Artificial metallopeptides for enantioselective hydration of enones

Ruben Maaskant
s1791117

MSc project
15-08-2014

Supervisors:

Dr. Almudena García Fernández
Prof. Dr. Gerard Roelfes

Abstract

Artificial metalloenzymes are hybrid catalysts composed of a metal complex and a biomolecular scaffold, for example proteins or peptides. In recent years this type of catalysts was employed in the catalysis of a wide range of reactions with excellent reactivities and enantioselectivities. The design and synthesis of artificial metallopeptides will be presented in this report. Two ligands were selected as the first coordination sphere. After selection of the ligands computational studies were performed to aid the design of the biomolecular scaffold. These scaffolds, peptides, were synthesized and modified to obtain the artificial metallopeptide.
The metallopeptides were subsequently employed in the catalysis of the hydration of an α,β-unsaturated ketone, yielding up to 38% conversion and up to 29% e.e.

Contents

Abstract 2
1. Introduction 5
1.1. Structure of artificial metalloenzymes 5
1.2. Artificial metalloenzymes in catalysis 5
1.3. Goal 10
2. Ligands 11
2.1. Introduction 11
2.1.1. Structure of metallopeptides 11
2.1.2. Bidentate ligands 11
2.1.3. Pyridine derived ligands 11
2.2. Results and discussion 12
2.2.1. Synthesis of bipyridylalanine ligand (**10**) 12
2.2.1.1. Synthesis of 5-methyl-2,2'-bipyridine (**2**) 13
2.2.1.2. Bromination of **2** 14
2.2.1.3. Alkylation of **4** 14
2.2.1.4. Hydrolysis of **7** 20
2.2.2. Synthesis of phenanthroline-acetamide ligand 21
2.3. Summary 21
2.4. Experimental section 22
3. Computation studies 28
3.1. Introduction 28
3.1.1. Aims and challenges 28
3.1.2. Selection of the peptide 29
3.2. I-TASSER 30
3.3. CORINA 32
3.4. GROMOS forcefield 33
3.5. Summary 35
4. Peptides 37
4.1. Introduction 37
4.1.1. Expression versus synthesis 37
4.1.2. Selection of the peptide 37
4.1.3. Fmoc solid phase peptide synthesis 37
4.2. Synthesis of truncated bPP 38
4.3. Synthesis of peptide bPP-Y20C 39
4.3.1. Introduction post-synthetic modification 39
4.3.2. Position for mutation 40
4.3.3. Synthesis of mutant bPP-Y20C 40
4.4. Synthesis of peptide bPP-Y20Phen 41
4.4.1. Deprotection of cysteine 41

4.4.2. Functionalization of bPP-Y20C 43
4.5. Conclusions 43
4.6. Experimental section 44
5. Catalysis 46
5.1. Introduction 46
5.1.1. Hydration of unsaturated compounds 46
5.1.2. Hydration using artificial metalloenzymes 46
5.2. Synthesis of substrate 47
5.3. Catalysis 47
5.3.1. Initial catalytic trials 47
5.3.2. Catalysis using bPP-Y20Phen 48
5.3.3. Catalysis using bPP-Y20C 49
5.4. Summary 52
5.5. Experimental section 53
6. Conclusions 54
References 55
Appendix A: List of abbreviations 59
Appendix B: Characterization of organic compounds 60
Appendix C: Characterization of peptides 85
Appendix D: HPLC-traces of correction factor and catalysis 94

1. Introduction

1.1. Structure of artificial metalloenzymes

In recent years the use of artificial metalloenzymes in catalysis has seen a growth. Artificial metalloenzymes were developed in a bid to combine the best of traditional homogeneous metal catalysis with enzymatic catalysis. By combining the broad substrate scope of homogeneous catalysis with the selectivity and rate acceleration of enzymatic catalysis, a potent hybrid catalyst can be obtained. These metalloenzymes have shown to efficient catalysts for a wide range of transformations, often with excellent enantioselectivities if applicable.[1–4] Additionally, reactions that do not have a counterpart in traditional metal catalysis could be performed.[5–7]
The structure of metalloenzymes can be divided in two parts, the metal complex and the biomolecular scaffold (Figure 1). The metal-ligand complex can be defined as the first coordination sphere, where the substrate binds, whereas the biomolecular scaffold can be defined as the second coordination sphere.

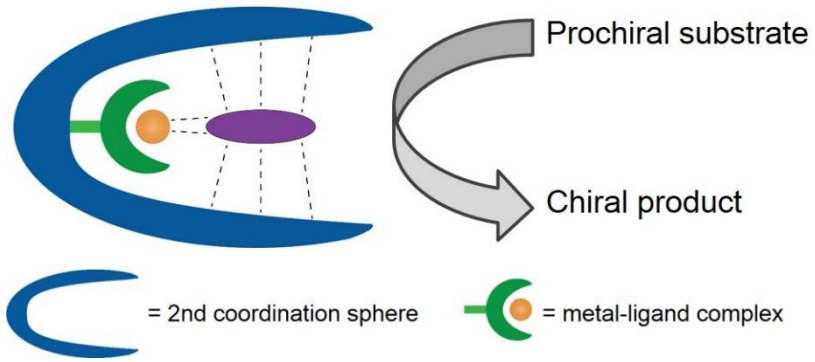

Figure 1: Representation of an artificial metalloenzyme with the first coordination sphere (metal-ligand complex) and the second coordination sphere.

This second coordination sphere provides additional interactions to stabilize the first coordination sphere, the substrate or transition states. As such, the second coordination sphere and its nature are of high importance. In addition to the stabilizing effect of the second coordination sphere, it can also be used to induce or enhance enantioselectivity obtained. Steric bulk of the scaffold can be used to block approaches or to force the substrate in a specific conformation.
In recent years, the use of computational studies in the design of a second coordination sphere increased.[8–12] These studies are attractive since it enables or enhances rational design and aids in the selection of scaffolds, providing an alternative for high throughput screening. By performing simulations a selection of suitable scaffolds or substrates can be made before the actual synthesis and catalysis, preserving material and time.

1.2. Artificial metalloenzymes in catalysis

Three main classes of biomolecules, used as scaffolds in previous studies, can be identified: DNA, proteins and peptides. In 2005 Roelfes and co-workers presented a first example of the use of DNA as scaffold in a copper catalyzed Diels-Alder reaction.[13] The presence of DNA improved the endo/exo selectivity and gave rise to excellent enantioselectivity of the reaction. In addition DNA was found to give a significant acceleration.[14] More recently other reactions, including Friedel-Crafts reactions, Michael

reactions and fluorinations, have been performed, also with excellent enantioselectivities (Scheme 1).[15,16]

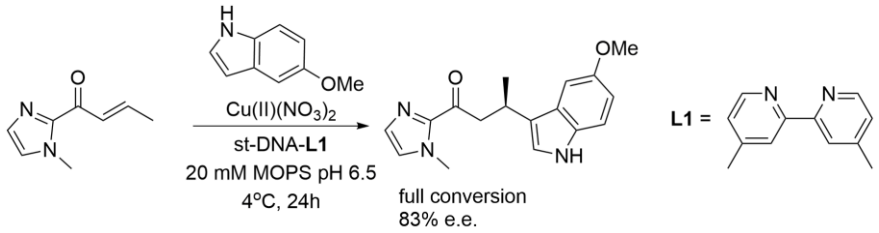

Scheme 1: DNA-catalyzed Friedel-Crafts reaction with an enone and 5-methoxyindole.

All of the systems use a metal-binding ligand that can interact (bind or intercalate) with DNA. The metal-binding ligand can go into the groove of the DNA and coordinate to a substrate. The substrate is activated via a Lewis acid mechanism by the transition metal catalyst. In all cases naturally sourced salmon testes DNA was used, synthetic DNA gave only marginally better results at a much higher cost. A range of well defined structures, both naturally occuring and engineered, is known.[17] However, the modification of DNA is difficult and structural diversity of the building blocks (bases) is limited, making rational design difficult.

Proteins can be easier modified and offer a greater structural diversity. Therefore they are often used as scaffolds in artificial metalloenzymes. Many of the proteins used as scaffold contain an existing pocket which is large enough to accommodate the metal complex and the substrate. Examples are bovine serum albumin and streptavidin.[3,18] A relatively small number of proteins contain such a large pocket, limiting diversity.

Ward and co-workers presented the use of streptavidin in the catalysis of several reactions, for example hydrogenations and sulfoxidations (Scheme 2).[3] A catalyst precursor is covalently anchored to biotin, which can subsequently coordinate strongly to streptavidin. The design of the catalyst-biotin moiety prior to incorporation into the protein makes variation and tuning of the first coordination sphere easier. In addition, streptavidin can be modified by mutation to enhance catalysis.[3,7,19] However, the strong binding to biotin should be retained.

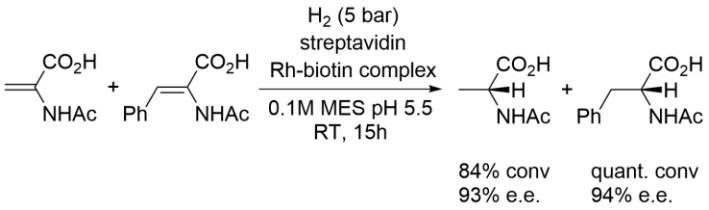

Scheme 2: Asymmetric hydrogenations using a streptavidin/Rh-biotin complex presented by Ward and co-workers.

Two approaches involving the creation of a binding site or pocket were presented by Ueno and co-workers and Bos and co-workers.[2,20] Ueno and co-workers designed a scandium(III) binding site on a tubular protein by rational design using X-ray data. By covalently introducing a ligand, tetracoordinate coordination of scandium(III) with the ligand and two present tyrosines was obtained. This enzyme could subsequently be used to perform an epoxide ring-opening reaction giving rise to rate acceleration.

Bos and co-workers used a dimeric protein to create a binding pocket in between the protein strands.[6,20] By covalently attaching a metal-binding ligand, a catalyst was created that could catalyze Diels-Alder reactions and hydrations of enones (Scheme 3). Residues in the second coordination sphere were mutated, enhancing catalytic properties and proving the concept of rational design.

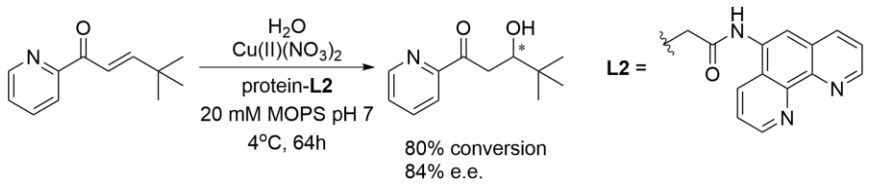

Scheme 3: Enantioselective hydration catalyzed by an artificial metalloprotein using a covalently attached phenanthroline moiety.

Proteins are excellent scaffolds for artificial metalloenzymes, providing structural diversity and a second coordination sphere capable of interacting with the metal complex or the substrate.
Peptides are smaller than proteins, consisting of up to 50 amino acids. Structural diversity and structural rigidity is however expected to be sufficient to establish a second coordination sphere and allow modifications. Peptides can be obtained synthetically and as such, extensive modifications can be introduced during the synthesis. A variety of reactions has been catalyzed using peptides and a range of metals, such as rhodium, iridium, palladium and copper.[21–27] Peptides were designed with natural or nonnatural ligands, which were either monodentate or bidentate. Whereas several systems use monomeric peptides, the use of dimeric or cyclic peptides has also been seen.
Mayer and Hilvert presented the use of a simple tripeptide in combination with iridium to efficiently perform transfer hydrogenations on ketones, aldehydes and imines.[21] In addition to the hydrogenation of these substrates, they performed the hydrogenation of NAD^+ in a selective manner (Scheme 4). The 1,4-hydrogenation of NAD^+ to NADH is a reaction of high importance in biological systems. Using the *in situ* formed complex of iridium and the tripeptide the 1,4-hydrogenation of NAD^+ was performed with over 10:1 selectivity compared to the 1,2 and 1,6-hydrogenations.

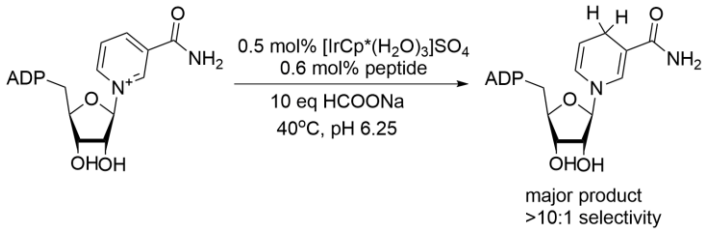

Scheme 4: 1,4-transfer hydrogenation of NAD^+ to NADH using an iridium source, a tripeptide and sodium formate.

Ball and co-workers presented an asymmetric Si-H insertion using a dirhodium catalyst and a peptide scaffold (Scheme 5).[22] Rhodium ions coordinated to two carboxylate groups from natural amino acids in the peptide, creating a peptide dimer by bridging. Using this catalyst excellent yields and enantioselectivities were obtained.
In more recent studies Ball and co-workers modified the catalytic procedure to perform enantioselective cyclopropanations (Scheme 6).[23,24] Where in earlier studies peptides were cleaved and purified after synthesis on resin, these studies used the peptides on resin in a high throughput screening. As such the time-consuming cleavage and purification steps were avoided.

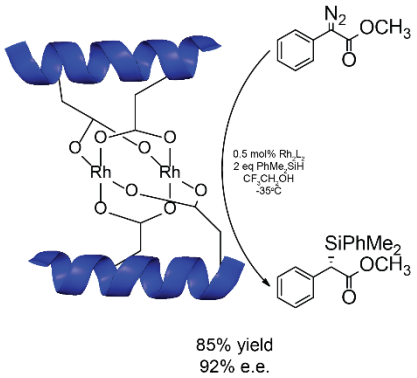

Scheme 5: Asymmetric Si-H insertion by Ball and co-workers using a dirhodium catalyst and a dimeric peptide.

It should be noted that monomeric peptides were used during the screening to avoid the formation of isomeric *bis*-peptides. It was assumed that the use of *bis*-peptides would give an enhancement of the monomeric peptides. After initial screening with *mono*-peptides, the sequence giving the optimal result was selected for the preparation of the corresponding *bis*-peptide. Using the *bis*-peptide, cyclopropanations of diazocompound and styrene were performed with up to 87% e.e., in contrast to 54% e.e. when using the *mono*-peptide on bead.

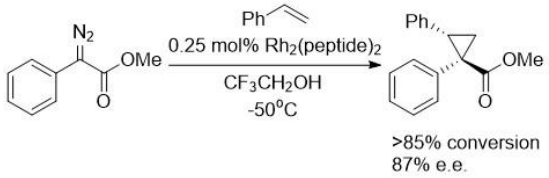

Scheme 6: Rhodium catalyzed cyclopropanation with styrene using a dirhodium *bis*-peptide complex.

In 2006 Gilbertson and co-workers presented studies that also involved catalyst screening with peptides on bead, obtained after parallel synthesis.[25] Several phosphine ligands were incorporated into the peptides by solid phase peptide synthesis. Tyrosines could be converted into phosphine ligands, possibly creating new possibilities for postsynthetic modification. These on bead peptides were employed in the rhodium catalyzed hydrogenations and the palladium catalyzed coupling of cyclic allylic acetates and malonates. Afterwards the best catalyst was cleaved from resin and used in solution. Whereas differences were found between 'on bead' catalysis and catalysis in solution, results were similar. In general, the yield was lower when using peptides in solution while the e.e. increased. High conversions and enantioselectivites were obtained in the coupling of acetates and malonates when using a peptide with a β-turn, which seemed to be essential for enantioselectivity (Scheme 7).[25]

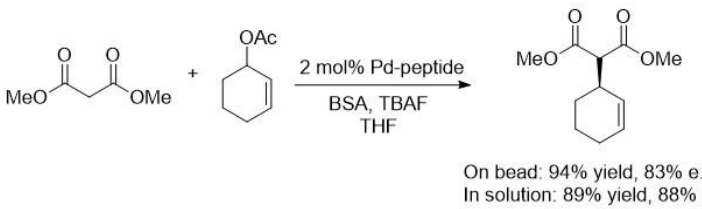

Scheme 7: Palladium catalyzed coupling of a cyclic allylic acetate and dimethyl malonate. Catalysis was performed with the peptide scaffold on bead as well as in solution, resulting in small differences in yield and enantioselectivity.

In 2009 another approach using synthetic peptides was presented by Coquière and co-workers (Scheme 8). The peptide bovine pancreatic protease (bPP) and several mutants, containing nonnatural pyridylalanine amino acids, were synthesized. These peptides were subsequently used in combination with copper(II) ions to catalyze Diels-Alder reactions and Michael additions with excellent conversions and enantioselectivities. The ligand, pyridylalanine, is monodentate and the system was designed to form a catalytically active dimer. It was later found that only a small percentage, roughly 10%, of the peptide dimerized and that the monomeric peptide was mainly present under the conditions used. However, this study showed the ease of modification by synthesis of the peptide.

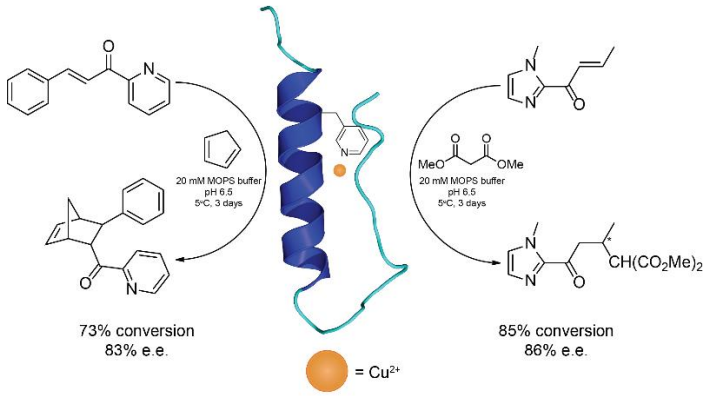

Scheme 8: Catalysis of Diels-Alder reactions and Michael additions using a copper-pyridylalanine complex linked to a helical peptide.

Peptides are smaller and can be obtained via expression or via synthesis. Synthesis of the peptide allows the facile incorporation of multiple nonnatural groups. In addition, peptide synthesis can be automated, reducing the time needed to obtain the scaffold.

A study using disulfide bridged cyclic peptides in combination with a copper(II) catalyst was presented in 2014 by Hermann and co-workers.[27] In this study, short nonapeptides with cysteine residues at both termini were synthesized and subsequently cyclized by intramolecular disulfide formation of the cysteine residues. The cyclic peptides were used in combination with copper(II) ions to catalyze Diels-Alder reactions and Friedel-Crafts reactions, obtaining high conversions and enantioselectivities (Scheme 9). It was shown that the disulfide bridge was important for catalysis, reduction of the disulfide with TCEP resulted in the loss of enantioselectivity. It was thought that the stability and rigidity of the peptide scaffold provided by the disulfide bridge is key to obtaining a high enantioselectivity. In this study, alanine scanning was applied. In alanine scanning, one residue is mutated to alanine in order to assess the importance of this specific residue to catalytic properties. As such, more mechanistic insight can be achieved.

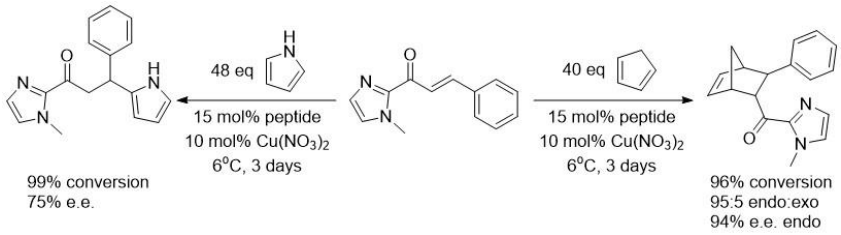

Scheme 9: Copper(II) catalyzed Diels-Alder and Friedel-Crafts reactions using a cyclic peptide. Upon reduction of the disulfide bridge, causing linearization, enantioselectivity was lost.

1.3. Goal

The aim of this project was the rational design and synthesis of artificial metallopeptides for applications in enantioselective catalysis. The rational design was to be aided by computational studies.

Suitable ligands had to be selected in order to establish a first coordination sphere and to bring the metal catalyst into the biomolecular scaffold.

After selection of the ligands, the design of the scaffold was done. Of the three discussed biomolecules, proteins, DNA and peptides, peptides offer the highest flexibility regarding structure modification and rational design. Peptides are relatively small biomolecules and can be acquired via expression or via synthesis. In addition, nonnatural amino acids can be built in, enabling a wide range of structural modifications.

The scaffold design was to be aided by computational studies and therefore a suitable computational method, enabling the acquisition of a large number of accurate structure predictions, had to be selected. After selection of suitable structures, the computational method should allow the detailed design and tuning of the second coordination sphere.

Structural motifs can be designed to tune the rigidity and overall structure of the peptide. Using computational studies, as well the overall structure of the peptide as the direct second coordination sphere can be changed before synthesizing the peptide. This reduces the number of mutants that should be synthesized and thus material and time are preserved.

The designed peptide scaffold had to be synthesized and a suitable method for the incorporation of the ligand had to be selected.

The final step in this project was to establish optimal conditions for catalysis using this hybrid catalyst.

The first part of this project, described in chapter 2, consists of the selection and synthesis of ligands for the first coordination sphere. With these ligands, computational studies could be performed. The screening of prediction software and results of these simulations are described in chapter 3. The synthesis and post-synthetic modification of peptides is described in chapter 4. These peptides were subsequently employed in catalysis, which is described in chapter 5.

2. Ligands

2.1. Introduction

2.1.1. Structure of metallopeptides

The structure of metallopeptides can be divided in two parts, the metal complex and the biomolecular scaffold (Figure 2). In this chapter the design and synthesis of two metal-binding amino acids will be discussed.
The design of the biomolecular scaffold will be discussed in chapter 3. The synthesis of the biomolecular scaffold and assembly of the catalyst will be discussed in chapter 4.

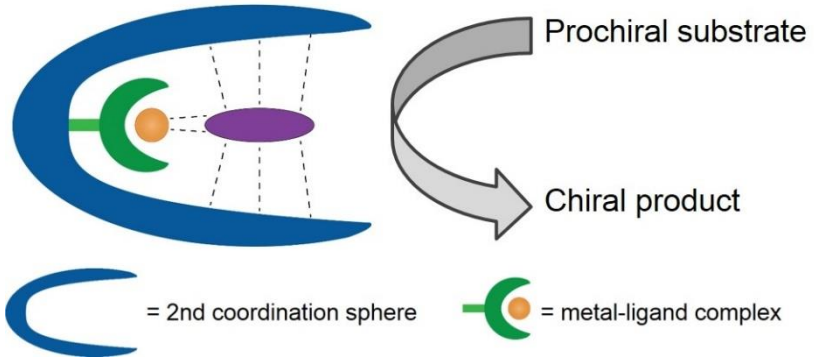

Figure 2: Schematic representation of a biomolecular catalyst.

2.1.2. Bidentate ligands

In order for a biomolecular scaffold to dissolve in aqueous media, a high number of sites that can interact with water molecules is required. Metal binding sites are difficult to design with natural amino acids, however a good metal binding site is necessary to efficiently coordinate metal ions and prevent leaching of the metal into the polar aqueous media. In order to gain more control over the localization of the metal ions, bidentate chelating ligands can be used instead of monodentate ligands. By introducing a group with two strongly coordinating atoms in close proximity, a higher affinity of the metal ions for this specific group is established. When a metal ion coordinates to a monodentate ligand, one counterion is displaced, whereas two counterions are displaced when coordinating to a bidentate ligand. More counterions are displaced, which means a gain in entropy of disorder when using a bidentate ligand. Therefore, the binding affinity of the metal ions for this specific site increases. This in turn increases the extent to which rational design can take place. By localization of the metal ion one can define the actual second coordination sphere and possible modifications of the latter to improve catalytic properties.

2.1.3. Pyridine derived ligands

In transformations with transition metal catalysts, the use of nitrogen-based ligands is frequently observed.[28,29] The pyridine group is known to have a strong binding with metal ions, ligands often contain one or more pyridine moieties to coordinate metal ions.[28,29,30] The resulting complexes are known to be efficient catalysts of a wide range of organic reactions.[28–30] Bipyridine complexes have been shown to be stable under catalytic conditions in both organic solvents and aqueous media.

Two bidentate metal-binding ligands with established catalytic properties, both planar aromatic molecules with a pyridine motif, were selected for synthesis.[15] Both ligands have been used in similar approaches.[15,20] Since the planar pyridine groups are achiral, any enantioselectivity is expected to be induced by the second coordination sphere.

Two approaches will be used for incorporation of the ligand into the peptide. The first approach is the direct incorporation of the ligand as an amino acid. The first ligand that will be discussed contains a bipyridine moiety as metal binding group and an amino acid group (Figure 3). It can be Fmoc-protected and introduced in the peptide via solid phase peptide synthesis (SPPS), thus following a linear approach.

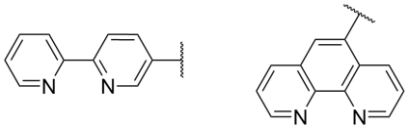

Figure 3: Left) The bipyridine moiety in the first ligand. Right) The phenanthroline moiety in the second

The second approach is introduction of the ligand by postsynthetic modification of a cysteine. This ligand carries a phenanthroline group as metal binding group and an electrophile-containing linker (Figure 3). This ligand can be introduced in the peptide via alkylation of the cysteine with the electrophile in the linker. This is a convergent approach, since both the ligand and the biomolecular scaffold will be synthesized separately and then combined.

2.2. Results and discussion

2.2.1. Synthesis of bipyridylalanine ligand (10)

The bipyridylalanine ligand will be incorporated into the peptide as an amino acid using solid phase peptide synthesis (SPPS). This method of incorporation has certain requirements: the S-enantiomer of the non-natural amino acid has to be obtained enantiopure to get a well-defined catalyst and the amino acid has to be Fmoc-protected to make it compatible with SPPS. The following retrosynthetic route was proposed for the synthesis of ligand **10** (Scheme 10). The protected amino acid **10** is obtained after Fmoc-protection of amino acid **9** (step ***6***). Enantiopure amino acid **9** is obtained by hydrolysis of the protected amino acid (step ***5***), it is important that racemization does not occur under the conditions used. Protected amino acid can be obtained by alkylation of a glycine derivative with a bipyridylalanine moiety (step ***4***). Since

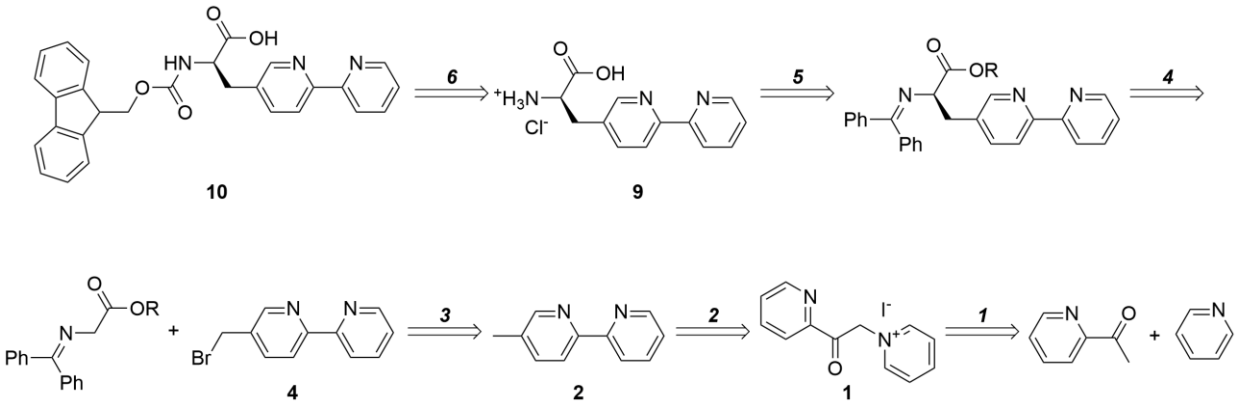

Scheme 10: Retrosynthesis of Fmoc-protected bipyridylalanine amino acid 10.

enantiopure amino acid is required, the alkylation is the key step of the synthesis. The enantioselectivity of the alkylation strongly influences the overall yield and the number of synthetic steps required.
Two precursors for the alkylation are required: a protected glycine residue and 5-(bromomethyl)-2,2'-bipyridine. The latter can be obtained by bromination of 5-methyl-2,2'-bipyridine (step ***3***). 5-methyl-2,2'-bipyridine can be obtained by performing a Kröhnke pyridine synthesis using compound **1** (step ***2***). This compound can be synthesized in a single step from commercially available materials (step ***1***).

2.2.1.1. Synthesis of 5-methyl-2,2'-bipyridine (2)

Compound **2**, was synthesized in a two-step synthesis adapting procedures from literature (Scheme 11).[31,32]
Initially, the reaction of commercially available 2-acetylpyridine with pyridine and iodine at 80°C for 4 hours, followed by stirring at room temperature overnight gives rise to the formation of **1**, as confirmed by ^{1}H-NMR, ^{13}C-NMR and mass spectrometry.

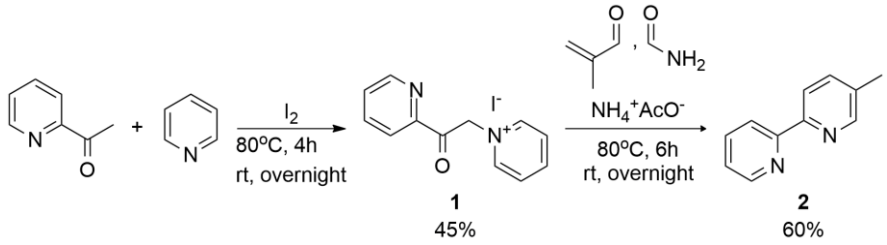

Scheme 11: The two-step synthesis to obtain 5-methyl-2,2'-bipyridine.

Subsequently compound **1** was converted to compound **2** via a Kröhnke pyridine synthesis with formamide, methacrolein and ammonium acetate as the base by stirring at 80°C for 6 hours, followed by overnight stirring at room temperature (Scheme 12). In the Kröhnke pyridine synthesis a pyridine ring is synthesized by condensation of a 1,5-diketone followed by aromatization via oxidation. After purification by column chromatography **2** was obtained pure and characterized by ^{1}H-NMR, ^{13}C-NMR and mass spectrometry.

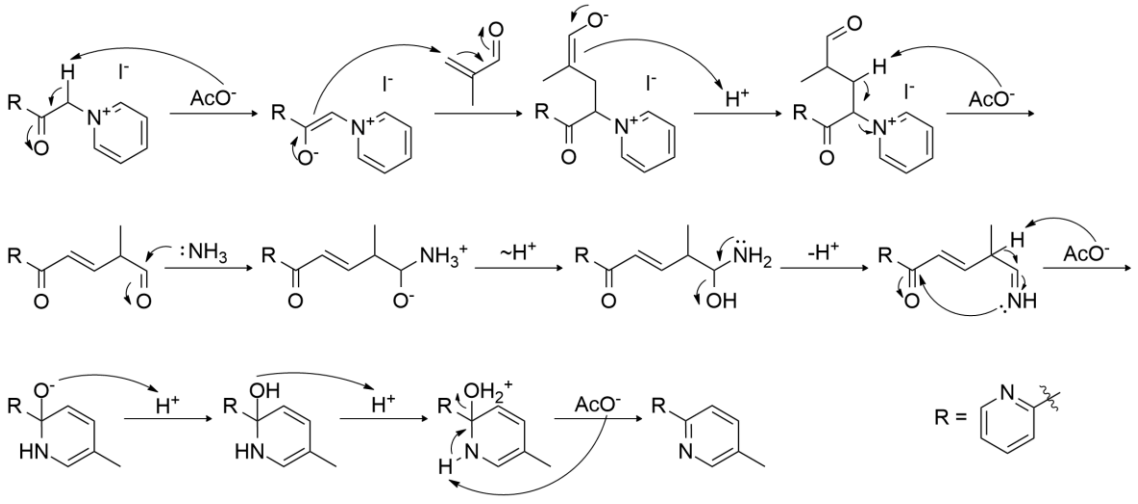

Scheme 12: Mechanism of the Kröhnke pyridine synthesis with **1**, ammonium acetate and methacrolein.

2.2.1.2. Bromination of 2

After the synthesis of **2** a bromination was performed to obtain the monobrominated electrophile.
Several procedures for the synthesis of the monobrominated compound from **2** are known. [33,34,35,31,36] Two of these approaches, using **2** as starting material, were followed.
In a first attempt, compound **2** was silylated with lithium diisopropylamine and trimethylsilyl chloride in THF at -78°C (Scheme 13).[33,34] The resulting compound **3** is then reacted with cesium fluoride and hexabromoethane in DMF by stirring at 25°C for 4 hours.

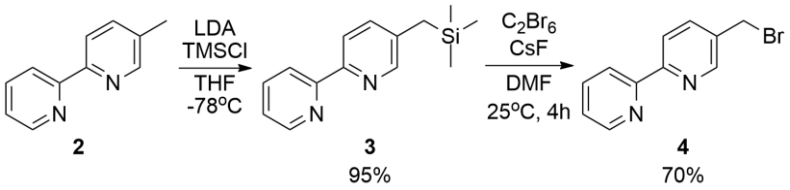

Scheme 13: Alternative synthesis to yield electrophile **4** via intermediate **3**.

After purification by column chromatography compound **4** was obtained, which was characterized by ^{1}H-NMR, ^{13}C-NMR and mass spectrometry. Although the two step reaction gave a good overall yield of 67%, availability of starting material, hexabromoethane and 1,2-dibromo-1,1,2,2-tetrafluoroethane, was an issue, limiting the applicability of this synthetic strategy.
In a different approach compound **2** was stirred at reflux with NBS in CCl_4 for 2 hours with AIBN as the initiator of the radical bromination. The reaction could be followed by TLC, which revealed the formation of a second compound. During the reaction approximately 10% of dibrominated compound was formed due to the use of a slight excess (1.1 equivalents) of NBS.

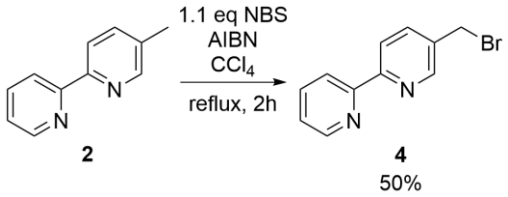

Scheme 14: Radical monobromination of **2** to yield electrophile **4**.

Allowing a longer reaction time to fully convert **2** leaves only monobrominated and dibrominated compound to be separated. After purification by recrystallization pure **4** was obtained in moderate yield of 50%.

2.2.1.3. Alkylation of 4

The synthesis of amino acid **9** requires introduction of an amino acid motif to compound **4**. One method to introduce an amino acid motif to an electrophile is by performing an alkylation on a glycine residue.
A method for the synthesis of amino acids, using nickel(II) complexes, was developed by Belokon and coworkers.[37] A chiral nickel(II)-complex was alkylated using a Michael addition on an alkene (Scheme 15).[37] The nickel(II)-complex, Gly-Ni-BPB, contained a (*S*)-benzylproline group as chiral auxiliary and a glycine residue. The glycine residue was deprotonated and subsequently a Michael addition using an unsaturated compound was performed, which yielded the alkylated Gly-Ni-BPB complex. After separation of the

diastereomers by column chromatography, general acid catalyzed hydrolysis yielded a range of enantiopure amino acids in moderate to good yields (40-80%).

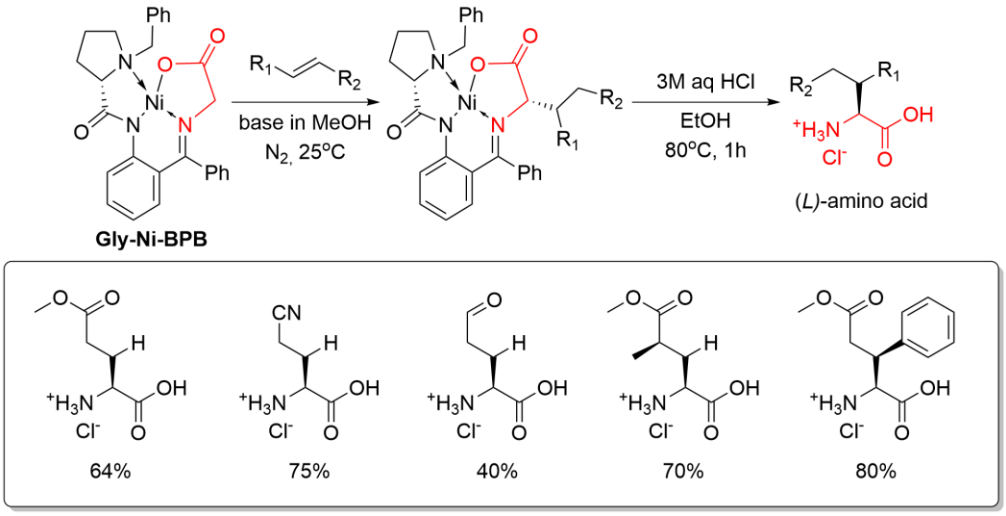

Scheme 15: Scope of L-amino acids that could be generated using the chiral nickel(II)-benzylproline (Gly-Ni-BPB complex).[19]

Using this strategy different nickel(II) complexes, containing masked glycine residues, have been reported to be suitable for alkylation with electrophiles.[37] In general, amino acids can be obtained after hydrolyzing the alkylated complex. The nickel(II) complexes used for these reactions can be synthesized in two or three steps and have the advantage that, after hydrolysis, the precursor of the nickel(II) complex can be recovered and recycled after a condensation with glycine and a nickel(II) salt.
In an attempt to use this methodology, several experiments were performed to alkylate Gly-Ni-BPB with 5-(bromomethyl)-2,2'-bipyridine (**4**)(Scheme 16).

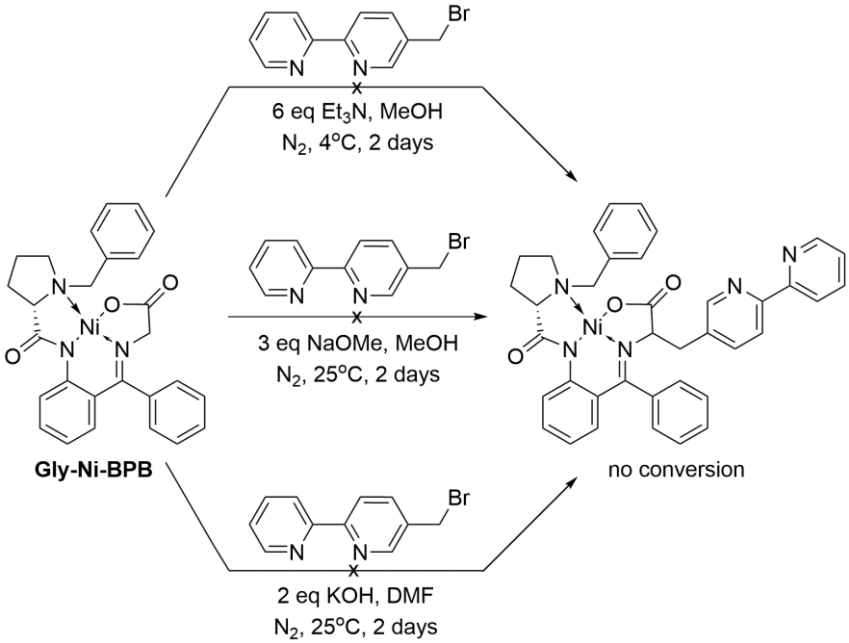

Scheme 16: Preliminary experiments to facilitate the alkylation of Gly-Ni-BPB using different conditions did not give conversion.

A reaction of the nickel(II)-benzylproline complex with **4** and triethylamine as the base in methanol at 4°C for 2 days did not show conversion according to ^{1}H-NMR. The lack of conversion can be explained by the low reaction temperature or the use of a hindered base (or a combination thereof).
However, performing the reaction using sodium methoxide as base in methanol at 25°C for 2 days also gave no conversion according to ^{1}H-NMR. Solid potassium hydroxide as base and DMF as solvent did not give any reaction. In all cases the starting material was isolated after reaction.
Since no conversion was observed in the reactions with the nickel(II)-benzylproline complex, experiments were performed with a nickel(II)-pyridine complex (Gly-Ni-PBP).
It has been reported that this non-chiral complex can be alkylated with aryl bromides in an enantioselective reaction using (*R*) or (*S*)-NOBIN as chiral catalyst and sodium hydroxide as base (Scheme 17).[38,39] After hydrolysis of the alkylated Gly-Ni-PBP, a range of amino acids could be obtained in good yields (62-92%) and with high enantiomeric excesses (93-98.5%). A recrystallization can be performed to obtain the enantiopure product, in case of (*R*)-phenylalanine the e.e. increased from 97% to >99.8%. In addition, it was shown that the enantiopreference of the reaction can be tuned with the NOBIN enantiomer used. Thus (*R*)-NOBIN gives (*R*)-amino acid and (*S*)-NOBIN gives (*S*)-amino acid.

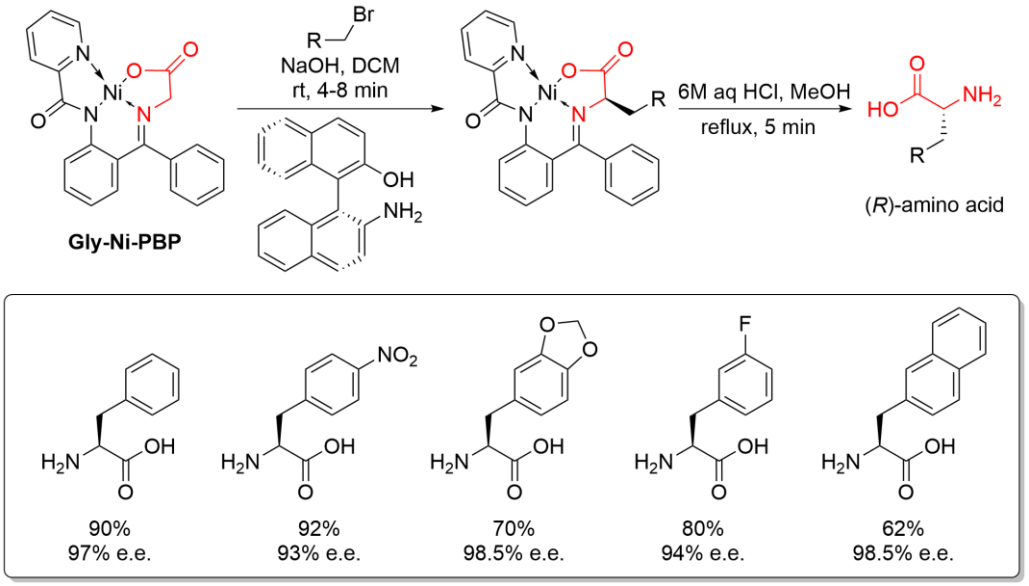

Scheme 17: Asymmetric alkylation of Gly-Ni-PBP with aryl bromides and (*R*)-NOBIN as catalyst. Hydrolysis of the alkylated complex yielded a range of amino acids with high enantiomeric excesses.[20,21]

Following this methodology, the reaction of the nickel(II)-pyridine complex with **4**, (*S*)-NOBIN as catalyst and solid sodium hydroxide as base in DCM at 20°C for 1 day yielded the alkylated nickel(II) complex **8** (Scheme 18). After recrystallization from dichloromethane/acetone at room temperature the complex was analyzed by ^{1}H-NMR, ^{13}C-NMR and mass spectrometry.
Compound **8** was subsequently hydrolyzed using aqueous hydrochloric acid and methanol at reflux. An extraction was performed to remove the precursor to the complex from the mixture and the aqueous phase was subsequently lyophilized to obtain amino acid **9**. ^{1}H-NMR, ^{13}C-NMR, mass spectrometry confirmed the formation of **9**. Unfortunately reverse phase HPLC (rp-HPLC) showed that the (*R*)-amino acid was formed with an e.e. of only 19%. Interestingly, the (*R*)-amino acid was formed preferentially with (*S*)-NOBIN.

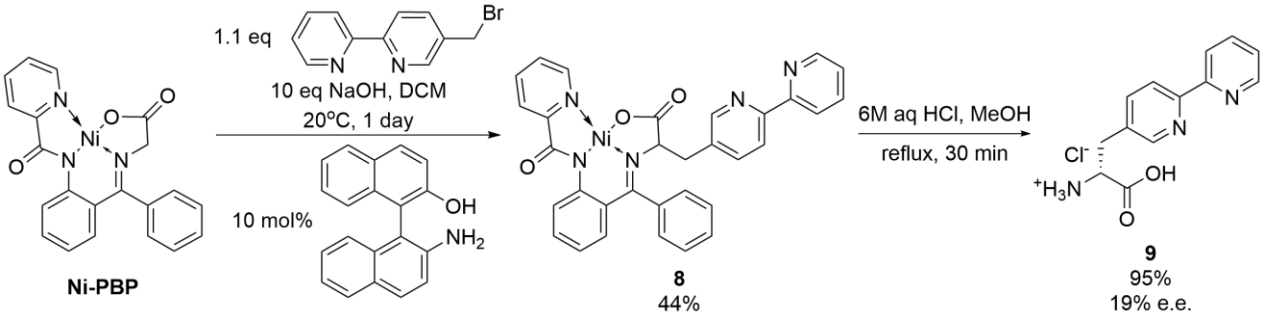

Scheme 18: Alkylation of the nickel(II)-pyridine complex using (S)-NOBIN as catalyst yielded the alkylated complex. After hydrolysis of the complex the unwanted enantiomer of the amino acid was obtained with an e.e. of 19%.

Additionally, the attempts to crystallize one of the enantiomers from the mixture were unsuccessful. Probably, the starting e.e. was too low to selectively crystallize one enantiomer. It can be concluded that although nickel(II) complexes are suitable reagents for the synthesis of α-amino acids, in our case alkylation with compound **4** as electrophile does not give the desired results.

In an alternative strategy, chiral phase transfer catalysts are also reported for the enantioselective alkylation of glycine residues.[40,41,42] Several chiral phase transfer catalysts can be synthesized or acquired from commercial sources, such as the Maruoka catalysts and cinchonidine based catalysts. All of these catalysts, based on quaternary ammonium salts, alkylate protected glycine esters with moderate to good enantioselectivities.[35,40,41,42,43,44,32,45,46]

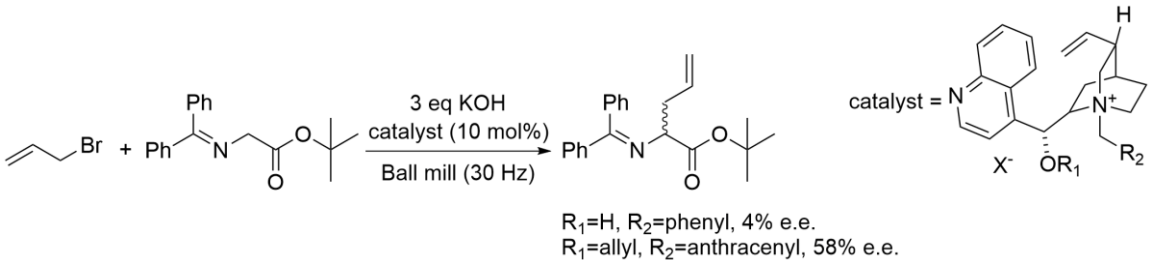

Scheme 19: Alkylation of benzophenonimine protected glycine *tert*-butyl ester with allyl bromide, catalyzed by the two selected cinchonidine salts.[24]

In our case, two cinchonidine based catalysts were tested, both of which have been reported for the alkylation of the benzophenonimine protected glycine *tert*-butyl ester (Scheme 19, Figure 4).[42]

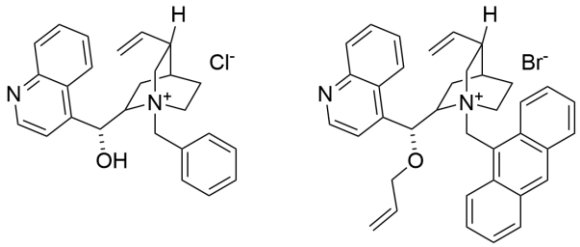

Figure 4: Left) (8S,9R)-(-)-N-benzylcinchonidinium chloride. Right) Cinchonidine based catalyst **12**.

(8S,9R)-(-)-N-benzylcinchonidinium chloride is commercially available and has been used in our group in the alkylation of the protected glycine methyl ester with **4** (unpublished results). Catalyst **12** was

synthesized using a two-step procedure and has been used in combination with the *tert*-butyl ester (Scheme 20). In the first step of the synthesis, commercially available cinchonidine and 9-(chloromethyl)anthracene were heated under reflux in toluene for 2 hours. Upon addition of the reaction mixture to cold diethyl ether intermediate **11** precipitated as a powder in a yield of 96%, which was characterized by ^{1}H-NMR, ^{13}C-NMR and mass spectrometry. Allylation of **11** with allyl bromide and potassium hydroxide as base in DCM, followed by recrystallization of the crude from methanol/diethyl ether at -18°C gave **12** in 85% yield. **12** was characterized by ^{1}H-NMR, ^{13}C-NMR and mass spectrometry.

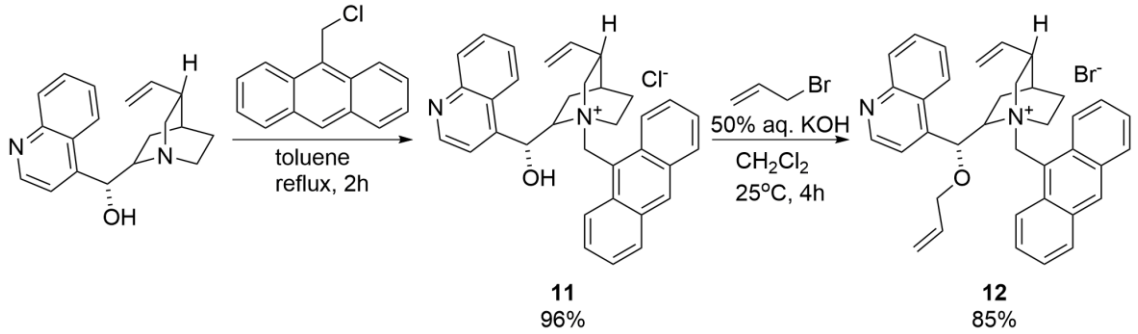

Scheme 20: Two-step synthesis of phase transfer catalyst **12** using cinchonidine, 9-(chloromethyl)anthracene and allyl bromide.

To make these glycine residue suitable as nucleophile for alkylation, the amine has to be protected as an imine group, often benzophenonimine, and the acid as an ester group. Several esters have been used in alkylations. For our study the methyl and *tert*-butyl esters were selected.[40,41,42] The benzophenonimine protected glycine methyl ester was obtained from commercial sources. The benzophenonimine protected glycine *tert*-butyl ester was synthesized in a single step by stirring commercially available *tert*-butyl 2-bromoacetate and benzophenonimine with diisopropylethylamine as base by heating under reflux for 12 hours (Scheme 21). Recrystallization of the reaction mixture yielded compound **6**, which was characterized by ^{1}H-NMR, ^{13}C-NMR and mass spectrometry.

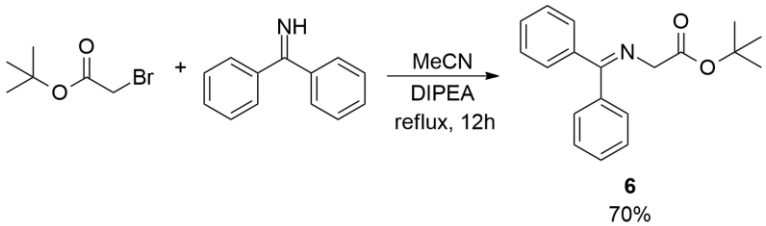

Scheme 21: One-step procedure to obtain the benzophenonimine protected glycine *tert*-butyl ester.

It was observed that for the alkylation of the benzophenonimine protected glycine methyl and *tert*-butyl esters with **4**, using aqueous sodium hydroxide as the base, only commercially available (8S,9R)-(-)-N-benzylcinchonidinium chloride and the protected glycine methyl ester gave conversion (Scheme 22).

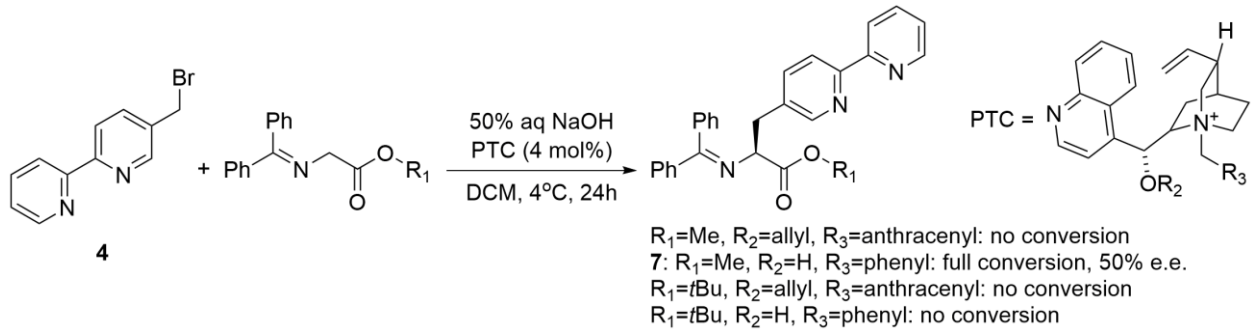

Scheme 22: Asymmetric phase-transfer catalyzed alkylation of the protected glycine ester with 5-(bromomethyl)-2,2'-bipyridine.

np-HPLC analysis showed a moderate 50% e.e. The lack of conversion in the reactions with the benzophenonimine protected glycine *tert*-butyl ester could be explained by the low reaction temperature or the use of a bulky ester and a bulky electrophile (or a combination thereof).

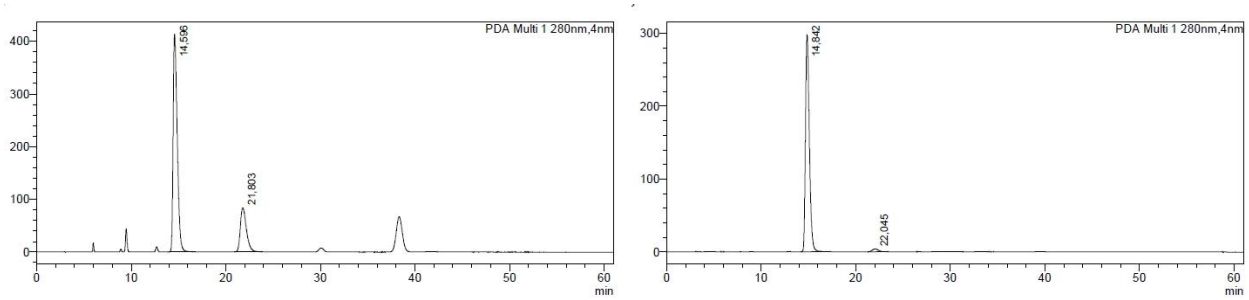

Figure 5: Left) HPLC analysis of crude **7** showed an e.e. of 50%. Right) HPLC analysis of **7** purified by column chromatography showed an e.e. of 96%.

However to our surprise, protected amino acid with 96% e.e. was obtained after purification by column chromatography (Figure 5). Upon dissolving the crude product in the eluent for the column, an insoluble residue was observed. This solid residue might be racemic material forming a conglomerate while the dominant enantiomer dissolved. Analysis of this residue by ^{1}H-NMR and np-HPLC showed protected amino acid with lower enantiomeric excess, which seems to confirm this hypothesis (Figure 6).

The isolation of amino acid with 96% e.e. could be repeated up to three times, at the fourth time amino acid with a lower e.e. was isolated. The isolated enantiopure compound **7** was obtained in 40% yield and was characterized by ^{1}H-NMR, ^{13}C-NMR and mass spectrometry.

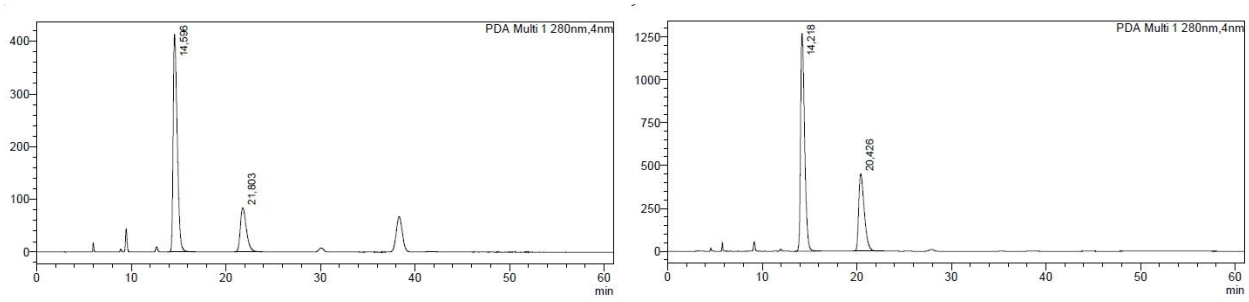

Figure 6: Left) HPLC analysis of crude **7** showed an e.e. of 50%. Right) HPLC analysis of solid residue showed the presence of **7** with lower e.e.

2.2.1.4. Hydrolysis of 7

The final step in the synthesis of enantiopure amino acid **9** requires the deprotection of **7**. Both protecting groups can be removed by acid catalyzed hydrolysis, avoiding harsh conditions to prevent racemization. Thus, both protecting groups were hydrolyzed using aqueous hydrochloric acid and diethyl ether at room temperature for 18 hours (Scheme 23). After removing benzophenone from the mixture by extraction, the aqueous phase was lyophilized to obtain 2-([2,2'-bipyridin]-5-yl)-1-carboxyethanaminium chloride **9** in

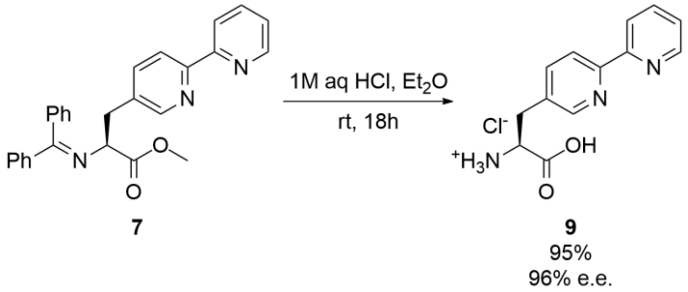

Scheme 23: Hydrolysis of enantiopure (*S*)-**7** using hydrochloric acid yielded enantiopure (*S*)-**9**.

95% yield. Compound **9** was analyzed by ^{1}H-NMR, ^{13}C-NMR, mass spectrometry and reverse phase HPLC (rp-HPLC). rp-HPLC showed that the e.e. of the isolated amino acid still was 96%.

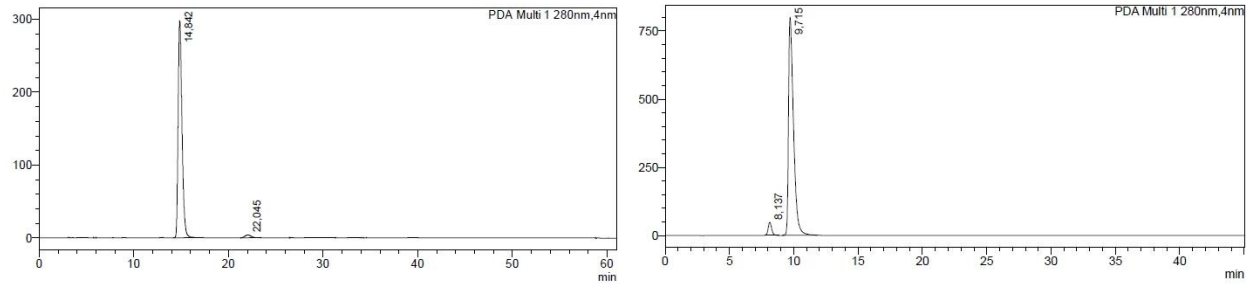

Figure 7: Left) HPLC analysis of **7** showed an e.e. of 96%. Right) HPLC analysis of **9** showed an e.e. of 96%.

HPLC analysis showed that enantiopure (*S*)-**9** was obtained without racemization during the hydrolysis (Figure 7). Overall yield of **9** was 5% after 6 steps.

The Fmoc-protection of **9** is required for its introduction in the peptide via SPPS. An experiment was performed using literature procedures, however significant amounts of unidentified impurities were observed in ^{1}H-NMR (Scheme 24).[32,45]

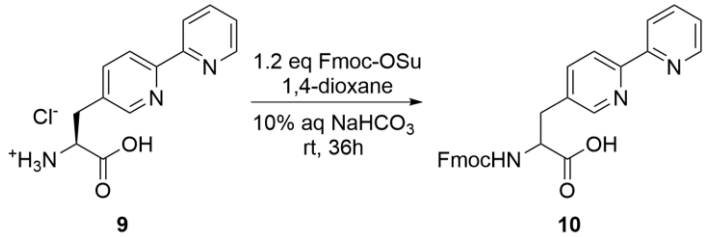

Scheme 24: Synthesis of Fmoc-protected amino acid **10**. The reaction did not proceed cleanly and no pure **10** was isolated.

Since the reaction did not proceed cleanly and the availability of **9** was limited, no further experiments were performed.

2.2.2. Synthesis of phenanthroline-acetamide ligand

In a different approach, we also want to explore the possibility to couple a ligand to the peptide scaffold by post-synthetic modification. This strategy required the presence of a linker with a nucleophile in the ligand structure, in order to facilitate the coupling with a residue from the peptidic chain.

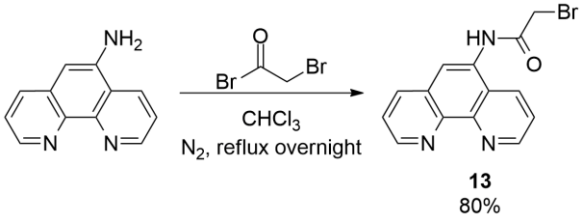

Scheme 25: Coupling of 1,10-phenanthrolin-5-amine to 2-bromoacetyl bromide to yield **13**.

Based on this design and following a procedure from literature, 1,10-phenanthrolin-5-amine was coupled to 2-bromoacetyl bromide in chloroform by heating to reflux overnight under inert atmosphere (Scheme 25).[20,6,47] After recrystallization from methanol compound **13** was obtained in a yield of 80%. Characterization was done by ^{1}H-NMR, ^{13}C-NMR and mass spectrometry.

2.3. Summary

After an optimization, two ligands have been synthesized for incorporation into the peptide scaffold.
Enantiopure amino acid (*S*)-**9**, containing a bipyridyl moiety, was synthesized in six steps from commercially available reagents with an overall yield of 5%. Compound **9** needs to be Fmoc-protected to enable introduction in the peptide by SPPS.
Ligand **13**, based on a 1,10-phenanthroline moiety, was obtained in 80% yield. Compound **13** can be introduced to the peptide via post-synthetic modification by reaction of the electrophile in the linker with a cysteine residue.

2.4. Experimental section

General remarks

All chemicals were obtained from Sigma Aldrich or Acros Organics and used without further purification, unless states otherwise. (8S,9R)-(-)-N-benzylcinchonidinium chloride was obtained from TCI Europe and used without further purification. ^{1}H-NMR and ^{13}C-NMR spectra were recorded on a Varian 400 (400 and 100 MHz respectively) or a Varian 200 (200 and 50 MHz respectively). Chemical shifts (δ) are denoted in ppm using residual solvent peaks as internal standard (δ_C = 77.2 and δ_H = 7.26 for $CDCl_3$, δ_C = 39.5 and δ_H = 2.50 for DMSO-d6, δ_C = 49.0 and δ_H = 3.31 for CD_3OD). Mass spectra (HRMS) were recorded on a LTQ Orbitrap XL. Melting temperatures were measured on a Büchi B-545 melting point apparatus. Column chromatography was performed using silica gel 60 Å (Merck, 200-400 mesh). Enantiomeric excess determination was performed by HPLC analysis on Shimadzu 10AD-VP or 20AD systems.

1-(2-oxo-2-(pyridin-2-yl)ethyl)pyridin-1-ium iodide (1)

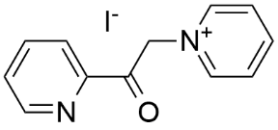

Procedure adapted from literature.[31,32] To a solution of iodine (40.0 g, 157.5 mmol) in anhydrous pyridine (150 ml) under inert atmosphere was added 2-acetylpyridine (18 ml, 160.5 mmol). The mixture was heated at 80°C for 4 hours and stirred overnight at room temperature. The suspension was filtered and the solid was washed with pyridine. The solid was dissolved in hot methanol (150 ml) and activated carbon (5 g) was added. The suspension was filtered over Celite and the filtrate was stored at -18°C overnight. Material crystallized overnight, these crystals were washed with ice-cold methanol. Product **1** was obtained as light yellow crystals (21.9 g, 67.1 mmol, 45%). ^{1}H NMR (400 MHz, DMSO-d6) δ 9.05 (d, *J* = 6.1 Hz, 2H), 8.92 (d, *J* = 4.2 Hz, 1H), 8.77 (t, *J* = 7.8 Hz, 1H), 8.32 (t, *J* = 6.7 Hz, 2H), 8.18 (t, *J* = 7.7 Hz, 1H), 8.12 (d, *J* = 7.7 Hz, 1H), 7.88 (t, 1H), 6.55 (s, 2H). ^{13}C NMR (101 MHz, DMSO-d6) δ 191.4, 150.4, 149.5, 146.3, 138.1, 129.1, 127.7, 122.0, 66.6. HRMS calcd for $C_{12}H_{11}N_2O$ (**1** -I^-) $[M+H]^+$ 199.087, found 199.086. m.p.: decomposes >195°C.

5-methyl-2,2'-bipyridine (2)

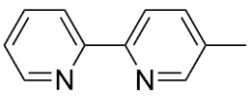

Procedure adapted from literature.[31,32] Ammonium acetate (12.0 g, 155.7 mmol) was added to a solution of product **1** (21.9 g, 67.1 mmol) in formamide (210 ml). Methacrolein (6.2 ml, 74.9 mmol) was added and the solution was stirred at 80°C for 6 hours. After stirring at room temperature overnight, the solution was diluted with water (100 ml) and aqueous $NaHCO_3$ solution (1 wt%, 50 ml). The aqueous phase was extracted with diethyl ether (4 x 100 ml). The combined organic layers were washed with aqueous $NaHCO_3$ solution (1 wt%, 2 x 100 ml), dried over sodium sulphate and concentrated. After column chromatography (SiO_2, dichloromethane/methanol: 20/1) product **2** was obtained as a colorless oil (6.9 g, 40.3 mmol, 60%). ^{1}H NMR (400 MHz, $CDCl_3$) δ 8.67 (d, *J* = 4.7 Hz, 1H), 8.51 (s, 1H), 8.37 (d, *J* = 8.0 Hz, 1H), 8.30 (d, *J* = 8.1 Hz, 1H), 7.81 (td, *J* = 7.8, 1.8 Hz, 1H), 7.64 (dd, *J* = 8.1, 2.2 Hz, 1H), 7.32 – 7.27 (m, 1H), 2.40 (s, 3H). ^{13}C NMR (101 MHz, $CDCl_3$) δ 156.1, 153.5, 149.5, 149.0, 137.3, 136.7, 133.2, 123.2, 120.6, 120.4, 18.2. HRMS calcd for $C_{11}H_{11}N_2$ $[M+H]^+$ 171.092, found 171.092.

5-((trimethylsilyl)methyl)-2,2'-bipyridine (3)

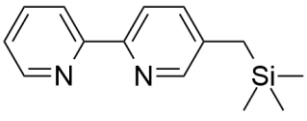

Prepared following literature procedures.[33] A solution of diisopropyl amine (0.2 ml, 1.5 mmol) in THF (10.5 ml) was cooled to -78°C and a solution of n-butyllithium in hexane (1.6M, 0.9 ml, 1.4 mmol) was added dropwise. After stirring for 10 minutes at -78°C the mixture was allowed to warm to room

temperature and stirred for 10 minutes. The mixture was cooled to -78°C and a solution of 5-methyl-2,2'-bipyridine (209.0 mg, 1.2 mmol) in THF (1.5 ml) was added. The mixture was stirred for 1 hour at -78 °C and trimethylsilyl chloride (0.2 ml, 1.5 mmol) was added. Cooling was removed and absolute ethanol (0.8 ml) was added rapidly. The cold mixture was poored into a separatory funnel with saturated aqueous $NaHCO_3$ (12 ml). The mixture was diluted with water (5 ml) and extracted with dichloromethane (3 x 12 ml). The combined organic layers were dried over sodium sulphate and concentrated. After purification by column chromatography (SiO_2, heptane/ethyl acetate/triethylamine: 50/50/2) product **3** was obtained as a white solid (283.2 mg, 1.2 mmol, 95%). ^{1}H NMR (400 MHz, $CDCl_3$) δ 8.66 (d, *J* = 4.5 Hz, 1H), 8.40 – 8.34 (m, 2H), 8.27 (d, *J* = 8.1 Hz, 1H), 7.81 (t, *J* = 7.9 Hz, 1H), 7.47 (d, *J* = 6.6 Hz, 1H), 7.29 (d, *J* = 7.1 Hz, 1H), 2.13 (s, 2H), 0.03 (s, 9H). ^{13}C NMR (101 MHz, $CDCl_3$) δ 156.5, 152.3, 149.1, 148.6, 136.9, 136.7, 136.1, 123.2, 120.6, 120.6, 24.1, -1.9. HRMS calcd for $C_{14}H_{19}N_2Si$ $[M+H]^+$ 243.131, found 243.130. m.p.: 53-55°C.

5-(bromomethyl)-2,2'-bipyridine (4)

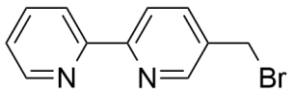

Method A:

Procedure adapted from literature.[31,32] This experiment was conducted under minimum exposure to light. N-bromosuccinimide (10.9 g, 61.2 mmol) and AIBN (142.8 mg, 0.9 mmol) were added to a solution of product **2** (10.0 g, 58.8 mmol) in dry CCl_4 (210 ml) under inert conditions. The mixture was heated under inert atmosphere at reflux until TLC (SiO_2, dichloromethane/methanol: 20/1) showed disappearance of the starting material. The mixture was cooled to room temperature and filtered. After evaporation of the solvent the crude was recrystallized from hot, dry hexane to yield a mixture of mono- and dibrominated crystalline material. To separate **4** and the dibrominated material a second recrystallization from absolute ethanol was performed, afterwards cooling to -18°C. Product **4** was obtained as white crystals (7.3 g, 29.4 mmol, 50%). ^{1}H NMR (400 MHz, $CDCl_3$) δ 8.68 (d, *J* = 2.4 Hz, 2H), 8.40 (d, *J* = 8.1 Hz, 2H), 7.83 (ddd, *J* = 9.4, 8.0, 2.0 Hz, 2H), 7.31 (m, 1H), 4.53 (s, 2H). ^{13}C NMR (101 MHz, $CDCl_3$) δ 156.1, 155.5, 149.4, 149.3, 137.6, 137.0, 133.7, 124.0, 121.3, 121.1, 29.8. HRMS calcd for $C_{11}H_9BrN_2$ $[M+H]^+$ 249.002, found 249.002. m.p.: 72-74°C.

Note: benzene can be used as substituent for CCl_4 as the solvent. Preliminary experiments shows a similar ratio of monobrominated and dibrominated compound, although the reaction time increases.

Method B :

Procedure adapted from literature.[33] Product **3** (280.1 mg, 1.2 mmol), hexabromoethane (1.2 g, 2.3 mmol) and cesium fluoride (349.4 mg, 2.3 mmol) were dissolved in dimethylformamide (11 ml). The solution was stirred at 25 °C for 4 hours. The mixture was poured into a separatory funnel with water (50 ml) and extracted with ethyl acetate (3 x 40 ml). The combined organic layers were washed with water (100 ml) and brine (100 ml), dried over sodium sulphate and concentrated. After purification by column chromatography (SiO_2, heptane/ethyl acetate/triethylamine: 70/30/2) product **4** was obtained as a white solid (200.3 mg, 0.8 mmol, 70%).

Methyl 2-((diphenylmethylene)amino)acetate (5)

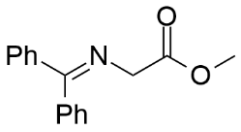

Benzophenone (46.1 g, 252.4 mmol), glycine methyl ester hydrochloride (15.9 g, 126.0 mmol), p-toluenesulfonic acid (2.5 g, 12.9 mmol) and toluene (70 ml) were added to a Dean-Stark setup and heated at reflux. N,N-diisopropyl-N-ethylamine (43.3 ml, 248.6 mmol) was added slowly and the mixture was refluxed for 2 hours. After cooling to room temperature the reaction mixture was diluted with water (100 ml) and toluene (40 ml). The layers were separated and the aqueous phase was extracted with 50 ml toluene. After drying and concentrating the organic layer the crude was purified using column chromatography (SiO_2, pentane/ethyl acetate/triethylamine: 85/15/1). Product **5** was obtained as a white

solid (14.7 g, 58.0 mmol, 46%). ^{1}H NMR (400 MHz, $CDCl_3$) δ 7.68 (d, *J* = 7.4 Hz, 2H), 7.50 – 7.39 (m, 4H), 7.36 (d, *J* = 7.7 Hz, 1H), 7.34 (d, *J* = 7.2 Hz, 1H), 7.21 – 7.17 (m, 2H), 4.24 (s, 2H), 3.75 (s, 3H). ^{13}C NMR (101 MHz, $CDCl_3$) δ 172.0, 171.1, 139.3, 136.0, 130.6, 128.9, 128.8, 128.8, 128.1, 127.7, 55.6, 52.1. HRMS calcd for $C_{16}H_{16}NO_2$ $[M+H]^+$ 254.118, found 254.117. m.p.: 41-42°C.

Note: Product **5** can also be obtained from Activate Scientific with a purity of >95%. Extensive purification was required in the synthesis of product **5**, therefore the commercially available material was used without further purification.

***tert*-Butyl 2-((diphenylmethylene)amino)acetate (6)**

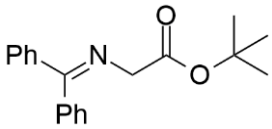

Prepared following literature procedures.[46] To a solution of *tert*-butyl 2-bromoacetate (7.1 g, 36.4 mmol) and benzophenonimine (6.5 g, 35.8 mmol) in acetonitrile (40 ml) was added diisopropylethylamine (6.3 ml, 4.7 g, 36.2 mmol). The mixture was heated under reflux for 12 hours. After cooling to room temperature, the mixture was concentrated and water (40 ml) and diethyl ether (80 ml) was added to the residue. The layers were separated and the aqueous phase was extracted with diethyl ether (80 ml). The combined organic layers were dried over magnesium sulphate and concentrated until the mixture became turbid. After cooling the mixture at 4°C overnight the mixture was filtrated yielding product **6** as a white solid (7.3 g, 24.7 mmol, 70%). ^{1}H NMR (400 MHz, $CDCl_3$) δ 7.69 (d, *J* = 7.5 Hz, 2H), 7.49 – 7.45 (m, 3H), 7.42 (t, *J* = 7.2 Hz, 1H), 7.35 (t, *J* = 7.5 Hz, 2H), 7.22 – 7.17 (m, 2H), 4.15 (s, 2H), 1.46 (s, 9H). ^{13}C NMR (101 MHz, $CDCl_3$) δ 171.6, 169.9, 139.4, 136.2, 130.5, 128.9, 128.7, 128.1, 127.8, 81.2, 56.4, 28.2. HRMS calcd for $C_{19}H_{22}NO_2$ $[M+H]^+$ 296.165, found 296.165. m.p.: 110-113°C.

Methyl 3-([2,2'-bipyridin]-5-yl)-2-((diphenylmethylene)amino)propanoate (7)

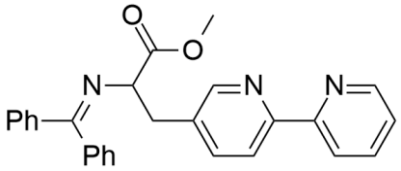

Enantioselective method for (*S*)-7:

Procedure adapted from literature.[32] To a solution of compound **4** (2.0 g, 8.1 mmol), glycine methyl ester **5** (1.8 g, 6.9 mmol) and (8S,9R)-(-)-N-benzylcinchonidinium chloride (143.4 mg, 0.3 mmol) in cold dichloromethane (60 ml, cooled to 4°C for 24 hours) was added a cold aqueous solution of sodium hydroxide (50 wt%, 4.5 ml, cooled to 4°C for 24 hours). The mixture was stirred for 24 hours at 4°C. The aqueous phase was extracted with dichloromethane (3 x 20 ml). After drying the combined organic phases over sodium sulphate and evaporation of the solvent, the product was purified using column chromatography (SiO_2, pentane/ethyl acetate/triethylamine: 70/30/2). Product **7** was obtained as a yellow solid (1.2 g, 2.8 mmol, 40%, 96% e.e. of L-enantiomer). ^{1}H NMR (400 MHz, $CDCl_3$) δ 8.68 – 8.63 (m, 1H), 8.38 (d, *J* = 1.7 Hz, 1H), 8.34 (d, *J* = 8.0 Hz, 1H), 8.23 (d, *J* = 8.1 Hz, 1H), 7.79 (td, *J* = 7.8, 1.8 Hz, 1H), 7.59 (dd, *J* = 8.3, 1.2 Hz, 2H), 7.51 (dd, *J* = 8.1, 2.2 Hz, 1H), 7.41 – 7.27 (m, 7H), 6.72 (d, *J* = 6.0 Hz, 2H), 4.33 (dd, *J* = 8.9, 4.4 Hz, 1H), 3.75 (s, 3H), 3.35 – 3.22 (m, 2H). ^{13}C NMR (101 MHz, $CDCl_3$) δ 171.9, 171.6, 156.1, 154.4, 150.4, 149.2, 139.1, 138.3, 136.9, 135.9, 133.8, 130.6, 128.9, 128.7, 128.5, 128.2, 127.5, 123.6, 121.0, 120.6, 66.6, 52.4, 36.8. HRMS calcd for $C_{27}H_{24}N_3O_2$ $[M+H]^+$ 422.186, found 422.186. m.p.: 117-119°C.

E.e.'s were determined by HPLC analysis on a Shimadzu 10AD-VP system (Chiracel OD-H, heptane/iPrOH 97:3, 1 ml/min). Retention times: 14.4 (L) and 21.5 (D) mins.

Method for racemic 7:

Procedure adapted from literature.[45] LDA (0.4 ml, 0.4 mmol, 1.3 eq) was added to a solution of product **5** (87.4 mg, 0.4 mmol) in dry THF (1.2 ml) at -78°C under inert atmosphere. The reaction mixture was stirred for 45 minutes at -78°C and a solution of compound **4** (100.0 mg, 0.4 mmol, 1.3 eq) in dry THF (1 ml) was

added. The reaction mixture was allowed to warm to room temperature and stirred overnight. Saturated aqueous ammonium chloride (2 ml) was added and the layers were separated. The aqueous layer was extracted with ethyl acetate (3 x 2 ml) and the combined organic layers were dried over sodium sulphate and concentrated. The material was coated on silica before purifying by column chromatography (SiO_2, pentane/ethyl acetate/triethylamine: 80/20/2). Racemic product **7** was obtained as a yellow solid (133.8 mg, 0.3 mmol, 90%).

Alkylation of Gly-Ni-PBP complex with bipyridine 3 (8)

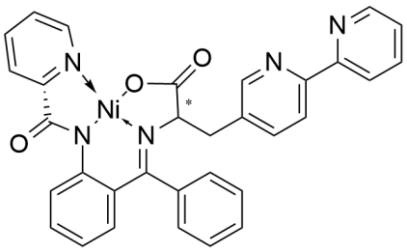

Procedure adapted from literature.[39] Gly-Ni-PBP complex (216.0 mg, 0.5 mmol), (*S*)-NOBIN (15.1 mg, 51.0 µmol) and sodium hydroxide (210.2 mg, 5.2 mmol) were added to dry dichloromethane (3 ml) under inert atmosphere. After stirring the mixture at 20°C for 30 minutes, product **4** (150.1 mg, 0.6 mmol) in dichloromethane (1 ml) was added. After stirring the mixture at 20°C for 24 hours, the reaction was quenched by adding aqueous acetic acid (10%, 1.5 ml) and diluted with dichloromethane (30 ml). The aqueous layer was extracted with dichloromethane (3 x 60 ml). The combined organic layers were washed with brine (60 ml), dried over sodium sulphate and concentrated. After recrystallization from dichloromethane/acetone (3/1) product **8** was obtained as red crystals. Product **8** could be further purified by recrystallization from dichloromethane/heptane (131.2 mg, 0.2 mmol, 44%). ^{1}H NMR (400 MHz, $CDCl_3$) δ 8.70 – 8.63 (m, 2H), 8.51 (d, *J* = 4.4 Hz, 1H), 8.15 (dd, *J* = 16.0, 8.0 Hz, 2H), 7.76 (d, *J* = 8.0 Hz, 1H), 7.69 (t, *J* = 7.6 Hz, 1H), 7.55 (dd, *J* = 9.0, 4.0 Hz, 4H), 7.31 – 7.24 (m, 3H), 7.23 – 7.18 (m, 2H), 7.15 (d, *J* = 6.0 Hz, 1H), 7.04 (t, *J* = 6.2 Hz, 1H), 6.77 – 6.70 (m, 2H), 4.38 – 4.32 (m, 1H), 3.09 (dd, *J* = 13.5, 2.1 Hz, 1H), 2.89 (dd, *J* = 13.5, 5.6 Hz, 1H). ^{13}C NMR (101 MHz, $CDCl_3$) δ 177.6, 171.8, 169.2, 155.4, 155.1, 152.6, 151.1, 148.8, 146.4, 143.4, 139.4, 139.3, 136.6, 134.5, 133.6, 131.9, 130.3, 129.5, 129.3, 127.7, 127.5, 127.2, 126.5, 123.9, 123.7, 123.6, 121.5, 121.1, 120.3, 72.5, 37.2 with one carbon missing. HRMS calcd for $C_{32}H_{24}N_5NiO_3$ $[M+H]^+$ 584.123, found 584.122. m.p.: decomposes >265°C**.**

2-([2,2'-bipyridin]-5-yl)-1-carboxyethanaminium chloride (9)

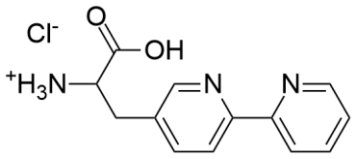

Method A:

Procedure adapted from literature.[32] A suspension of enantiopure product (*S*)-**7** (1.0 g, 2.4 mmol) in diethyl ether (30 ml) was cooled to 0°C. 1M HCl (5.0 ml, 5.0 mmol) was added dropwise and the mixture was stirred at room temperature for 18 hours. After separation of the phases the aqueous phase was extracted with diethyl ether (2 x 30 ml) and dichloromethane (2 x 30 ml). After lyophilization of the aqueous phase product **9** was obtained as a white solid (630.5 mg, 2.3 mmol, 95%, 96% e.e. of L-enantiomer). ^{1}H NMR (400 MHz, CD_3OD) δ 8.90 (d, *J* = 6.3 Hz, 2H), 8.75 (d, *J* = 8.2 Hz, 1H), 8.63 (td, *J* = 8.0, 1.5 Hz, 1H), 8.55 (d, *J* = 8.3 Hz, 1H), 8.29 (dd, *J* = 8.3, 2.1 Hz, 1H), 8.07 – 8.02 (m, 1H), 4.48 (t, *J* = 6.8 Hz, 1H), 3.78 (s, 1H), 3.49 (dq, *J* = 14.6, 6.9 Hz, 2H). ^{13}C NMR (50 MHz, CD_3OD) δ 170.5, 150.3, 148.9, 147.3, 146.6, 145.5, 143.3, 136.6, 128.4, 125.2, 124.4, 54.3, 34.1. HRMS calcd for $C_{13}H_{14}N_3O_2$ (**9** -HCl) $[M+H]^+$ 244.108, found 244.107. m.p.: decomposes >165°C.

E.e.'s were determined by HPLC analysis on a Shimadzu 20AD system (Daicel Crownpak CR(+), 30 mM perchloric acid pH 1.5, 0.5 ml/min). Retention times: 8.1 (D) and 9.7 (L) mins.

Method B:

Procedure adapted from literature.[39] A suspension of complex **8** (90.6 mg, 0.2 mmol) in 6M HCl (1.0 ml, 6.0 mmol) and methanol (1.5 ml) was refluxed for 30 minutes, during which the red color of the complex

disappeared. The solvent was evaporated and water (2 ml) was added to the residue. After filtering and washing the solid with water, the pH of the aqueous layer was adjusted to 8 with aqueous NH_3 (25 wt%). After extraction of the aqueous layer with chloroform (3 x 5 ml), the aqueous layer was evaporated to dryness to obtain the product as a white solid (41.3 g, 0.2 mmol, 95%, 19% e.e. of D-enantiomer).

2-((((9H-fluoren-9-yl)methoxy)carbonyl)amino)-3-([2,2'-bipyridin]-5-yl)propanoic acid (10)

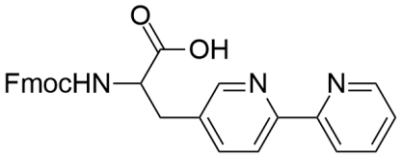

Procedure adapted from literature.[32,45] After precooling a solution of product L-**9** (500.3 mg, 1.8 mmol) in aqueous $NaHCO_3$ (10%, 10 ml) in an ice bath for 30 minutes, a solution of N-(9-fluorenylmethoxycarbonyloxy)succinimide (720.1 mg, 2.1 mmol) in 1,4-dioxane (10 ml) was added dropwise. The mixture was allowed to warm to room temperature and stirred for 36 hours. The mixture was diluted with water (60 ml) and extracted with diethyl ether (3 x 40 ml). The aqueous phase was cooled in an ice bath and the pH was adjusted to 2 with concentrated HCl. The suspension was centrifuged at 4000 rpm for 15 min. The solution was decanted and the solid material was washed with water (2 x 20 ml), centrifuged (2 x 15 min) and decanted. The solid was dissolved in methanol and concentrated. 1H-NMR showed product formation, although it contained significant amounts of unidentified impurities. ^{1}H NMR (400 MHz, DMSO-d6) δ 8.68 (s, 1H), 8.60 (s, 1H), 8.36 (d, *J* = 7.4 Hz, 1H), 8.31 (d, *J* = 7.6 Hz, 1H), 7.94 (t, *J* = 7.4 Hz, 1H), 7.88 – 7.81 (m, 4H), 7.68 (d, *J* = 7.4 Hz, 1H), 7.65 – 7.57 (m, 2H), 7.48 – 7.22 (m, 4H), 4.32 – 4.12 (m, 4H), 3.23 – 3.15 (m, 1H), 3.02 – 2.91 (m, 1H).

(1S,4S,5R)-1-(anthracen-9-ylmethyl)-2-((R)-hydroxy(quinolin-4-yl)methyl)-5-vinylquinuclidin-1-ium chloride (11)

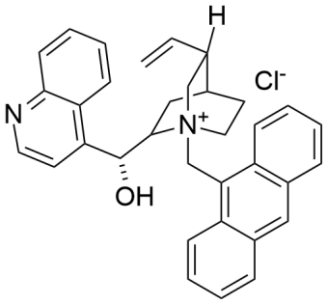

Prepared following literature procedures.[40] To a suspension of cinchonidine (1.0 g, 3.4 mmol) in toluene (10 ml) was added 9-(chloromethyl)anthracene (805.0 mg, 3.6 mmol). The reaction mixture was stirred at reflux for 2 hours and then cooled to room temperature. The mixture was poured onto 50 ml of diethyl ether. The solid material was filtered and washed with cold diethyl ether. Product **11** was obtained as a light yellow solid (1.7 g, 3.3 mmol, 96%). ^{1}H NMR (400 MHz, $CDCl_3$) δ 9.00 (d, *J* = 8.4 Hz, 1H), 8.89 – 8.80 (m, 2H), 8.73 (d, *J* = 8.9 Hz, 1H), 8.19 (d, *J* = 3.9 Hz, 1H), 8.07 (d, *J* = 4.0 Hz, 1H), 8.01 (s, 1H), 7.74 (d, *J* = 8.3 Hz, 1H), 7.65 (d, *J* = 8.0 Hz, 1H), 7.60 (d, *J* = 8.3 Hz, 1H), 7.44 – 7.36 (m, 1H), 7.31 – 7.18 (m, 4H), 7.11 (t, *J* = 7.4 Hz, 1H), 7.08 – 7.02 (m, 1H), 6.73 (dd, *J* = 42.2, 13.5 Hz, 2H), 5.49 – 5.35 (m, 1H), 5.22 (d, *J* = 17.3 Hz, 1H), 4.90 (d, *J* = 10.5 Hz, 1H), 4.78 – 4.64 (m, 2H), 4.00 (d, *J* = 12.5 Hz, 1H), 2.59 (t, *J* = 11.6 Hz, 1H), 2.44 (t, *J* = 11.2 Hz, 1H), 2.13 (bs, 1H), 1.83 (dd, *J* = 25.6, 14.1 Hz, 2H), 1.70 (s, 1H), 1.14 (dd, *J* = 18.1, 10.7 Hz, 1H), 1.07 – 0.95 (m, 1H). ^{13}C NMR (101 MHz, $CDCl_3$) δ 149.4, 147.0, 145.8, 136.4, 133.2, 132.7, 131.1, 130.3, 130.1, 129.1, 128.6, 128.4, 128.2, 127.6, 127.4, 126.8, 126.4, 125.5, 124.8, 124.7, 124.2, 120.1, 118.2, 117.7, 67.4, 66.7, 61.3, 54.7, 50.3, 38.5, 25.9, 25.7, 23.5. HRMS calcd for $C_{34}H_{33}N_2O$ (**11** -Cl^-) $[M]^+$ 485.259, found 485.243. m.p.: decomposes >160°C.

(1S,4S,5R)-2-((R)-(allyloxy)(quinolin-4-yl)methyl)-1-(anthracen-9-ylmethyl)-5-vinylquinuclidin-1-ium bromide (12)

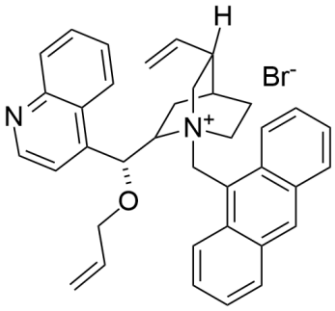

Prepared following literature procedures.[40] Allyl bromide (0.5 ml, 5.9 mmol) and aqueous KOH (50 wt%, 1.0 ml, 9.5 mmol) were added to a suspension of product **11** (1.0 g, 1.9 mmol) in dichloromethane (10 ml). The mixture was stirred at 25°C for 4 hours. The mixture was diluted with water (10 ml) and extracted with dichloromethane (3 x 10 ml). The combined organics layers were dried over sodium sulphate and concentrated. The solid material was dissolved in methanol, after which diethyl ether was added until the solution turned cloudy. After storing the mixture at -18°C and filtration of the crystallized material product **12** was obtained as a light orange solid (1.0 g, 1.6 mmol, 85%). ^{1}H NMR (400 MHz, CD_3OD) δ 9.04 (d, *J* = 4.5 Hz, 1H), 8.90 (s, 1H), 8.75 (d, *J* = 9.0 Hz, 1H), 8.57 (d, *J* = 7.2 Hz, 1H), 8.46 (d, *J* = 9.1 Hz, 1H), 8.30 – 8.20 (m, 3H), 8.00 – 7.90 (m, 3H), 7.84 – 7.74 (m, 2H), 7.69 – 7.61 (m, 2H), 6.96 (s, 1H), 6.48 – 6.34 (m, 2H), 5.89 (d, *J* = 13.9 Hz, 1H), 5.75 – 5.64 (m, 2H), 5.56 (d, *J* = 10.6 Hz, 1H), 5.01 (d, *J* = 11.2 Hz, 1H), 4.97 (d, *J* = 4.4 Hz, 1H), 4.59 – 4.39 (m, 4H), 3.82 – 3.74 (m, 1H), 3.24 (t, *J* = 11.5 Hz, 1H), 2.96 – 2.85 (m, 1H), 2.52 – 2.39 (m, 2H), 2.24 – 2.12 (m, 1H), 1.97 (d, *J* = 2.4 Hz, 1H), 1.68 – 1.54 (m, 2H). ^{13}C NMR (50 MHz, CD_3OD) δ 151.0, 149.3, 143.0, 138.5, 134.8, 134.7, 134.7, 134.6, 133.9, 133.1, 133.0, 131.5, 131.3, 131.1, 130.6, 129.5, 129.4, 129.2, 127.1, 126.7, 126.6, 125.5, 125.0, 124.6, 121.7, 119.0, 118.9, 117.8, 71.4, 70.0, 63.5, 57.4, 53.6, 39.5, 27.3, 26.3, 23.4. HRMS calcd for $C_{37}H_{37}N_2O$ (**11** -Br^-) $[M+H]^+$ 525.290, found 525.289. m.p.: 167-171°C.

2-bromo-N-(1,10-phenanthrolin-5-yl)acetamide (13)

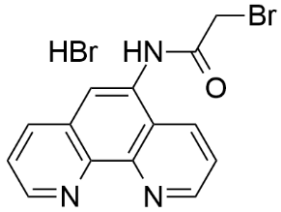

Prepared following literature procedures.[20] To a solution of 1,10-phenanthrolin-5-amine (195.0 mg, 1.0 mmol) in anhydrous chloroform (30 ml) under inert atmosphere was added 2-bromoacetyl bromide (0.1 ml, 1.2 mmol). The mixture turned red and was heated at reflux overnight. After cooling to room temperature the suspension was filtered and the solid was washed with cold chloroform. After recrystallization of the solid from methanol (50 ml) product **13** was obtained as a yellow solid (316.0 mg, 0.8 mmol, 80%). ^{1}H NMR (400 MHz, DMSO-d6) δ 10.94 (s, 1H), 9.33 (dd, *J* = 4.5, 1.0 Hz, 1H), 9.22 (dd, *J* = 5.0, 1.2 Hz, 1H), 9.16 (d, *J* = 8.3 Hz, 1H), 9.09 (d, *J* = 8.5 Hz, 1H), 8.57 (s, 1H), 8.32 (s, 1H), 8.26 – 8.19 (m, 2H), 4.38 (s, 2H). ^{13}C NMR (50 MHz, DMSO-d6) δ 172.4, 149.0, 145.4, 143.1, 138.2, 136.3, 135.0, 133.3, 129.5, 125.8, 125.7, 125.4, 119.2, 62.0. HRMS calcd for $C_{14}H_{11}BrN_3O$ (**13** -HBr) $[M+H]^+$ 316.008, found 316.008. m.p.: decomposes >260°C.

3. Computational studies

3.1. Introduction

3.1.1. Aims and challenges

The use of computational studies for the structure prediction of proteins or peptides gained popularity and due to this increase in use more systems are algorithms are being developed or refined.[48–50] This increase in use can be attributed due to several reasons. Computational tools can provide large numbers of possible structures of peptides or proteins. Using these predicted structures a preselection of possibly suitable biomolecular scaffolds can be made. The ability to make such a selection using simulations saves material, for the synthesis or expression of biomolecules, and the time which preparation of all biomolecules would cost. Thus it is an excellent tool for the first selection of a number of molecules from an extensive library.

The ability to predict structures could also be used more in detail for the design of the structure of one specific biomolecule. After selection of one molecule computational studies can be used to design or tune a second coordination sphere or to predict the structures of closely related mutants. This way of rational design could provide optimal catalytic properties while reducing the invested time and money preparing the catalyst.

In the last years computational studies have been used for various topics, examples are the docking of molecules (e.g. drugs), the design of an active site or rationalization of reaction pathways.[51–54] Maréchal and co-workers recently reported the use of docking programmes in a study on the metabolism of quinidine by P450s.[51] Using docking programmes possible binding sites and conformations of quinidine, an inhibitor for this P450 mutant, were identified. This was done by optimizing the interactions of quinidine with the heme group and residues close to the binding sites. After identifying the binding residues in the P450 mutant and the most probable conformations of quinidine, computational studies were used to convert this P450 mutant so quinidine could be accepted as a substrate instead of as an inhibitor. The conformations that were probably needed to convert quinidine were identified, however no results of the actual reaction were presented.

A similar approach was followed by Baker and co-workers to catalyze Kemp eliminations.[53] Enzymes were designed for a number of reactions, however only low activities were obtained. Rational mutational analysis gave small improvements of activities. The use of docking programmes to enhance catalytic properties led to a significant improvement of two magnitudes of order. Residues in the active site were modified to provide optimal stabilization for the transition state, resulting in a predicted k_{cat}/k_{uncat} of 1.6×10^4. After computational studies and subsequent directed evolution a k_{cat}/k_{uncat} of 1.18×10^6 was obtained. The large improvement demonstrates the power of computational studies.

Another study involving design of an active site using molecular docking was presented by Ward and co-workers.[19] In this study molecular docking was used to position a crucial histidine residue in order to optimize e.e.'s obtained in an asymmetric transfer hydrogenation. In addition to increasing enantioselectivities, the opposite enantiomer could be obtained after positioning the histidine on a different residue. Molecular docking provided the insight needed for this repositioning. The (*S*)-enantiomer was obtained with an e.e. of 96%, whereas the (*R*)-enantiomer was obtained with an e.e. of 79%. In a recent study of Ward and Maréchal a combination of protein-ligand docking and quantum/molecular mechanical calculations are used to investigate the reaction pathways to synthesize both enantiomers.[54] Using these computational methods conformational differences between the transition states, leading to either of the enantiomers, are analyzed and as such the enantioselectivity of

this reaction is rationalized. Where an enantiomeric excess of 80% for the (*S*) enantiomer was predicted, 96% was obtained in a real experiment.
Although the field is very young, it is shown that computational studies are powerful tools. In addition to longer known aspects as aiding catalyst design and predicting kinetic parameters, recent advances show these studies can aid in the rationalization of reaction mechanisms and in the origin of enantioselectivity. Several studies have been published on simulations involving transition metal compounds, however are not yet used to predict actual catalytic properties.
A study by Baker and co-workers focused on the binding of various metal ions by 2,2'-bipyridine in a proteins.[55] Docking simulations are performed to enhance the binding affinity of cobalt(II), zinc(II) and nickel(II) for the active site of a protein containing 2,2'-bipyridine. Additional groups which could stabilize the metal ions were added, resulting in an increase in binding affinity. However, this designed metalloprotein was not applied in catalysis.
A similar study was recently published by Maréchal and co-workers, in which they studied the interaction between proteins and organometallic compounds using computational methods.[56] It was stated that, while methods for the docking of ligands in proteins are readily available and well studied, the docking of organometallics compounds in protein-ligand complexes is far less studied. Therefore, the docking of organometallic ligands in proteins is studied using four different methods in order to establish a benchmark and points of improvement. A number of organometallic ligands, containing ruthenium, iron or osmium, is used for calculations and the resulting conformations are then compared to reported X-ray structures. Whereas this study gave some insight in the reliability of various methods, all complexes were inert and the first coordination sphere did not change upon binding. This is a limitation common to available methods, as the correct modelling of geometries available to all methods is difficult. This is partly due to the large number of geometries available to transition metals. Although this drawback limits the use of these methods for organometallic compounds at the moment, it is expected that reliable methods will come available to this important field.
However, when using computational methods one should always keep in mind that these programmes or algorithms give an indication of the structure. The most reliable predictions can be obtained by calculating all the acting forces on the molecule, including nonbonding and through-space interactions. If more interactions taken into account, more calculations have to be done and the time required to produce one prediction increases.
Two requirements for the computational tool can be established.
The system should have the ability to incorporate non-natural amino acids, namely the bipyridine and phenanthroline containing amino acids, in the prediction.
In addition the inclusion of copper(II) ions in the simulations should be possible. The latter requirement is difficult since very few systems are capable of handling metal ions, due to the large number of possible geometries that can be obtained with metal ions.
Since there was no previous experience with simulation systems, three systems were selected for the computational studies.

3.1.2. Selection of the peptide

Whereas a peptide can be designed *de novo*, a large number of peptides and related structures is already known. Although one has total freedom when designing a peptide *de novo*, determining the exact structure of the peptide can be difficult. The use of an exisiting peptide can simplify rational design if the structure of the peptide is known. The analysis of predicted structures of mutants could be more reliable when using the known peptide structure as a reference, especially when structure of the native peptide is predicted as well.

In earlier work the peptide bovine pancreatic protease, bPP, has been used in catalysis.[26] bPP was characterized by Li and co-workers using solution NMR.[57] Since a structure is known the evaluation of a predicted structure could be made more reliable. bPP is a peptide consisting of 36 amino acids and three structure domains (Figure 8).

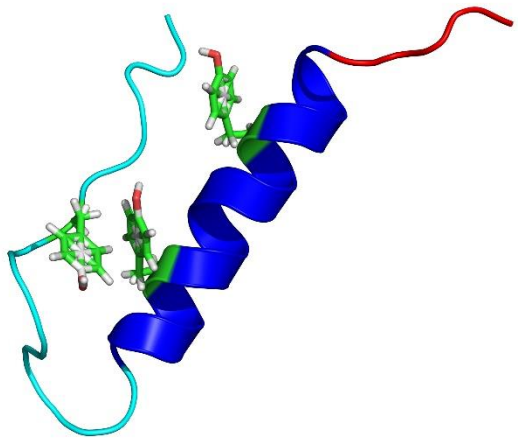

Figure 8: Solution NMR structure of bPP from the PDB database (1BBA).[ref] The polyproline loop is highlighted in light blue, the α-helix in dark blue and the disordered tail in red. Three tyrosines are present in bPP, one in the polyproline loop and two in the α-helix.

bPP consist of a polyproline loop, which is folded onto an α-helix. On the opposite side of the α-helix is a tail, consisting of several residues, which is disordered according to NMR. The α-helix provides rigidity to the structure, which makes rational design easier. The polyproline loop folds back onto the α-helix, providing a hydrophobic pocket and shielding. The hydrophobic pocket interface make bPP more tolerant towards the incorporation of big hydrophobic ligands, since the ligands are less exposed to the aqueous environment. The shielding could be used to induce stereoselectivity. Three tyrosine residues are present, two in the α-helix and one in the polyproline loop. Since a large aromatic moiety will be introduced in the peptide, mutating an existing aromatic group was expected to reduce the change of the structure. Since these tyrosine residues were the largest aromatic moieties present, these sites were selected for mutation.
Since a NMR structure of bPP in solution is known and the peptide has successfully been employed in catalysis, bPP was selected as biomolecular scaffold.

3.2. I-TASSER

The first method used in the computational studies is the I-TASSER structure prediction server. The I-TASSER server is an online tool developed by Zhang and co-workers for the prediction of protein or peptide structures.[58,59] Users can submit a protein or peptide sequence and after the required time, varying from hours to several days, the five most likely structures are predicted by the server. The system divides the submitted amino acid sequence in a number of fragments, which can overlap eachother. Subsequently these fragments are compared to known sequences from the PDB library and ranked according to similarity. In the second step, the structures belonging to the known matching sequences are reassembled into a structure. During reassembly lowest free-energy states of the possible combinations of structures are calculated. After building the most likely structures with the lowest free-energy states, a check is performed in order to avoid steric clashes.

The reliance on the extensive PDB database and the occurrence of relationships between amino acid motifs and structures could provide a reliable simulation. Non-natural amino acids cannot be used in the I-TASSER server, as such the synthesized ligand can't be included in any structure prediction. Tryptophan was used as substitute, since it possesses an aromatic indole group. Whereas the similarity is limited, the ease of use and calculation speed of the I-TASSER server make it an attractive option.
Although the structure of bPP is incorporated in the PDB database, a prediction of the structure of bPP was made for verification of the algorithm. As expected, a perfect similarity was obtained with bPP in the PDB database and the resulting prediction was excellent (Figure 9).

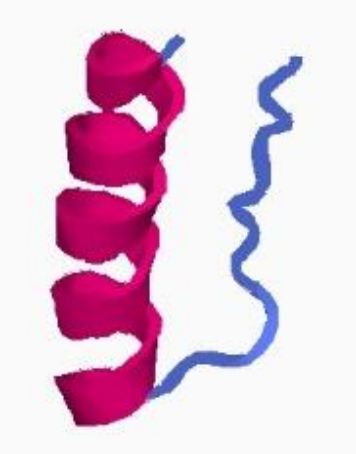

Figure 9: I-TASSER prediction of native bPP. A perfect match with the NMR structure was obtained, which was expected since the structure of bPP is included in the PDB database.

All three tyrosines present in bPP were mutated to tryptophan and submitted to the I-TASSER server. After simulation three similar structures were obtained (Figure 10).

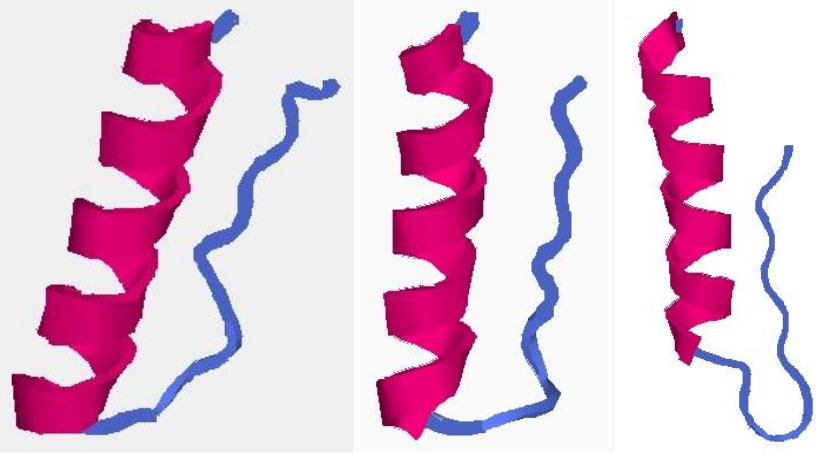

Figure 10: Structures of three bPP mutants as predicted by the I-TASSER server. Left) mutation of Tyr7 in the polyproline loop. Middle) mutation of Tyr20 in the α-helix, after the fold. Right) mutation of Tyr27 at the end of the α-helix.

Whereas the predicted structures of the mutations at position 20 and 27 were expected to be highly similar, since both residues are located in the α-helix, the mutation at position 7 was expected to give a distortion. Residue 7 is located in the more flexible polyproline loop and is expected to have a bigger effect on the structure. The reason for this high similarity of all structures to eachother and native bPP might be the prediction method. I-TASSER bases predictions solely on statistics, the similarity of fragments to known sequences. If the number of mutated residues is low, a high similarity will still be

obtained. The nature of the residues and mutations is ignored by I-TASSER programme. Therefore no structural change is observed even when changing the complete nature (hydrophilic, hydrophobic or charged) of the amino acid. Since bPP consists of 36 amino acids a mutation of one amino acid will have a minimal effect on the statistical similarity.
Since the I-TASSER does not take into account interactions, is solely based on statistics, and non-natural amino acids could not be incorporated this method was deemed not suitable for this project.

3.3. CORINA

All structures predictions with CORINA were performed by Milon Mondal in the group of Dr. Anna Hirsch. CORINA is a software suite capable of converting small to medium sized molecules from 2D structures into 3D structures.[60,61] CORINA accepts the 2D structures in a range of formats, meaning that a ChemDraw file can be converted into a 3D structure. As such, the incorporation of non-natural amino acids or other residues is possible.
The energies of all possible torsion angles of a bond are taken from a database. The lowest possible total energy is calculated by combining the energies of all torsion angles of all bonds. This lowest possible total energy corresponds to the most probable conformation of the molecule, which is the 3D structure. A bulky aromatic ligand will cause some torsion angles to be impossible or have very high energy due to hinderance and ring strain. As such, the structure should be affected by the presence of such a moiety. Since CORINA was designed for small to medium sized molecules, initially two smaller helical peptides were used.
The first peptide to be used was Tachykinin Peptide Eledoisin (PDB code: 1MXQ), which is a short helical peptide consisting of 11 amino acids.[62] A solution NMR structure is known, which makes evaluation of the predicted structure easier and more reliable. A bipyridine moiety was included on position 6, mutated from a phenylalanine. Generation of the 3D structure by CORINA did not yield a helical peptide, like the known structure, but a nearly linear peptide chain (Figure 11).

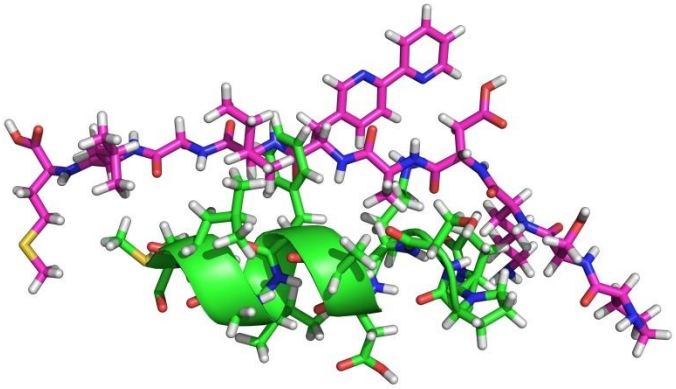

Figure 11: Solution NMR structure of the peptide (PDB: 1MXQ) in green and the 3D structure of the peptide with the bipyridine moiety in purple.

It was thought that the introduction of a large aromatic moiety would lead to aggregation of the peptide chain in order to encapsulate the large hydrophobic residue. This could be a reason why the short helical peptide, lacking the great number of interactions in bPP, would unfold. However, this would lead to a ball-like structure instead of a linear chain. It was realized that the linearity could be explained by the fact that CORINA does not take any nonbonding interactions into account. These interactions are the reason peptides and proteins form secondary, tertiary and quaternary structures. Ignoring these interactions would mean that there is no driving force for the formation of helices. To further strengthen

this theory, two more structures were generated. In both structures a bipyridine moiety was included on position 6 or 7 (Figure 12).

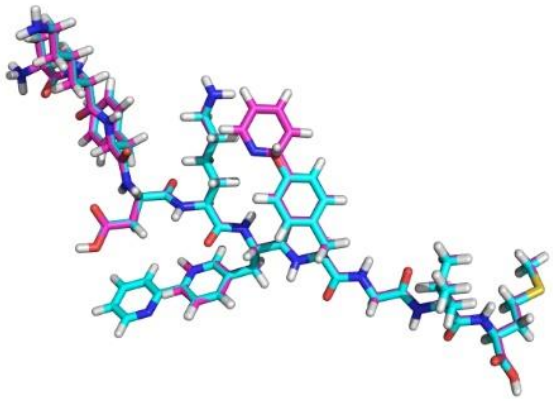

Figure 12: 3D structures of the peptides with a bipyridine moiety on position 6 (blue) or 7 (purple). As with previous calculations, structures were linear.

When overlapping the structures of the peptides, both using the same sequence as Tachykinin Peptide Eledoisin with a single mutation, very similar conformations are obtained. Although the bipyridine rings are located on different positions, exact overlays are obtained. Both bipyridine moieties are stretched and located on the outside of the peptide. Since the aromatic rings provide the least steric hinderance, thus the lowest energy, if they are oriented away from the peptide linear structures are obtained. In these linear structures, all atoms are located away from each other as far as possible minimizing the energy.
Although CORINA gave the possibility to include non-natural amino acids, the algorithm of CORINA was not suitable for this project. Since only torsion angles are taken into account and very important nonbonding interactions were ignored, the generated 3D structures were not accurate.

3.4. GROMOS forcefield

All structure predictions with the GROMOS forcefield were performed by Dr. Alex de Vries and Tjalle Matthijssen in the Molecular Dynamics group of Prof. Dr. Marrink. Structures generated with CORINA showed that nonbonding interactions were essential for a good prediction of the secondary and tertiary structure of peptides. More advanced simulation would be required, this was done in the form of Molecular Dynamics (MD) simulations. In Molecular Dynamics the structure of a molecule is built while taking both bonded and nonbonded interactions into account. A reliable structure can be obtained, since all important interactions are calculated. Other molecules, such as water, can be added. As such, the incorporation of nonnatural amino acids is possible. The specific software package used in this project was GROMACS in combination with the GROMOS forcefield.[63] In a forcefield the relative strength of all interactions, bonded and nonbonded, are described. Per forcefield these values are different and therefore the output of forcefields might differ. The bonded interactions are applied on the backbone on the biomolecule, in this case the peptide backbone. By removing the backbone from the peptide only the side chains of the amino acids are preserved, leaving a number of small molecules. In a forcefield the partition coefficient (between octanol and water) of a large number of small molecules is described. The small molecules from the amino acid side chains are either described in the forcefield or can be related to a similar described molecule. As such, for each small molecule (amino acid side chain) the nonbonded interactions are known. Subsequently the molecule is assembled and the energy of the conformation is calculated. Atoms are moved a little bit and again the energy of the conformation is calculated. Such a

state, the position of the atoms and the corresponding energies, is called a timeframe. By calculating a large number of timeframes and varying the positions of the atoms a bit per timeframe, a large amount of conformations and corresponding energies is obtained. The change of the structure and the total energy can be followed through time. While generating timeframes, the total energy of the conformation is reduced. When generating enough timeframes a minimum will be found and following conformations will have a higher energy. It is this conformation with the minimal energy that is the most probable structure. However, the existence of other structures with a similar energy is not excluded. In order to get a reliable predictions enough timeframes have to be obtained. Since a large amount of calculations are required per timeframe, a lot of time and computing power is required. Due to these requirements this method is less suitable for the screening of a library of mutants, since this would require a significant amount of time and computing power.
The incorporation of metal ions is difficult due to the large number of geometries a metal-complex can attain. Simple models for metal ions exist, however they are limited to ions as calcium with a low number of possible geometries. Copper(II) ions can attain a large number of geometries and no models exist at this moment.
The first simulation was performed on bPP without mutations as a benchmark (Figure 13).
To reduce the amount of timeframes required to get the structure with the lowest energy, the structure of bPP at the start of the simulation was defined manually to resemble the known NMR structure. The structure found in solution NMR was probably of low energy and since the simulations are performed in water (solution) the predictions might require less timeframes.

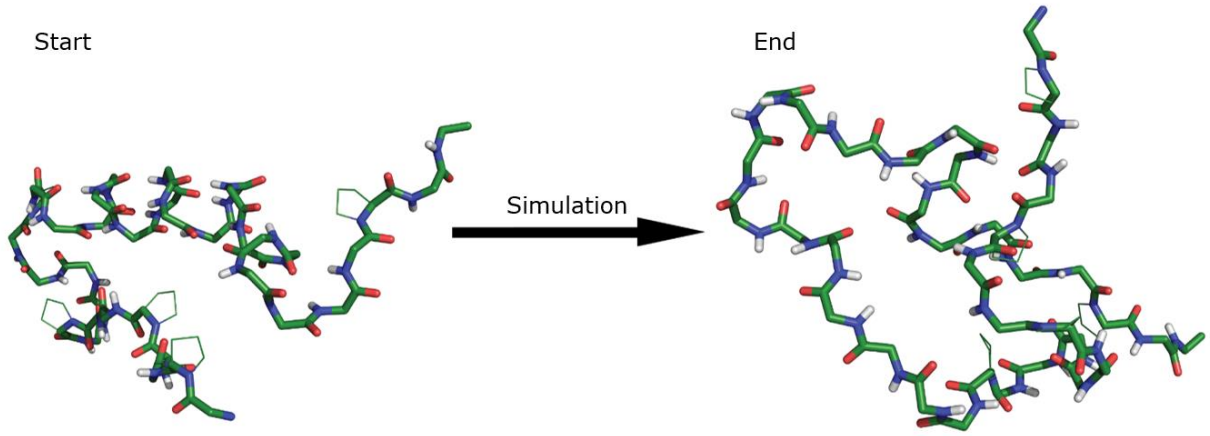

Figure 13: MD simulation of bPP using the GROMOS forcefield. The conformation of bPP at the start of the simulation was defined manually to resemble the known NMR structure.

However, after simulation the structure of bPP unfolded into a disordered folding chain. The reason of unfolding of the chain is not known. Although the simulated structure does not match the NMR structure, a simulation was performed with bipyridine incorporated into the peptide.
In this simulation the tyrosine at position 20 was mutated to the bipyridine amino acid, again the structure was defined manually to resemble the NMR structure (Figure 14).
During simulation the peptide chain seemed to unfold and refold around the bipyridine ring. At the start of the simulation the bipyridine ring is located on the outside of the peptide. The large aromatic group is exposed to the aqueous environment of the peptide, which is highly unfavourable. By folding the peptide chain around the bipyridine ring the exposure of the bipyridine ring to the aqueous environment, and thereby the total energy, is reduced. This could explain the folding in this particular simulation. Since the simulation of native bPP did not correspond to the known structure, it is not known if simulations with this forcefield are reliable.

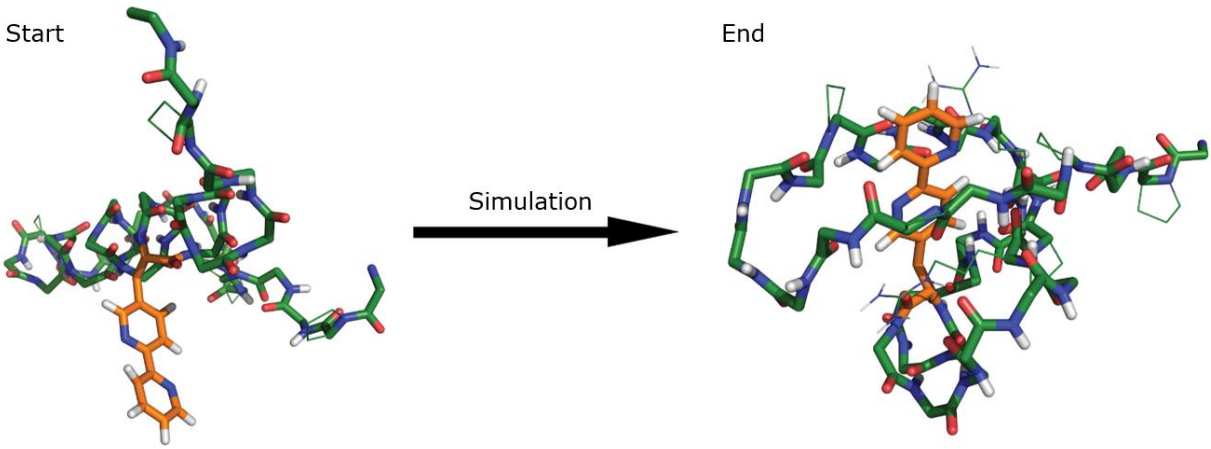

Figure 14: MD simulation of a bPP mutant using the GROMOS forcefield. The conformation of bPP at the start of the simulation was defined manually to resemble the known NMR structure.

In order to get a more matching simulation of native bPP other forcefields could be used. It was suggested that the folding of the bPP mutant might be caused by dominant hydrophobic interactions this particular version of GROMOS. Other versions, in which the hydrophobic interactions are scaled, could be used to assess the behaviour of the peptide. The determination which forcefield works the best for this kind of peptides would be empirical.
Due to the amount of time required to perform the simulations, Molecular Dynamics are not suitable for rational design. Therefore no further simulations were performed.

3.5 Summary

In these computational studies three different methods were used.
The first method, the I-TASSER server, gave good structure predictions. However, these predictions were based solely on statistics and not on interactions. Therefore mutations could be ignored. In addition, non-natural amino acids could not be used.
The second method, CORINA, was used to build 3D structures of small helical peptides. These predictions were not reliable, linear chains were obtained. This was caused by the fact that CORINA does not take nonbonded interactions into account, although these interactions are crucial in the formation of secondary, tertiary and quaternary structures of peptides.
All structures predictions with CORINA were performed by Milon Mondal in the group of Dr. Anna Hirsch.
The third method involved MD simulations, which take into account both bonded and nonbonded interactions. Using the GROMOS forcefield simulations were performed on native bPP and a bPP mutant, containing a bipyridine ring. In the simulation of the bPP mutant it was observed that the peptide chain folds around the bipyridine ring, which could be caused by the hydrophobicity of the residue. The simulation of native bPP did not resemble the reported NMR structure. Simulations of native bPP using different forcefields should show which forcefield gives the optimal results for this kind of peptides. However, since MD simulations are time consuming and do not fit the purpose of rational design, no further simulations were performed.
All structure predictions with the GROMOS forcefield were performed by Dr. Alex de Vries in the Molecular Dynamics group of Prof. Dr. Marrink.

None of the used methods met all requirements for the design of the peptide. Future studies could focus on the use of docking software. Whereas in docking the structure of the peptide is not dynamic like in

MD simulations, usually only residues in the binding pocket will be affected, docking software is more readily accessible and is less time consuming.

4. Peptides

4.1. Introduction

4.1.1 Expression versus synthesis

In addition to a metal binding ligand, the catalytic system consisted of a peptide as the biomolecular scaffold.
Peptides can be obtained either by expression or by synthesis. Whereas one has limited freedom where it comes to incorporation of non-natural amino acids using expression and one has to develop a method for expression of the peptide with non-natural residues, the synthetic approach is likely to work from the start. In addition, the expression of small peptides can prove difficult. In addition, one can in principle incorporate multiple non-natural residues during peptide synthesis.

4.1.2. Selection of the peptide

In earlier work the peptide bPP has been synthesized using standard Fmoc SPPS on a Rink amide resin as the full-length peptide (36 residues) and a truncated version (31 residues).[26] Furthermore non-natural residues were introduced in bPP by SPPS. Since bPP has been successfully synthesized with non-natural residues, bPP was selected as the biomolecular scaffold.
Synthesizing a longer peptide involves more reactions which eventually lowers the yield, for this reason the truncated version of bPP was selected as the scaffold.

4.1.3. Fmoc solid phase peptide synthesis

In solid phase peptide synthesis (SPPS) a solid bead is used as a support to grow a peptide chain on. The advantage of using a solid bead is the easy purification of the product. Excess reagents are added and can be washed away after reaction, leaving just the bead with the coupled molecules. In Fmoc SPPS, the base-labile N-(9-fluorenylmethoxycarbonyloxy)succinimide (Fmoc, Figure 15) is used as protecting group of the main chain, whereas the side chains of amino acids are protected with acid-labile protecting groups.

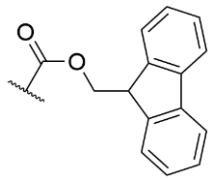

Figure 15: N-(9-fluorenylmethoxycarbonyloxy)succinimide (Fmoc) protecting group.

Because of this orthogonal protecting groups, the direction of reaction (growth of main chain or side chains) can be controlled. The solid residue is protected with a Fmoc group, which is deprotected using a base (typically piperidine or piperazine). Subsequently, a solution of protected amino acid and activator is added to the deprotected peptide containing the free Nα amine (Scheme 26). The C-terminus of the amino acid is activated and the amine can couple to the amino acid. Since the N-terminus of the amino acid is protected only one amino acid will couple to the resin. After reaction the reagents are washed away and another cycle of deprotection, activation/reaction and washing can be performed. After coupling of all amino acids the peptide can be cleaved from the support and undergo deprotection of the side chains by the addition of an acidic mixture. This mixture, typically composed of TFA with additives to

prevent side reactions, is added to the solid support. After the reaction the mixture is filtrated, the deprotected and cleaved peptide is obtained in solution.

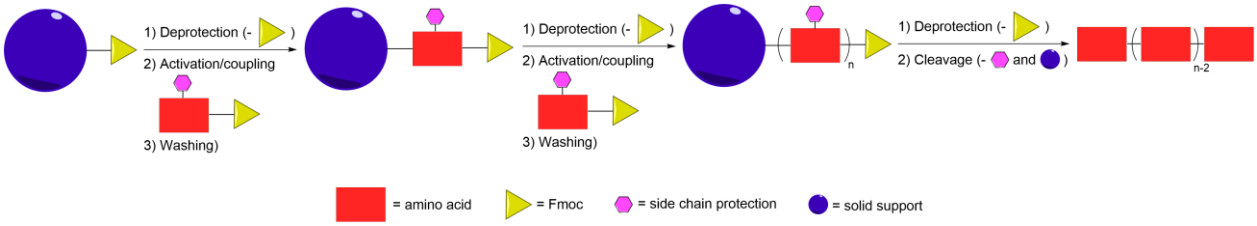

Scheme 26: Schematic representation of Fmoc SPPS. Deprotection, activation/coupling and washing cycles are repeated until the desired peptide is obtained. Subsequently the side chain protection and the solid support are cleaved, yielding the peptide.

As the peptide chain grows, reactive ends can fail to couple due to hindrance of the rest of the peptide chain. The longer the peptide chain becomes, the higher the probability to obtain unreacted ends. These unreacted ends can react with the next amino acid, causing a deletion in the chain. This phenomenon decreases the final yield of the desired peptide and it is also the reason why the maximum chain length that can be obtained with SPPS is typically around 50 amino acids. In addition the presence of peptides containing deletions significantly increases the difficulty of the purification, since peptides are obtained that are highly similar to the desired peptide and therefore have similar characteristics. The yield can be improved by using a bigger excess of amino acid, by performing more couplings, by increasing the coupling time or by using microwave or infrared assistance. The purification can be simplified by reacting the unreacted peptide ends with a small molecule, rendering them unreactive. This process, capping, was not applied in this study.
In this study automated Fmoc SPPS with microwave assistance was used to synthesize the peptides.

4.2. Synthesis of truncated bPP

In first instance truncated bPP, consisting of residues 1-31 of bPP, was synthesized using Fmoc SPPS on a Rink amide AM resin to find initial conditions for synthesis and purification of the peptides and to use it as a blank in catalysis (see Experimental Section for conditions). After synthesis and purification by rp-HPLC

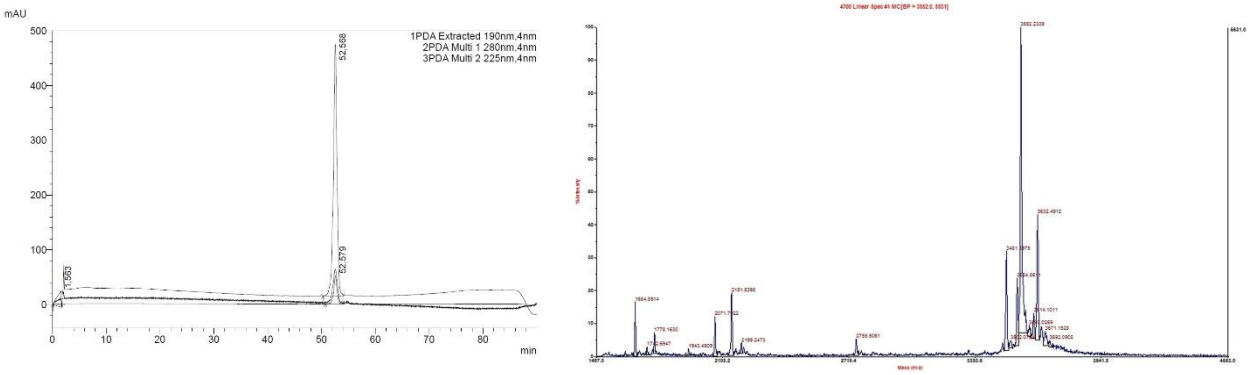

Figure 16: Left) HPLC trace of bPP-Y20Y showed one peak, which seemed to indicate that the peptide was pure. Right) MALDI-TOF however showed several peaks. The main peak is of the expected product, with one satellite indicating aspartimide formation and a second peak indication deletion.

the peptide was characterized by MALDI-TOF. Although the single peak in the HPLC trace seemed to indicate that only one product was isolated, MALDI-TOF showed two masses in the sample (Figure 16). One mass corresponded to the peptide, while a second less intense mass of 18 amu less was observed. It was initially believed that, due to ionization, a molecule of water was released from the peptide resulting

in a lower mass. However, literature suggested that the second mass could be attributed to the formation of aspartimide side product, when water is not able to hydrolyze this side product(Scheme 27).[26] Aspartimide formation occurs when an aspartate containing sequence of amino acids is present, in this case an aspartate (position 10) and asparagine (position 11). Therefore, as suggested by literature, a mutation of aspartate to glutamate (D10E) was applied in future syntheses to prevent aspartimide formation.[26]

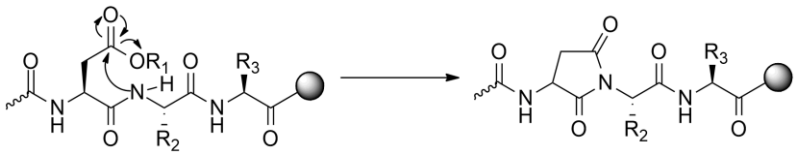

Scheme 27: The mechanism of aspartimide formation with an aspartic acid residue.

After successful isolation of bPP-Y20Y a first mutant suitable for post-synthetic modification was developed.

4.3. Synthesis of peptide bPP-Y20C

4.3.1. Introduction post-synthetic modification

In post-synthetic modification of a peptide a chemical group is coupled to an amino acid in the synthesized peptide, often via a linker. Amino acids such as cysteines or lysines are often used in the post-synthetic chemical modification of peptides.[64,65,66,67] The main advantage of this approach is the use of the chirality of the existing amino acid, one can incorporate an achiral ligand and avoid enantioselective synthesis. Two challenges of this approach are the selective modification of amino acids and the introduction of bulky groups. In large systems such as peptides and proteins one often encounters similar or identical functional groups, complicating the selective modification of a single group. Since the peptide used in this project is synthesized, this could be overcome by using protecting groups with orthogonal deprotection procedures. One can selectively deprotect a single residue, perform the modification and subsequently deprotect the other residues. This complication does not arise when functional groups such as cysteines or lysines are not present in the native peptide, as is the case with bPP. The second challenge, the introduction of bulky groups, has no standard solution. Solutions that one could think of are denaturation of the biomolecule to reach buried sites, the use of harsher reaction conditions or changing the nature of either nucleophile or electrophile.

Since the described phenanthroline-acetamide ligand has already been applied in post-synthetic modification and catalysis using a protein, we selected the same approach for the peptide-based system.[20]

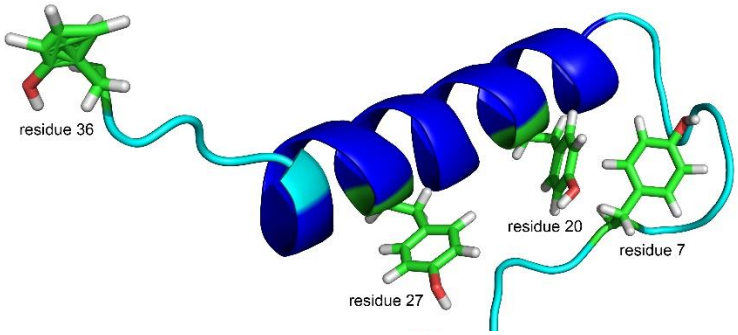

Figure 17: Solution NMR structure of wildtype bPP with the four tyrosine residues marked. Where the proline loop is semi-ordered the last five residues are disordered according to solution NMR.

In the protein-based system a free cysteine, a good nucleophile, is used to couple the ligand via the electrophilic halide. Since the selected peptide scaffold, bPP, does not contain cysteine residues by nature no issues concerning the selectivity of the modification were expected.[57] This also implies, however, that a new mutant of bPP with a cysteine residue should be developed.

4.3.2. Position for introduction of cysteine

Since the ligands contain bulky aromatic groups, introducing them on sites where aromatic groups are already present will minimize the structural change. This reduces the effect of the bulky aromatic groups on both stability and solubility of the peptide. bPP contains several aromatic groups which can be selected for mutation. Four aromatic amino acids, all tyrosines, are present in the peptide (Figure 17). One is present in the proline loop (residue 7), two in the α-helix (residues 20 and 27) and one in the disordered end (residue 36). In order to keep the structure as defined as possible, one could introduce the mutation in the rigid α-helix on positions 20 or 27. Position 20 is located in the middle of the sequence, whereas position 27 is located near the end of the sequence. In order to have a hydrophobic pocket which could stabilize the aromatic ligand one would prefer to have a range of amino acids in the vicinity of the mutation. Therefore the tyrosine on position 20 was selected for mutation into cysteine.

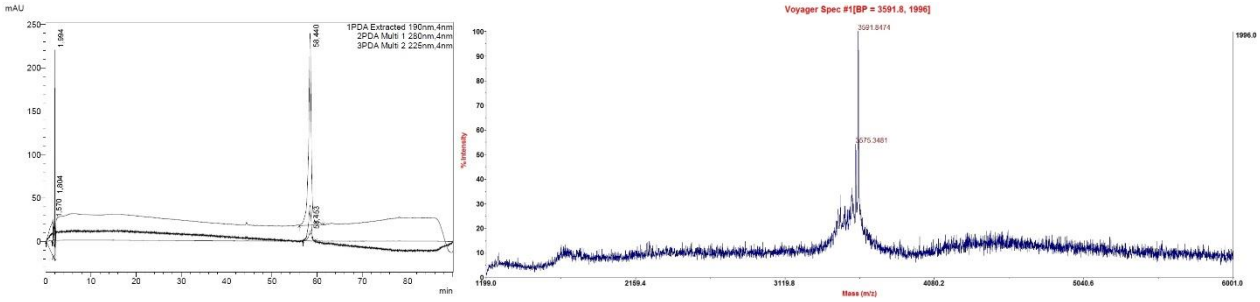

Figure 18: Left) HPLC trace of peptide bPP-Y20C shows only one peak, suggesting that the peptide is pure. Right) MALDI-TOF showed the correct mass of bPP-Y20C. Aspartimide formation was not observed.

4.3.3. Synthesis of mutant bPP-Y20C

In the synthesis of the cysteine containing mutant, referred to as bPP-Y20C, the mutation to prevent aspartimide formation (D10E) was included as well. In the synthesis of this mutant the cysteine had *t*Buthio-disulfide protection, which should not be affected during cleavage from the resin. Keeping the cysteine protected has the advantage that one does not encounter dimerization, which makes the extensive and time-consuming purification by rp-HPLC easier and increases the overall yield. After synthesis and purification with the same conditions as used for bPP-Y20Y, characterization was performed by MALDI-TOF and LCMS. A single peak was present in the HPLC trace, while MALDI-TOF showed a mass of 3591.8 amu. The mass corresponds to the calculated mass of bPP-Y20C and this in combination with the single peak observed on HPLC indicated that the peptide was pure and that the disulfide protection of the cysteine was intact (Figure 18). Absence of the second mass as observed for truncated bPP (18 amu lower) in MALDI-TOF showed that, as expected, the D10E mutation prevented aspartimide formation (Figure 18).

4.4. Synthesis of peptide bPP-Y20Phen

4.4.1. Deprotection of cysteine

After synthesis of bPP-Y20C the post-synthetic modification could be performed, which consists of two steps. Since the structural differences between the peptides in the different stages of modification are expected to be minimal where it comes to purification, it was made sure that all steps of modification go to completion. As mentioned earlier bPP-Y20C was synthesized with a *t*Buthio-disulfide protection which has to be removed prior to functionalization.
The deprotection of the disulfide-protected cysteine poses two main challenges. The first challenge is to perform the deprotection oxygen-free. When oxygen is present, free cysteines can readily oxidize to disulfides, preventing post-synthetic modification. Therefore one should perform the deprotection oxygen-free. This involves performing the reaction under inert atmosphere (by degassing the buffers with N_2) and using a purification method which can be performed fast in order to minimize disulfide formation. The second challenge is the complete removal of the disulfide reductant during purification. The second step of the modification involves coupling by a good nucleophile. Since common reductants (e.g. DTT or TCEP) contain good nucleophiles (thiols or phosphines) these should be removed prior to functionalization to prevent formation of reductant-ligand derivatives.[67,68]
The second step of the modification involves coupling of the ligand to the free cysteine of the peptide. As with the deprotection, the functionalization should be performed under inert atmosphere to minimize disulfide formation. Another key aspect is the pH of the buffer used for functionalization. The buffer should be basic enough to deprotonate the cysteine and enable reaction, but not too basic since this can promote disulfide formation if the mixture is not completely oxygen-free.

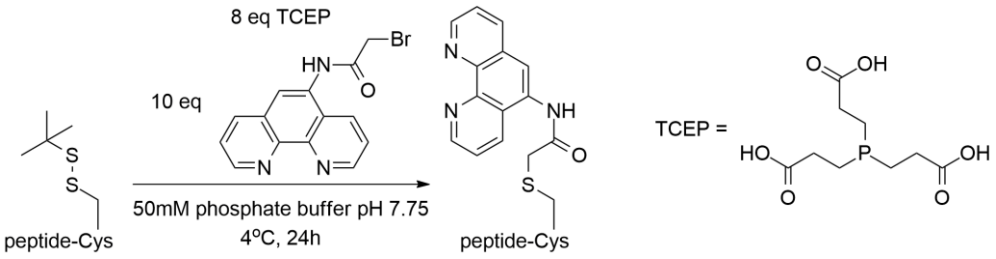

Scheme 28: Initial conditions used in the simultaneous deprotection and derivatization of the cysteine residue with TCEP and the phenanthroline-acetamide ligand **13**.

Several methods were used to perform the deprotection of the cysteine. In the first method the phosphine-based reducing agent TCEP was used, since it is able to reduce disulfides while limiting the extent of sidereactions of the phosphine with acetamides (Scheme 28).[68] Due to this limited compatibility a one pot procedure was developed to avoid purification of the unstable free cysteine before functionalization, which would be necessary when using reducing agents like DTT. An initial experiment was performed with 8 equivalents of TCEP and 10 equivalents of phenanthroline-acetamide at 4°C. After 24 hours the reaction was analyzed by MALDI-TOF. MALDI-TOF showed a main peak with a mass of 3591 amu, corresponding to the protected peptide, and a smaller peak with a mass of 3739, correspond to the functionalized peptide (Figure 19). Deprotected peptide could not be observed.

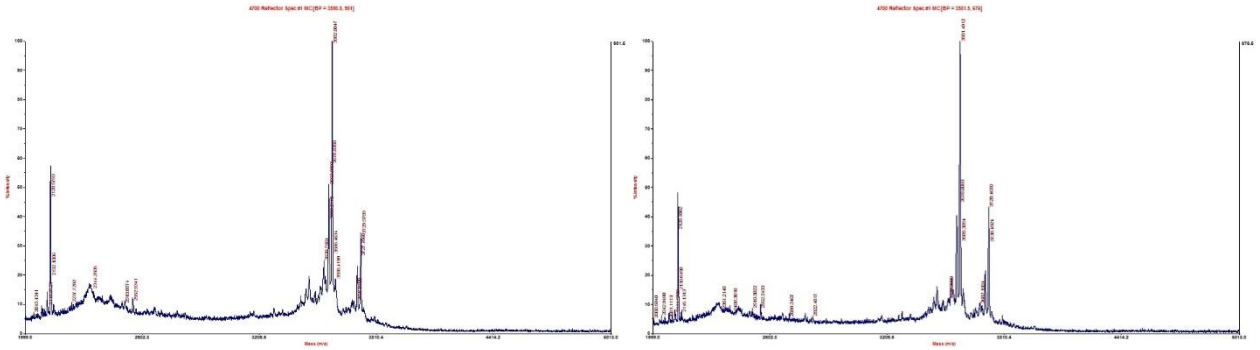

Figure 19: Left) Analysis by MALDI-TOF after 24 hours reaction time showed both starting material and functionalized peptide. Right) Analysis by MALDI-TOF after 48 hours reaction time showed a slightly higher signal for the functionalized peptide compared to 24 hours reaction time.

Another 8 equivalents of TCEP and 10 equivalents of phenanthroline-acetamide were added and after another 24 hours (48 hours total reaction time) the reaction was analyzed by MALDI-TOF. Again peaks for both protected peptide and functionalized peptide were observed and although the relative intensity of the latter peak was higher compared that in the first sample, the reaction was far from complete. It was therefore concluded that the envisioned one pot procedure was not suitable and that is was necessary to carry out the deprotection and functionalization separately. This, however, will require a purification after deprotection. Since TCEP has only minimal solubility in organic solvent (including alcohols) a more time-consuming technique such as size-exclusion chromatography has to be performed with the risk of dimer formation.

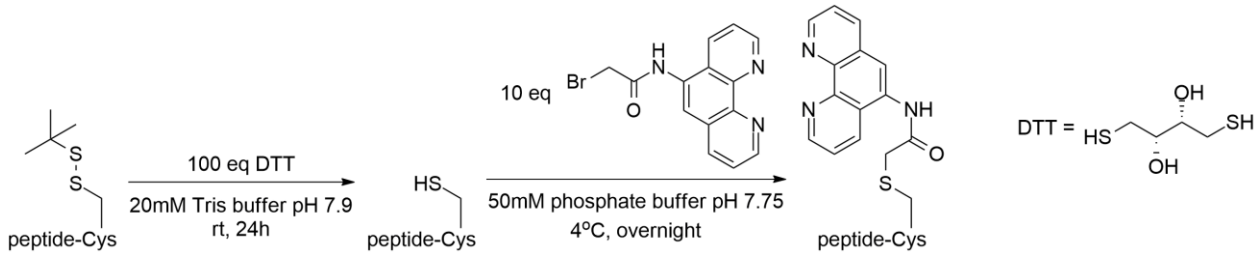

Scheme 29: Conditions used in the deprotection and subsequent modification of the cysteine with DTT and the phenanthroline-acetamide ligand **13**.

It was therefore decided to use DTT as reducing agent, since DTT is in principle soluble in organic solvents such as ethanol and even diethyl ether. In an initial experiment the deprotection was performed with 100 equivalents of DTT overnight at 4°C. Since analysis of a sample by MALDI-TOF still showed protected peptide, the reaction was performed with a longer reaction time of 24 hours leading to disappearance of the signal of protected peptide (Scheme 29). Before the deprotected peptide could be functionalized, excess DTT should be separated from the peptide. Although size-exclusion chromatography could be used to separate the two compounds, there were some practical issues related to dimer formation. To avoid oxidation on the column, one would have to equilibrate the column carefully with degassed buffer to remove oxygen. Moreover, since size-exclusion chromatography can be time-consuming one increases the chance of oxidation. A different purification was developed, where an initial extraction of the mixture with cold diethyl ether was performed to remove part of the DTT followed by lyophilization. After lyophilization the solid material was washed with cold diethyl ether to dissolve the DTT. After centrifugation and decanting the organic solvent the peptide was dried with N_2. Since the free cysteine had to be derivatized as quickly as possible to minimize oxidation of the cysteines to residual oxygen, no characterization of the peptide with the free cysteine was performed.

4.4.2. Functionalization of bPP-Y20C

The next step in the post-synthetic modification was the functionalization of the peptide with the ligand. Literature conditions were used for the coupling. The deprotected cysteine was reacted with 10 equivalents of **13** overnight at 4°C in phosphate buffer, which resulted in complete conversion. After the reaction the peptide was separated from excess ligand by size-exclusion chromatography. Further purification was done by rp-HPLC. After purification, the obtained peptide was analyzed by rp-HPLC, MALDI-TOF and LCMS. A single peak was observed in rp-HPLC, indicating the presence of one compound (Figure 20). MALDI-TOF showed a mass of 3740.10 amu, which corresponds to the theoretical mass of 3740.74 amu. LCMS showed a mass of 3741.75 amu, with a theoretical mass of 3740.74 amu (Figure 21). Double (1871.38 amu), triple (1247.92 amu) and quadruple (936.19 amu) charged states were also observed (Figure 21). The found masses corresponded to the theoretical masses for the double (1870.88 amu), triple (1247.58 amu) and quadruple (935.94 amu) charged states. Pure bPP-Y20Phen was obtained, which could subsequently be used in catalysis.

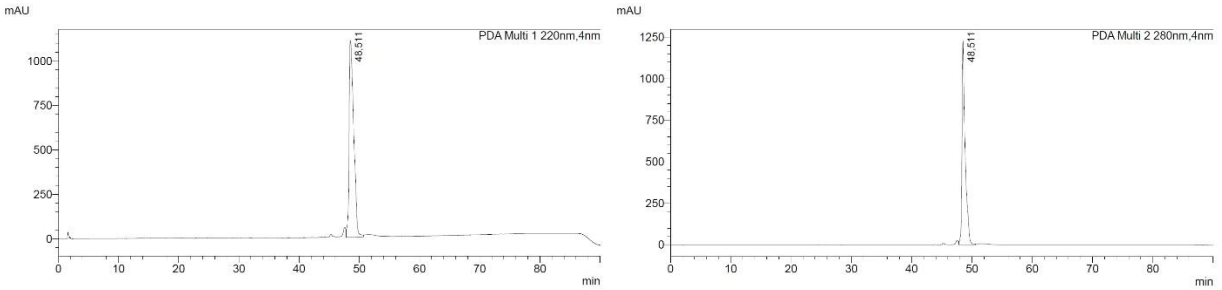

Figure 20: rp-HPLC traces of bPP-Y20Phen after purification.

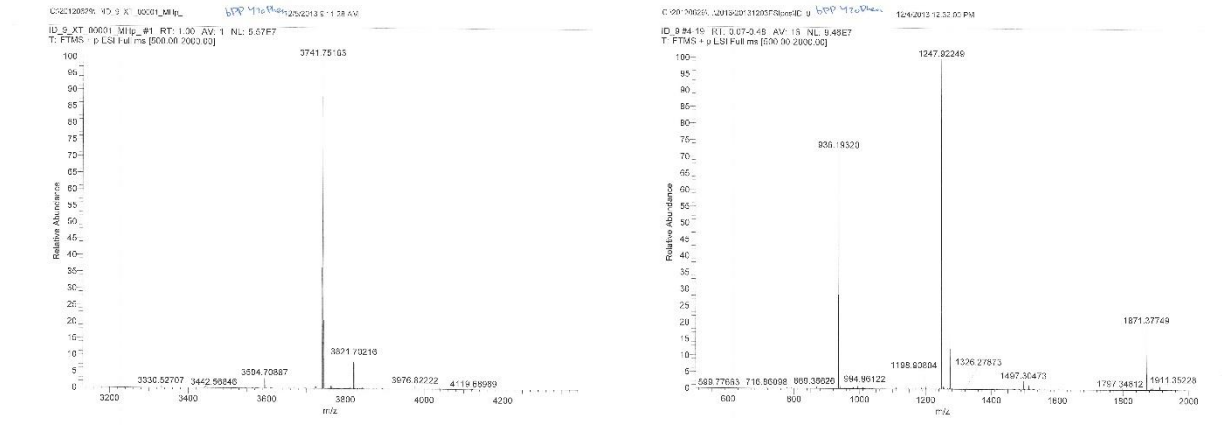

Figure 21: LCMS showed a single charged state (left) and double, triple and quadruple charged states (right).

4.5. Summary

Three peptides were synthesized using automated Fmoc SPPS and purified by rp-HPLC. After successful synthesis of the first peptide, truncated bPP, a mutant containing a cysteine group was synthesized. After synthesis and purification of this mutant, bPP-Y20C, postsynthetic modification could be performed. A phenanthroline group was coupled via a linker to the free cysteine, yielding the ligand-containing mutant bPP-Y20Phen. This peptide could subsequently be applied in catalysis, with truncated bPP and bPP-Y20C as reference peptides.

4.6. Experimental section

General remarks
All solvents were obtained from Biosolve. Piperazine was obtained from Sigma Aldrich. All Fmoc-protected amino acids and resins (Rink amide AM, substitution either 0.49 or 0.23) were obtained from Novabiochem. Amino acids with standard TFA-cleavable side chain protecting groups were used, except for cysteine (tButhio-protecting group).

Synthesis
Peptide synthesis (sequence APLEPEYPGENATPEQMAQXAAELRRYINML from N to C terminus, double couplings underlined) was performed using standard Fmoc-chemistry on a CEM Discover microwave synthesizer. Cleavage of the peptide from the resin was performed by mixing the resin for 3 hours at room temperature with 3 ml of a mixture of trifluoroacetic acid/dichloromethane/triisopropylsilane (95/2.5/2.5). After cleavage the mixture was filtered and the resin was washed with the cleavage mixture (2 x 0.5 ml). The solution was cooled on ice and ice-cold diethyl ether (5 ml) was added to precipitate the peptide. After centrifugation (10 min, 4000 rpm, 4°C) the solvent was decanted and the precipitate was washed with ice-cold diethyl ether (5 ml). After performing this centrifugation, decanting and washing cycle for a total of three times, the solution was decanted and the solid was dried with N_2. Subsequently the solid was dissolved in a mixture of water/acetonitrile/trifluoroacetic acid (95/5/0.1) for purification.

Peptide purification and analysis were performed by HPLC on a Shimadzu 20AD system using XTerra Prep MS C18 10 µm and XTerra MS C18 3.5 µm columns respectively. A gradient of water/acetonitrile with 0.1% of trifluoroacetic acid was used: 95/5 for 5 min to 40/60 over 65 min, 40/60 for 10 min to 95/5 over 2.5 min, 95/5 for 7.5 min. Pure fractions were pooled and lyophilized.

Mass spectra (UPLC-TOF/MALDI-TOF) were recorded on a Waters Acquity Xevo G2 TOF and Applied Biosystems 4700 or Voyager 6363 respectively. Peptide concentrations were determined using the A280 method (280 nm) on a Nanodrop 2000 UV-Vis spectrophotometer. Extinction coefficients were calculated using the ExPASy ProtParam tool or measured using UV-Vis spectroscopy.[11]

General procedure for deprotection of tbuthio-protected cysteines
Peptide (final concentration 150 µM) and DTT (final concentration 15 mM) were dissolved in degassed buffer (20 mM Tris-HCl pH 7.9, 0.1 mM EDTA, 1 mM DTT). After degassing with N_2 for 30 min the solution was mixed for 24 hours by rotation at room temperature. The solution was washed with 5 portions of cold diethyl ether and residual ether was evaporated by bubbling N_2 through the solution. After freeze-drying the solids were washed with 3 portions of diethyl ether to remove any DTT present. After drying the solid with N_2 for 15 min the solid was derivatized immediately.

General procedure for coupling of 2-bromo-N-(1,10-phenanthrolin-5-yl)acetamide to free cysteines
10 eq of 2-bromo-N-(1,10-phenanthrolin-5-yl)acetamide **13** (final concentration 1.5 mM), dissolved in a minimal amount of DMSO, was added to a solution of reduced peptide (final concentration 150 µM) in phosphate buffer (50 mM, pH 7.75). After degassing the solution with N_2 for 15 min the solution was mixed overnight by rotation at 4°C. The peptide was separated from remaining starting material **13** by using a GE Healthcare Illustra NAP-10 column Sephadex G-25 DNA Grade, loading 1 ml of solution and eluting with subsequently 1.5 and 1 ml of double distilled water. Fractions were analyzed using a Nanodrop A280 method, combined and freeze-dried. The solids were dissolved in a minimal amount of solvent (double distilled water/acetonitrile: 95/5 + 0.1% TFA) and purified and analyzed using rp-HPLC. Yields varied

between 30% and 55%. MALDI-TOF calcd for $C_{165}H_{248}N_{45}O_{49}S_3$ $[M+H]^+$ 3739.74, found 3739.10. HRMS calcd for $C_{165}H_{248}N_{45}O_{49}S_3$ $[M+H]^+$ 3740.75, found 3741.75.

5. Catalysis

5.1. Introduction

5.1.1. Hydration of unsaturated compounds

The assembled artificial metallopeptide bPP-Y20Phen was, as well as bPP-Y20Y and bPP-Y20C, applied in the catalysis of a hydration reaction.
The hydration reaction is an insertion of a molecule of water in an unsaturated compound (Scheme 30). Due to the small size of the nucleophile it is difficult to perform the insertion in a selective manner, be it regioselective or enantioselective. An additional challenge is the use of water as solvent in several existing systems, which results in a high concentration of nucleophiles.[6,69] In industry hydration reactions are typically used to produce alcohols from alkenes.[70] Using a acid catalyst, for example strong sulfuric acid, simple alcohols as ethanol, isopropanol and 2-butanol are generated from their corresponding alkenes. However, the harsh conditions would make it difficult to perform the hydration in a(n) (enantio)selective fashion.

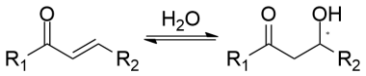

Scheme 30: General scheme of a hydration reaction of an α,β-unsaturated ketone.

Although several two step systems have been developed which perform hydrations in an enantioselective fashion, all systems that perform the hydration enantioselectively and in a single step use artificial metalloenzymes.[6,69,71,72]

5.1.2. Hydration using artificial metalloenzymes

Several developed systems use water-soluble biomolecular scaffolds in combination with metal-binding ligands and a copper(II) source in aqueous buffer to catalyze the reaction in an enantioselective fashion. The metal-binding ligands, all containing bidentate aromatic nitrogen-containing groups, were introduced to the scaffolds either covalently or by intermolecular interactions. All of the substrates applied contain an α,β-unsaturated ketone motif combined with an auxiliary group to bind in a bidentate fashion. Using various conditions, substrates and biomolecular scaffolds such as proteins and DNA high e.e.'s were obtained (Scheme 31).[6,69]
Whereas high e.e.'s were obtained, structural changes to the catalyst might improve the enantioselectivity of the system due to creation of a better defined active site or to improve delivery of the nucleophile. The DNA source used in these experiments was usually salmon testes, which gives a random sequence. Synthetic DNA could be used, however the increase of e.e. was marginal whereas the cost of the DNA increased significantly.[69] Whereas proteins can be modified, it is difficult to introduce multiple nonnatural residues if desired. The protein that was used in this system is a homodimeric protein.[6] Thus, one change in the amino acid sequence will result in two changes in the assembled protein. It is expected that with a synthetic peptide more freedom in structure modification can be obtained.
A challenge in the existing systems using this substrate is the reversibility of the reaction. If the equilibrium of the reaction is reached the enantiomeric excess is lowered and eventually racemic product is obtained.

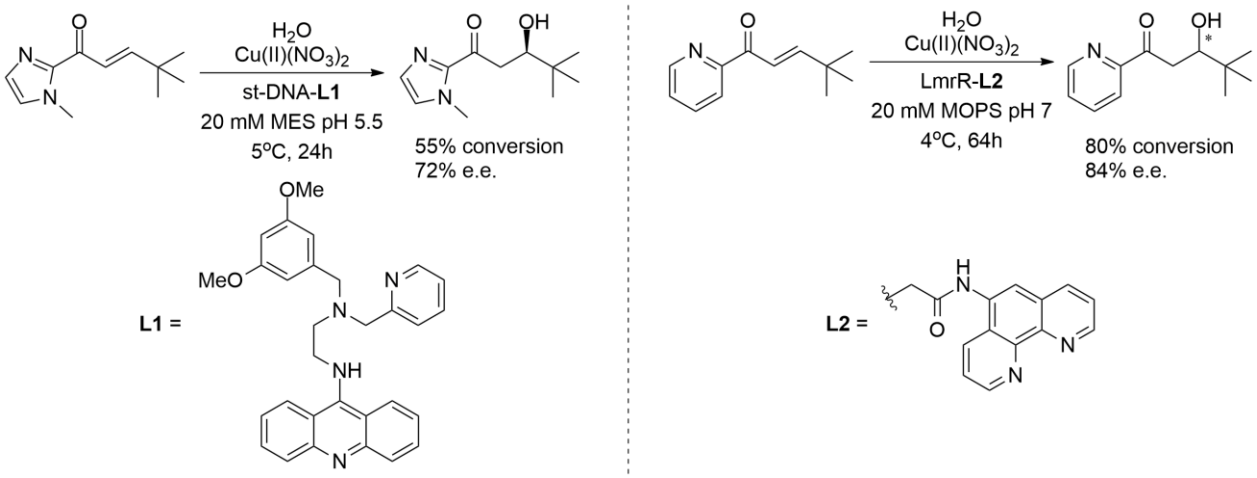

Scheme 31: Enantioselective hydration of two substrates using different biomolecular scaffolds in buffered solution.

5.2. Synthesis of substrate

It was decided to use a substrate which was used in earlier studies on hydrations.[69]
An α,β-unsaturated 2-acyl N-methylimidazole with tert-butyl group at the β position was used as substrate (Scheme 32). The substrate, compound **14**, was synthesized via an aldol condensation of 2-acyl N-methylimidazole and pivaldehyde in THF at room temperature for 48 hours using potassium hydroxide in ethanol as the base. Compound **14** was purified by column chromatography and characterized by ^{1}H-NMR, ^{13}C-NMR, mass spectrometry and normal phase HPLC analysis.

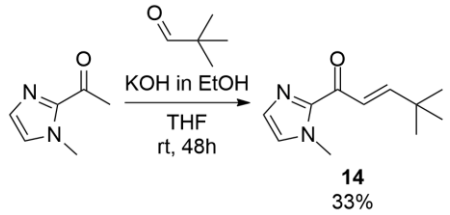

Scheme 32: Synthesis of enone **14** via a base catalyzed aldol condensation.

5.3. Catalysis

5.3.1. Initial catalytic trials

Initial experiments were performed using conditions from previous catalytic trials with bPP[26], however MES buffer pH 5.5 was used as medium since this gave the best results in the DNA-catalyzed hydration (Scheme 33).[6,69] In all cases experiments were performed *in duplo* from two stocks, so four experiments in total. Catalysis was performed with bPP-Y20Phen and bPP-Y20C as blank. In addition, experiments using peptide without copper(II), copper(II) without peptide and only buffer were performed.

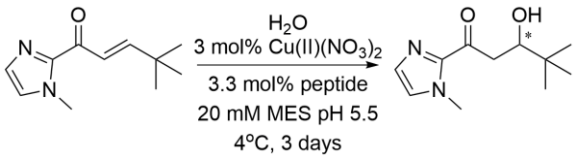

Scheme 33: Conditions used in the hydration of an enone with a peptide as biomolecular scaffold.

Initial experiments showed that copper-phenanthroline, whether bound to the peptide or as free complex, was found to be inactive under the used conditions (Table 1 entries 1 and 6). It was thought that copper(II) did bind to the peptide, however it is not known whether the copper(II) binds selectively to the phenanthroline moiety. Surprisingly, bPP-Y20C/Cu(II) gave a good conversion around 40%, a four-fold increase, albeit that no e.e. was obtained (Table 1 entries 3). From these experiments it was decided to perform experiments with bPP-Y20Phen to obtain conversion and additional experiments with bPP-Y20C to investigate the four-fold increase of conversion.

Entry	Peptide	Copper source	Conversion (%)	e.e. (%)
1	bPP-Y20Phen	$Cu(NO_3)_2$	<5	<5
2	bPP-Y20Phen	none	<5	<5
3	bPP-Y20C	$Cu(NO_3)_2$	40±12	<5
4	bPP-Y20C	none	<5	<5
5	none	$Cu(NO_3)_2$	10±1	<5
6	none	CuPhen	<5	<5
7	none	none	<5	<5

Table 1: Results from initial catalytic trials. Conditions: 20 mM MES buffer pH 5.5, 1 mM substrate, 30 µM $Cu(NO_3)_2$ (3 mol%), 33 µM peptide (3.3 mol%), 4°C for 3 days, mixing by continuous inversion, extraction with EtOAc. Conversion (corrected) and e.e. based on HPLC area.

5.3.2. Catalysis using bPP-Y20Phen

In all following catalytic experiments the number of experiments was decreased from four to two in a bid to preserve coupled peptide. As a results, ranges of conversions and e.e. are now mentioned instead of averages and standard deviations.

A number of catalytic experiments was performed using bPP-Y20Phen in order to obtain conversion and e.e. Both bPP-Y20Phen/Cu(II) as well as copper(II)-phenanthroline complex did not give any conversion at pH 5.5 (Table 2 entries 1 and 3). A four-fold increase of the concentration of bPP-Y20Phen/Cu(II) at pH 5.5 did not yield any conversion as well (Table 2 entry 5).

No conversion was obtained with bPP-Y20Phen/Cu(II) as catalyst at pH 7, however preformed copper(II)-phenanthroline complex gave 14-21% conversion at pH 7 (Table 2 entries 7 and 8).

Since at this pH the preformed complex is active and earlier experiments suggested that copper was bound to the peptide, it is likely that copper is bound to the peptide but subsequently deactivated. This deactivation could be caused by inability of the substrate to bind to the copper. This in turn could have two causes. The first cause is steric hindrance from the peptide chain, which would prohibit the substrate from reaching the active site. The second cause is binding of an additional ligand to copper(II), which would leave no vacant coordination sites for the substrate to bind.

Although the exact reason of deactivation is not known, a motivation and a possible solution to deactivation by steric hindrance by the peptide chain can be given.

Whereas three tyrosine residues were present in the peptide, the tyrosine residue in the turn between the α-helix and the polyproline loop was selected for mutation. This site could be the most shielded side since it is located in the middle of the peptide. A mutation of the other tyrosine residues could be

performed to restore activity of the system. One tyrosine is located in the polyproline loop, however this loop might possess too much structural flexibility to induce enantioselectivity. The other tyrosine residue is located at the end of the α-helix at position 27. Since this location is possibly less shielded while retaining rigidity of the chain, this site could be selected for mutation.

Entry	Peptide	Copper source	Conversion range (%)	e.e. (%)
1	bPP-Y20Phen	$Cu(NO_3)_2$	<5	<5
2	bPP-Y20Phen	none	<5	<5
3	none	CuPhen	<5	<5
4	none	none	<5	<5
5[a]	bPP-Y20Phen	$Cu(NO_3)_2$	<5	<5
6[a]	bPP-Y20Phen	none	<5	<5
7[b]	bPP-Y20Phen	$Cu(NO_3)_2$	<5	<5
8[b]	none	CuPhen	14-21	<5
9[b]	none	none	<5	<5

Table 2: Results from catalytic trials using bPP-Y20Phen. Conditions: 20 mM MES buffer pH 5.5, 1 mM substrate, 30 µM $Cu(NO_3)_2$ (3 mol%), 33 µM peptide (3.3 mol%), 4°C for 3 days, mixing by continuous inversion, extraction with EtOAc. a) Four times the original catalyst loading was used, 3 mol% copper and 13.3 mol% peptide. b) Catalysis was performed in 20 mM MOPS buffer pH 7. Conversion (corrected) and e.e. based on HPLC area.

5.3.3. Catalysis using bPP-Y20C

Initial experiments at pH 5.5 showed a good conversion between 25 and 57%, a two to six-fold increase, when using bPP-Y20C and copper nitrate, albeit without e.e. (Table 3 entry 1).
Upon increase of the pH, conversion drops to maximum two-fold increase. Optimal results were obtained at pH 7, 25-26% conversion and 24 to 29% e.e were obtained (Table 3 entry 5). While the reaction showed to be stereoselective as well at pH 8, both conversion and e.e. were lower (Table 3 entry 6). Whereas the highest conversions can be obtained at pH 5.5, the highest enantioselectivity was obtained at pH 7. Since performing the reaction in an asymmetric fashion was one goal of this project, pH 7 was found to be the best pH for this particular reaction and therefore used as standard for further experiments.

Entry	Peptide	Copper source	buffer and pH	Conversion range (%)	e.e. (%)
1	bPP-Y20C	$Cu(NO_3)_2$	MES pH 5.5	26-58	<5
2	bPP-Y20C	none	MES pH 5.5	<5	<5
3	bPP-Y20C	CuPhen	MES pH 5.5	6-18	<5
4	bPP-Y20C	$Cu(NO_3)_2$	MOPS pH 6	6-11	<5
5	bPP-Y20C	$Cu(NO_3)_2$	MOPS pH 7	25-26	24-29
6	bPP-Y20C	$Cu(NO_3)_2$	MOPS pH 8	18-23	21-24
7	bPP-Y20C	$Cu(NO_3)_2$	CHES pH 9	7-10	<5
8	bPP-Y20C	none	MOPS pH 6	<5	<5
9	bPP-Y20C	none	MOPS pH 7	<5	<5
10	bPP-Y20C	none	MOPS pH 8	<5	<5
11	bPP-Y20C	none	CHES pH 9	<5	<5
12	none	$Cu(NO_3)_2$	MOPS pH 6	8-9	<5
13	none	$Cu(NO_3)_2$	MOPS pH 7	27-42	<5
14	none	$Cu(NO_3)_2$	MOPS pH 8	14-18	<5
15	none	$Cu(NO_3)_2$	CHES pH 9	8-11	<5

Table 3: Results from a pH screening of catalysis using bPP-Y20C. Conditions: 20 mM buffer, 1 mM substrate, 30 µM $Cu(NO_3)_2$ (3 mol%), 33 µM peptide (3.3 mol%), 4°C for 3 days, mixing by continuous inversion, extraction with EtOAc. Conversion (corrected) and e.e. based on HPLC area.

Since the peptide is the only source of chirality present, it can be concluded that this peptide is able to induce stereoselectivity. This finding supports the concept of using peptides as second coordination spheres.

Although promising results were obtained in catalysis at pH 7, the obtained conversion was not near equilibrium values obtained in similar systems.[69] In a bid to increase conversion as well as e.e. the reaction time was prolonged to 5 or 7 days.

Entry	Peptide	Copper source	reaction time (days)	Conversion range (%)	e.e. (%)
1	bPP-Y20C	$Cu(NO_3)_2$	3	25-26	24-29
2	bPP-Y20C	$Cu(NO_3)_2$	5	29-34	15-19
3	bPP-Y20C	$Cu(NO_3)_2$	7	34-38	21-25
4	bPP-Y20C	none	3	<5	<5
5	bPP-Y20C	none	5	<5	<5
6	bPP-Y20C	none	7	<5	<5
7	none	$Cu(NO_3)_2$	3	27-42	<5
8	none	$Cu(NO_3)_2$	5	46-50	<5
9	none	$Cu(NO_3)_2$	7	31-53	<5

Table 4: Time dependence of catalysis using bPP-Y20C. Conditions: 20 mM MOPS buffer pH 7, 1 mM substrate, 30 µM $Cu(NO_3)_2$ (3 mol%), 33 µM peptide (3.3 mol%), 4°C for 3 days, mixing by continuous inversion, extraction with EtOAc. Conversion (corrected) and e.e. based on HPLC area.

Conversion increased upon prolongation of the reaction time, eventually reaching 34-38% after 7 days (Table 4 entry 3). After 5 days the e.e. decreased from 24-28% to 15-18%, however after 7 days e.e.'s of 21-25% are obtained.

The drop in e.e. after 5 days can be explained by the setup of the reactions. Reaction volumes are small (300 µl) and therefore only one sample can be taken from each reaction. The samples after 3, 5 and 7 days do not come from the same mixture and as such differences can occur. This could explain why a

drop in e.e. is observed after 5 days, while after 7 days only a slight decrease is observed.
The conversion of the reactions with only copper reach a maximum of 46-50% after 5 days (Table 4 entry 8). This could indicate the establishment of the equilibrium under these conditions around 50% conversion. This in turn could contribute to the slight decrease in e.e. after 7 days of reaction with peptide and copper, since the conversion is nearing equilibrium values (Table 4 entry 3).
bPP-Y20C contained a mutation of a tyrosine residue to a protected cysteine residue. The cysteine is protected with a *tert*-butyl mercaptan, forming a disulfide moiety. It was suspected that this disulfide might contribute to a large extent to the binding of copper. Sulfur atoms are more polarizable and therefore good donors, the disulfide bridge could provide chelation. Sulfur compounds are soft bases and although copper(II) is borderline[73], there is no favorable soft-soft interaction, binding might occur. Experiments were performed with truncated bPP, lacking the disulfide.
Using truncated bPP/Cu(II) 13-19% conversion was obtained after 3 days, which increased to 18-25% after 7 days (Table 5). However, no e.e. was obtained.
Significantly higher conversions were obtained when using copper without peptide and it was hypothesized that copper is still bound to some extent by the peptide, although it is not known where copper(II) exactly binds. E.e. was lost when using truncated bPP instead of bPP-Y20C, in addition higher conversions were obtained with the latter peptide. This indicates that the disulfide moiety is important in catalysis, especially for the enantioselectivity. Since it is not known where copper(II) binds, it is not known why the disulfide moiety is so important. One possibility is binding of copper(II) by the disulfide in this specific site, which could induce chirality.

Entry	Peptide	Copper source	reaction time (days)	Conversion range (%)	e.e. (%)
1	bPP	$Cu(NO_3)_2$	3	13-19	<5
2	bPP	$Cu(NO_3)_2$	5	20-21	<5
3	bPP	$Cu(NO_3)_2$	7	18-25	<5
4	bPP	none	3	<5	<5
5	bPP	none	5	3-11	<5
6	bPP	none	7	4-18	<5
7	none	$Cu(NO_3)_2$	3	27-42	<5
8	none	$Cu(NO_3)_2$	5	46-50	<5
9	none	$Cu(NO_3)_2$	7	31-53	<5

Table 5: Time dependence of catalysis using truncated bPP. Conditions: 20 mM MOPS buffer pH 7, 1 mM substrate, 30 µM $Cu(NO_3)_2$ (3 mol%), 33 µM peptide (3.3 mol%), 4°C for 3 days, mixing by continuous inversion, extraction with EtOAc. Conversion (corrected) and e.e. based on HPLC area.

Mutations of amino acids in the vicinity of the disulfide could be performed in a bid to increase the enantioselectivity of the system further.
One glutamate residue on position 23 could be mutated to a neutral amino acid, since this might be a possible secondary binding site for the copper. This binding, if existent, could contribute in both positive and negative way by further defining the geometry of the bound copper or by competing with the disulfide. Since the disulfide seems to contribute to the binding of copper, two possibly competing methionines on positions 17 and 30 could be mutated to a similar hydrophobic amino acid such as leucines.

5.4. Summary

Catalytic trials with bPP-Y20Phen as scaffold did not give conversion. It seemed copper was bound to the peptide, but the system was not catalytically active. This could be due to the inability of the substrate to bind to the metal, by steric hinderance of the peptide chain or by binding of an extra ligand to the metal source. By mutating the tyrosine at position 27 instead of position 20, located more towards the end of the peptide chain and the α-helix, could decrease the steric hindrance. However, it might be possible that due to the introduction of a large hydrophobic moiety the peptide chain folds around the phenanthroline group. In this case, placing it more on the outside of the peptide chain might destabilize the system further and cause faster aggregation of the chain.
Good conversions up to 34-38% and e.e.'s up to 24-29% were obtained using bPP-Y20C as peptide scaffold. The disulfide moiety seemed to be of high importance for the enantioselectivity and to a lesser extent the conversion. The use of truncated bPP, lacking this moiety, resulted in a total loss of e.e. Mutations could be made in the vicinity of this disulfide moiety in order to increase the conversion and enantioselectivity. Charged residues, such as glutamate on position 23, could be mutated to non charged residues in order to avoid competition for the copper.

5.5. Experimental section

(E)-4,4-dimethyl-1-(1-methyl-1H-imidazol-2-yl)pent-2-en-1-one (14)

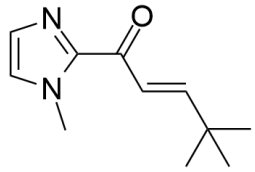

Prepared following a literature procedure.[69] To pivaldehyde (1.3 ml, 11.6 mmol) and N-methyl-2-acetylimidazole (1.4 g, 11.6 mmol) in THF (20 ml) was added potassium hydroxide (100 mg) in a minimal amount of absolute ethanol (approximately 2 ml). After the mixture was stirred for 48 hours at room temperature the solvent was evaporated. The crude product was dissolved in ethyl acetate (50 ml) and the organic layer was washed with brine (2 x 20 ml). The organic layer was dried over sodium sulphate and concentrated. After column chromatography (SiO_2, pentane/ethyl acetate: 4/1) product **14** was obtained as a colorless oil (740.0 mg, 3.8 mmol, 33%). ^{1}H NMR (400 MHz, $CDCl_3$) δ 7.34 (d, *J* = 15.9 Hz, 1H), 7.19 (s, 1H), 7.13 (d, *J* = 15.9 Hz, 1H), 7.04 (s, 1H), 4.05 (s, 3H), 1.15 (s, 9H). ^{13}C NMR (101 MHz, $CDCl_3$) δ 181.3, 158.5, 143.9, 129.2, 127.2, 121.3, 36.4, 34.2, 28.8. HRMS calcd for $C_{11}H_{17}N_2O$ $[M+H]^+$ 193.133, found 193.133.

Retention time was determined by HPLC analysis on a Shimadzu 20AD system (Chiracel AD-H, heptane/iPrOH 90:10, 0.5 ml/min).: 9.4 min.

3-hydroxy-4,4-dimethyl-1-(1-methyl-1H-imidazol-2-yl)pentan-1-one (15)

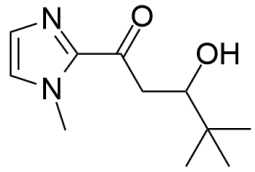

Prepared following a literature procedure.[69] Product **14** (100.0 mg, 0.5 mmol, final concentration 1 mM) predissolved in acetonitrile (1ml) and copper nitrate trihydrate (43.7 mg, 0.2 mmol, final concentration 0.3 mM) were dissolved in MES buffer (520 ml, pH 5.5) and stirred overnight at room temperature. The mixture was extracted with dichloromethane (4 x 200 ml), the combined organic layers were dried over sodium sulphate and concentrated. After column chromatography (SiO_2, pentane/ethyl acetate: 3/2) product **15** was obtained as a colorless oil (65.6 mg, 0.3 mmol, 60%). ^{1}H NMR (400 MHz, $CDCl_3$) δ 7.15 (s, 1H), 7.04 (s, 1H), 4.01 (s, 3H), 3.73 (dd, *J* = 9.1, 2.6 Hz, 1H), 3.24 – 3.15 (m, 2H), 0.97 (s, 9H). ^{13}C NMR (101 MHz, $CDCl_3$) δ 193.3, 143.3, 129.2, 127.2, 75.8, 42.7, 36.3, 35.0, 25.8. HRMS calcd for $C_{11}H_{19}N_2O_2$ $[M+H]^+$ 211.144, found 211.143.

E.e.'s were determined by HPLC analysis on a Shimadzu 20AD system (Chiracel AD-H, heptane/iPrOH 90:10, 0.5 ml/min). Retention times: 17.0 (S) and 19.3 (R) mins.

General procedure for metallopeptide-catalyzed hydration

Procedure for peptide-Cu^{II} catalyzed reactions adapted from literature.[20] To a solution of $Cu(NO_3)_2{\cdot}3H_2O$ (final concentration 30 µM) in 20 mm buffer (pH adjusted) at 0°C was added peptide (1.1 equiv based on $Cu(NO_3)_2{\cdot}3H_2O$, concentration determined using UV/Vis absorbance at 280 nm) to a final volume of 290 µl. A fresh stock solution (10 µl) of enone **14** in buffer/acetonitrile was added (final concentration 1 mM). The reaction was mixed for a set number of days by continuous inversion at 4°C. The product was isolated by extraction with ethyl acetate (3 x 1 ml). The organic phases were dried over Na_2SO_4 and the plug of Na_2SO_4 was flushed with ethyl acetate (1 ml). After evaporation of the solvent under reduced pressure the product was dissolved in isopropanol (120 µl, analytical grade). The conversion and ee value were determined by np-HPLC using a chiral stationary phase (Chiracel AD-H, heptane/iPrOH 90:10, 0.5 ml/min).

6. Conclusions

Two aromatic ligands have been selected and synthesized for incorporation into the peptide scaffold as the first coordination sphere. One ligand was ready for introduction while a second required a final protecting step.
Ligand **13**, based on a 1,10-phenanthroline group, was synthesized in one step in 80% yield. This ligand was ready for introduction in the peptide via post-synthetic modification, by reaction of the linker with a cysteine residue.
Amino acid (*S*)-**9**, containing a bipyridyl group, was synthesized in six steps from commercially available reagents with an overall yield of 5%. This amino acid needs to be Fmoc-protected to enable introduction in the peptide via solid phase peptide synthesis.

After selection of the ligands, a suitable computational method was to be found to design the peptide. For this purpose three methods, I-TASSER, CORINA and GROMOS, were used. However, none of the methods was found suitable for design of the peptide. Future studies could focus on the use of docking software for the design of the second coordination sphere.

No conversion to hydration product was obtained in catalytic trials with bPP-Y20Phen as peptide. It was thought copper(II) was bound to the peptide but subsequently was deactivated. This could be due to steric hindrance of the active site by the peptide chain. This might be overcome by mutation of the tyrosine at position 27 instead of position 20.
Surprisingly, good conversions and e.e.'s up to 38% and 29% respectively could be obtained using bPP-Y20C/Cu(II). The disulfide moiety seemed to be of high importance for the enantioselectivity and to a lesser extent the conversion. The use of truncated bPP, lacking this moiety, resulted in a total loss of e.e. Mutations could be made in the vicinity of this disulfide moiety in order to increase the conversion and enantioselectivity. Charged residues, such as glutamate on position 23, could be mutated to non charged residues in order to avoid competition for the copper.

In conclusion, it is shown that artificial metalloenzymes based on synthetic peptides are good catalysts for an enantioselective hydration reaction. In addition to the promising results obtained in catalysis, the ease with which modification can be applied to the scaffold using peptide synthesis is a big advantage. Although the power of computational methods in the design of biomolecules has been shown in other studies, the investigated methods did not give the desired results. Therefore the development of a general method for computational design would be a major step forward.

References

1. Lewis, J. C. Artificial Metalloenzymes and Metallopeptide Catalysts for Organic Synthesis. *ACS Catal.* **3,** 2954–2975 (2013).
2. Ueno, T., Tabe, H. & Tanaka, Y. Artificial Metalloenzymes Constructed From Hierarchically-Assembled Proteins. *Chem. – Asian J.* **8,** 1646–1660 (2013).
3. Ward, T. R. Artificial Metalloenzymes Based on the Biotin−Avidin Technology: Enantioselective Catalysis and Beyond. *Acc. Chem. Res.* **44,** 47–57 (2011).
4. Bos, J. & Roelfes, G. Artificial metalloenzymes for enantioselective catalysis. *Curr. Opin. Chem. Biol.* **19,** 135–143 (2014).
5. Oelerich, J. & Roelfes, G. DNA-based asymmetric organometallic catalysis in water. *Chem. Sci.* **4,** 2013–2017 (2013).
6. Bos, J., García-Herraiz, A. & Roelfes, G. An enantioselective artificial metallo-hydratase. *Chem. Sci.* **4,** 3578 (2013).
7. Hyster, T. K., Knörr, L., Ward, T. R. & Rovis, T. Biotinylated Rh(III) Complexes in Engineered Streptavidin for Accelerated Asymmetric C–H Activation. *Science* **338,** 500–503 (2012).
8. Lu, Y., Yeung, N., Sieracki, N. & Marshall, N. M. Design of functional metalloproteins. *Nature* **460,** 855–862 (2009).
9. Heinisch, T. & Ward, T. R. Design strategies for the creation of artificial metalloenzymes. *Curr. Opin. Chem. Biol.* **14,** 184–199 (2010).
10. Deuss, P. J., den Heeten, R., Laan, W. & Kamer, P. C. J. Bioinspired Catalyst Design and Artificial Metalloenzymes. *Chem. – Eur. J.* **17,** 4680–4698 (2011).
11. Ringenberg, M. R. & Ward, T. R. Merging the best of two worlds: artificial metalloenzymes for enantioselective catalysis. *Chem. Commun.* **47,** 8470–8476 (2011).
12. Yeung, N. *et al.* Rational design of a structural and functional nitric oxide reductase. *Nature* **462,** 1079–1082 (2009).
13. Roelfes, G. & Feringa, B. L. DNA-Based Asymmetric Catalysis. *Angew. Chem.* **117,** 3294–3296 (2005).
14. Boersma, A. J., Klijn, J. E., Feringa, B. L. & Roelfes, G. DNA-based asymmetric catalysis: sequence-dependent rate acceleration and enantioselectivity. *J. Am. Chem. Soc.* **130,** 11783–11790 (2008).
15. Boersma, A. J., Megens, R. P., Feringa, B. L. & Roelfes, G. DNA-based asymmetric catalysis. *Chem. Soc. Rev.* **39,** 2083–2092 (2010).
16. Shibata, N., Yasui, H., Nakamura, S. & Toru, T. DNA-Mediated Enantioselective Carbon-Fluorine Bond Formation. *Synlett* **2007,** 1153–1157 (2007).
17. Rothemund, P. W. K. Folding DNA to create nanoscale shapes and patterns. *Nature* **440,** 297–302 (2006).
18. Rosati, F. & Roelfes, G. Artificial Metalloenzymes. *ChemCatChem* **2,** 916–927 (2010).
19. Zimbron, J. M. *et al.* A Dual Anchoring Strategy for the Localization and Activation of Artificial Metalloenzymes Based on the Biotin–Streptavidin Technology. *J. Am. Chem. Soc.* **135,** 5384–5388 (2013).
20. Bos, J., Fusetti, F., Driessen, A. J. M. & Roelfes, G. Enantioselective Artificial Metalloenzymes by Creation of a Novel Active Site at the Protein Dimer Interface. *Angew. Chem. Int. Ed.* **51,** 7472–7475 (2012).
21. Mayer, C. & Hilvert, D. A Genetically Encodable Ligand for Transfer Hydrogenation. *Eur. J. Org. Chem.* **2013,** 3427–3431 (2013).
22. Sambasivan, R. & Ball, Z. T. Metallopeptides for Asymmetric Dirhodium Catalysis. *J. Am. Chem. Soc.* **132,** 9289–9291 (2010).

23. Sambasivan, R. & Ball, Z. T. Screening Rhodium Metallopeptide Libraries 'On Bead': Asymmetric Cyclopropanation and a Solution to the Enantiomer Problem. *Angew. Chem. Int. Ed.* **51,** 8568–8572 (2012).
24. Sambasivan, R. & Ball, Z. T. Studies of Asymmetric StyreneCyclopropanation with a Rhodium(II) Metallopeptide Catalyst Developed with a High-Throughput Screen. *Chirality* **25,** 493–497 (2013).
25. Agarkov, A. *et al.* Synthesis of phosphine containing amino acids: Utilization of peptide synthesis in ligand design. *Pept. Sci.* **84,** 48–73 (2006).
26. Coquière, D., Bos, J., Beld, J. & Roelfes, G. Enantioselective Artificial Metalloenzymes Based on a Bovine Pancreatic Polypeptide Scaffold. *Angew. Chem. Int. Ed.* **48,** 5159–5162 (2009).
27. Zheng, L., Marcozzi, A., Gerasimov, J. Y. & Herrmann, A. Conformationally Constrained Cyclic Peptides: Powerful Scaffolds for Asymmetric Catalysis. *Angew. Chem. Int. Ed.* **53,** 7599–7603 (2014).
28. Trost, B. M. in *Transition Metals for Organic Synthesis* (eds. Beller, essor M. & Bolm, essor C.) 2–14 (Wiley-VCH Verlag GmbH, 2004). at <http://onlinelibrary.wiley.com/doi/10.1002/9783527619405.ch1a/summary>
29. Chadwick, J. C., Duchateau, R., Freixa, Z. & Leeuwen, P. W. N. M. van. *Homogeneous Catalysts: Activity - Stability - Deactivation*. (John Wiley & Sons, 2011).
30. Rappoport, Z. & Marek, I. *The Chemistry of Organocopper Compounds*. (John Wiley & Sons, 2010).
31. Ballardini, R. *et al.* Photoinduced Electron Transfer in a Triad That Can Be Assembled/Disassembled by Two Different External Inputs. Toward Molecular-Level Electrical Extension Cables. *J. Am. Chem. Soc.* **124,** 12786–12795 (2002).
32. Imperiali, B. & Fisher, S. L. Stereoselective synthesis and peptide incorporation of (S)-.alpha.-amino-(2,2'-bipyridine)-6-propanoic acid. *J. Org. Chem.* **57,** 757–759 (1992).
33. Savage, S. A., Smith, A. P. & Fraser, C. L. Efficient Synthesis of 4-, 5-, and 6-Methyl-2,2'-bipyridine by a Negishi Cross-Coupling Strategy Followed by High-Yield Conversion to Bromo- and Chloromethyl-2,2'-bipyridines. *J. Org. Chem.* **63,** 10048–10051 (1998).
34. Smith, A. P., Fraser, C. L. & Lamba, Jaydeep J.S. Efficient Synthesis of Halomethyl-2,2'-bipyridines: 4,4'-bis(chloromethyl)-2,2'-bipyridine. *Org. Synth.* **78,** 82–88 (2002).
35. Imperiali, B., Prins, T. J. & Fisher, S. L. Chemoenzymic synthesis of 2-amino-3-(2,2'-bipyridinyl)propanoic acids. *J. Org. Chem.* **58,** 1613–1616 (1993).
36. Brunet, E., Alonso, M., Quintana, M. C., Juanes, O. & Rodríguez-Ubis, J.-C. Facile synthesis of new fullerene–Ru(bpy)3 dyads bearing phosphonate groups for hybrid organic–inorganic materials. *Tetrahedron Lett.* **48,** 3739–3743 (2007).
37. Belokon, Y. N. *et al.* Synthesis of enantio- and diastereo-isomerically pure β- and γ-substituted glutamic acids via glycine condensation with activated olefins. *J. Chem. Soc. [Perkin 1]* 1865–1872 (1986). doi:10.1039/P19860001865
38. Belokon', Y. N. *et al.* Asymmetric Michael addition of a glycine synthon to methyl methacrylate, mediated by disodium TADDOLate. *Mendeleev Commun.* **7,** 137–138 (1997).
39. Belokon, Y. N. *et al.* Highly Efficient Catalytic Synthesis of α-Amino Acids under Phase-Transfer Conditions with a Novel Catalyst/Substrate Pair. *Angew. Chem.* **113,** 2002–2005 (2001).
40. Corey, E. J., Xu, F. & Noe, M. C. A Rational Approach to Catalytic Enantioselective Enolate Alkylation Using a Structurally Rigidified and Defined Chiral Quaternary Ammonium Salt under Phase Transfer Conditions. *J. Am. Chem. Soc.* **119,** 12414–12415 (1997).
41. Respondek, T., Cueny, E. & Kodanko, J. J. Cumyl Ester as the C-Terminal Protecting Group in the Enantioselective Alkylation of Glycine Benzophenone Imine. *Org. Lett.* **14,** 150–153 (2012).
42. Nun, P., Pérez, V., Calmès, M., Martinez, J. & Lamaty, F. Preparation of Chiral Amino Esters by Asymmetric Phase-Transfer Catalyzed Alkylations of Schiff Bases in a Ball Mill. *Chem. – Eur. J.* **18,** 3773–3779 (2012).

43. Kitamura, M., Shirakawa, S. & Maruoka, K. Powerful Chiral Phase-Transfer Catalysts for the Asymmetric Synthesis of α-Alkyl- and α,α-Dialkyl-α-amino Acids. *Angew. Chem. Int. Ed.* **44,** 1549–1551 (2005).
44. Hashimoto, T. & Maruoka, K. Recent Development and Application of Chiral Phase-Transfer Catalysts. *Chem. Rev.* **107,** 5656–5682 (2007).
45. Strachan, J.-P., Whitaker, R. C., Miller, C. H. & Bhatti, B. S. Synthesis of Bicyclic Tertiary α-Amino Acids. *J. Org. Chem.* **71,** 9909–9911 (2006).
46. Danner, P., Bauer, M., Phukan, P. & Maier, M. E. Total Synthesis of Cryptophycin 3. *Eur. J. Org. Chem.* **2005,** 317–325 (2005).
47. Ng, C.-O., Lai, S.-W., Feng, H., Yiu, S.-M. & Ko, C.-C. Luminescent rhenium(I) complexes with acetylamino- and trifluoroacetylamino-containing phenanthroline ligands: Anion-sensing study. *Dalton Trans.* **40,** 10020–10028 (2011).
48. Bonneau, R. & Baker, D. AB INITIO PROTEIN STRUCTURE PREDICTION: Progress and Prospects. *Annu. Rev. Biophys. Biomol. Struct.* **30,** 173–189 (2001).
49. Floudas, C. A., Fung, H. K., McAllister, S. R., Mönnigmann, M. & Rajgaria, R. Advances in protein structure prediction and de novo protein design: A review. *Chem. Eng. Sci.* **61,** 966–988 (2006).
50. Simmerling, C., Strockbine, B. & Roitberg, A. E. All-Atom Structure Prediction and Folding Simulations of a Stable Protein. *J. Am. Chem. Soc.* **124,** 11258–11259 (2002).
51. Maréchal, J.-D. *et al.* Insights into drug metabolism by cytochromes P450 from modelling studies of CYP2D6-drug interactions. *Br. J. Pharmacol.* **153,** S82–S89 (2008).
52. Petrik, I. D., Liu, J. & Lu, Y. Metalloenzyme design and engineering through strategic modifications of native protein scaffolds. *Curr. Opin. Chem. Biol.* **19,** 67–75 (2014).
53. Brustad, E. M. & Arnold, F. H. Optimizing non-natural protein function with directed evolution. *Curr. Opin. Chem. Biol.* **15,** 201–210 (2011).
54. Muñoz Robles, V., Vidossich, P., Lledós, A., Ward, T. R. & Maréchal, J.-D. Computational Insights on an Artificial Imine Reductase Based on the Biotin–Streptavidin Technology. *ACS Catal.* **4,** 833–842 (2014).
55. Mills, J. H. *et al.* Computational Design of an Unnatural Amino Acid Dependent Metalloprotein with Atomic Level Accuracy. *J. Am. Chem. Soc.* **135,** 13393–13399 (2013).
56. Ortega-Carrasco, E., Lledós, A. & Maréchal, J.-D. Unravelling novel synergies between organometallic and biological partners: a quantum mechanics/molecular mechanics study of an artificial metalloenzyme. *J. R. Soc. Interface* **11,** 20140090 (2014).
57. Li, X., Sutcliffe, M. J., Schwartz, T. W. & Dobson, C. M. Sequence-specific proton NMR assignments and solution structure of bovine pancreatic polypeptide. *Biochemistry (Mosc.)* **31,** 1245–1253 (1992).
58. Roy, A., Kucukural, A. & Zhang, Y. I-TASSER: a unified platform for automated protein structure and function prediction. *Nat. Protoc.* **5,** 725–738 (2010).
59. Zhang, Y. I-TASSER server for protein 3D structure prediction. *BMC Bioinformatics* **9,** 40 (2008).
60. Sadowski, J. & Gasteiger, J. From atoms and bonds to three-dimensional atomic coordinates: automatic model builders. *Chem. Rev.* **93,** 2567–2581 (1993).
61. Sadowski, J., Gasteiger, J. & Klebe, G. Comparison of Automatic Three-Dimensional Model Builders Using 639 X-ray Structures. *J. Chem. Inf. Comput. Sci.* **34,** 1000–1008 (1994).
62. Grace, R. C., Chandrashekar, I. R. & Cowsik, S. M. Solution structure of the tachykinin Peptide eledoisin. *BIOPHYS.J.* **84,** 655–664 (2002).
63. Berendsen, H. J. C., van der Spoel, D. & van Drunen, R. GROMACS: A message-passing parallel molecular dynamics implementation. *Comput. Phys. Commun.* **91,** 43–56 (1995).
64. Kim, Y. *et al.* Efficient Site-Specific Labeling of Proteins via Cysteines. *Bioconjug. Chem.* **19,** 786–791 (2008).

65. Tyagarajan, K., Pretzer, E. & Wiktorowicz, J. E. Thiol-reactive dyes for fluorescence labeling of proteomic samples. *ELECTROPHORESIS* **24,** 2348–2358 (2003).
66. Monfregola, L., Leone, M., Calce, E. & De Luca, S. Postsynthetic modification of peptides via chemoselective N-alkylation of their side chains. *Org. Lett.* **14,** 1664–1667 (2012).
67. Chalker, J. M., Bernardes, G. J. L., Lin, Y. A. & Davis, B. G. Chemical Modification of Proteins at Cysteine: Opportunities in Chemistry and Biology. *Chem. – Asian J.* **4,** 630–640 (2009).
68. Shafer, D. E., Inman, J. K. & Lees, A. Reaction of Tris(2-carboxyethyl)phosphine (TCEP) with Maleimide and α-Haloacyl Groups: Anomalous Elution of TCEP by Gel Filtration. *Anal. Biochem.* **282,** 161–164 (2000).
69. Boersma, A. J. *et al.* Catalytic enantioselective syn hydration of enones in water using a DNA-based catalyst. *Nat. Chem.* **2,** 991–995 (2010).
70. Falbe, J., Bahrmann, H., Lipps, W. & Mayer, D. in *Ullmann's Encyclopedia of Industrial Chemistry* (Wiley-VCH Verlag GmbH & Co. KGaA, 2000). at <http://onlinelibrary.wiley.com/doi/10.1002/14356007.a01_279/abstract>
71. Schnapperelle, I., Hummel, W. & Gröger, H. Formal Asymmetric Hydration of Non-Activated Alkenes in Aqueous Medium through a 'Chemoenzymatic Catalytic System'. *Chem. – Eur. J.* **18,** 1073–1076 (2012).
72. Hartmann, E., Vyas, D. J. & Oestreich, M. Enantioselective formal hydration of α,β-unsaturated acceptors: asymmetric conjugate addition of silicon and boron nucleophiles. *Chem. Commun.* **47,** 7917–7932 (2011).
73. Pearson, R. G. Hard and soft acids and bases, HSAB, part 1: Fundamental principles. *J. Chem. Educ.* **45,** 581 (1968).

Appendix A: List of abbreviations

AIBN	= azobisisobutyronitrile
CCl_4	= carbon tetrachloride
DCM	= dichloromethane
DMF	= N,N-dimethylformamide
DTT	= 1,4-dithio-D-threitol
EDTA	= ethylenediaminetetraacetic acid
Fmoc	= 9-fluorenylmethoxycarbonyl
Gly-Ni-BPB	= glycine-nickel(II)-(N-benzylprolyl)-2-carboxylic acid(2-benzoyl-phenyl)-amide
Gly-Ni-PBP	= glycine-nickel(II)-pyridine-2-carboxylic acid(2-benzoyl-phenyl)-amide
LDA	= lithium diispropylamine
NBS	= N-bromosuccinimide
NOBIN	= 2-amino-2′-hydroxy-1,1′-binaphthalene
SPPS	= solid phase peptide synthesis
TFA	= trifluoroacetic acid
THF	= tetrahydrofuran
TOF	= time of flight

Appendix B: Characterization of organic compounds

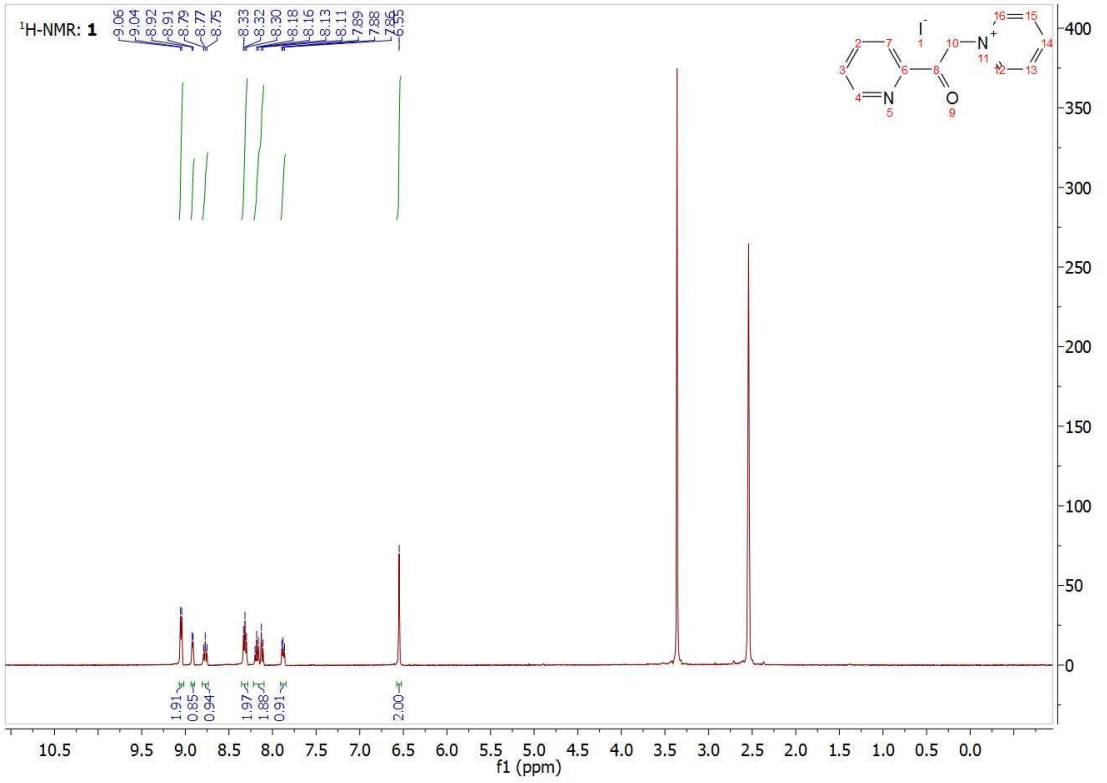

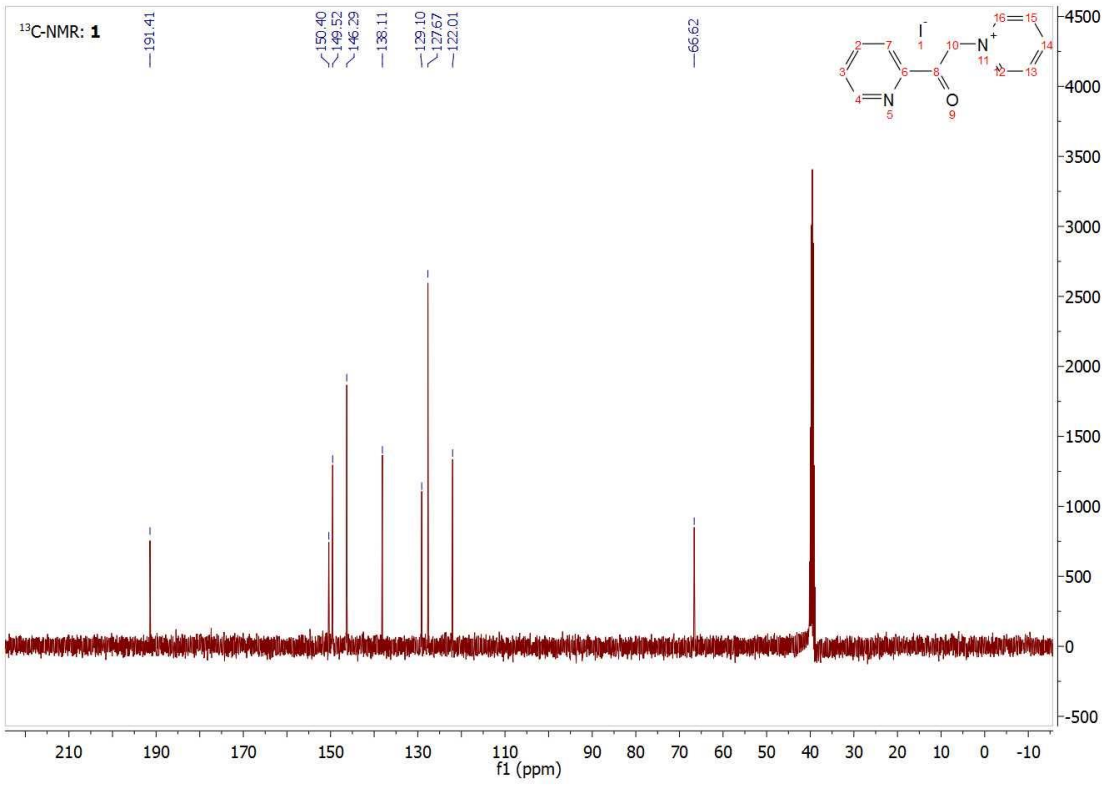

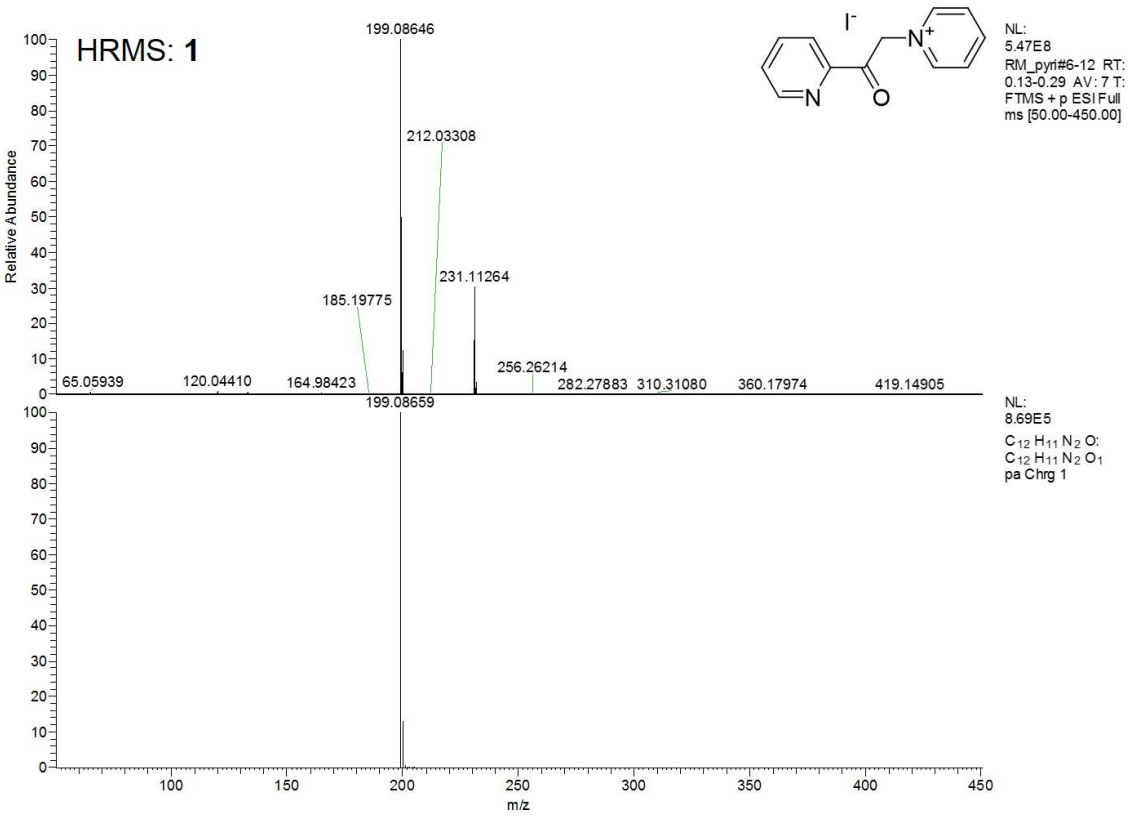
HRMS: 1
199.08646
212.03308
231.11264
185.19775
256.26214
65.05939
120.04410
164.98423
282.27883
310.31080
360.17974
419.14905
199.08659
Relative Abundance
m/z
NL:
5.47E8
RM_pyri#6-12 RT:
0.13-0.29 AV: 7 T:
FTMS + p ESI Full
ms [50.00-450.00]
NL:
8.69E5
C12 H11 N2 O:
C12 H11 N2 O1
pa Chrg 1

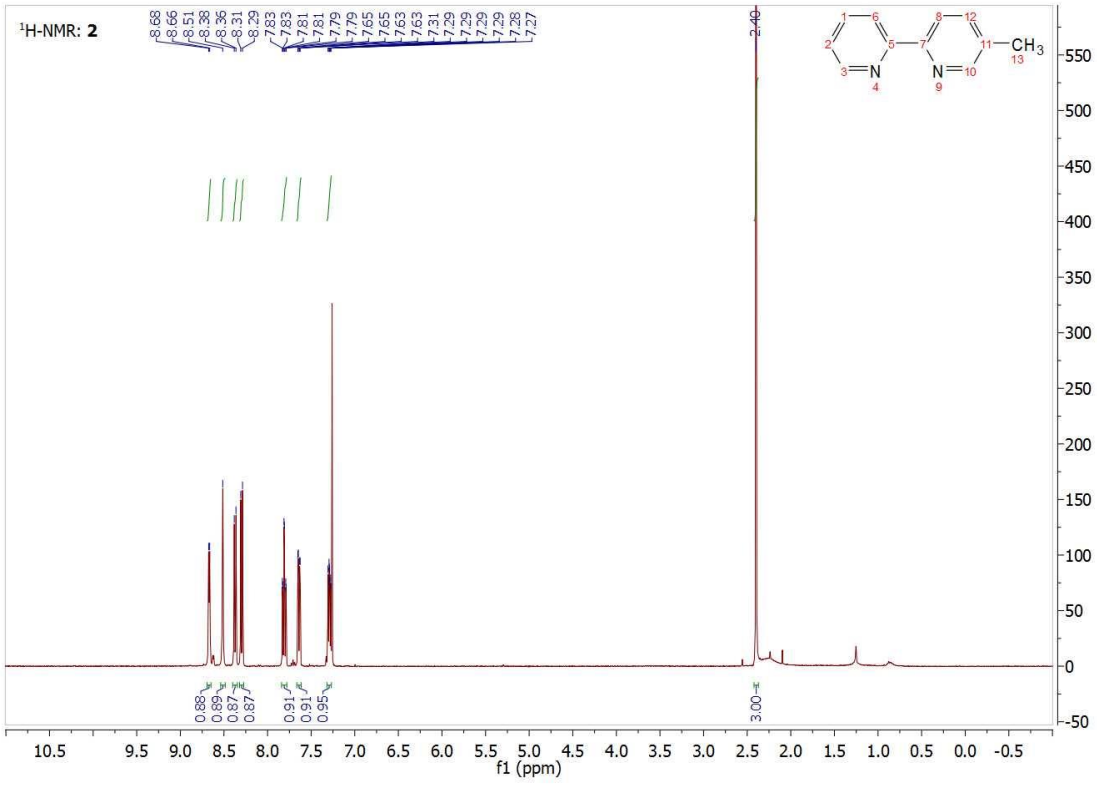
1H-NMR: 2
8.68
8.66
8.51
8.38
8.36
8.31
8.29
7.83
7.81
7.81
7.79
7.79
7.65
7.63
7.63
7.31
7.29
7.29
7.29
7.28
7.27
2.49
0.88
0.89
0.87
0.87
0.91
0.91
0.95
3.00
f1 (ppm)

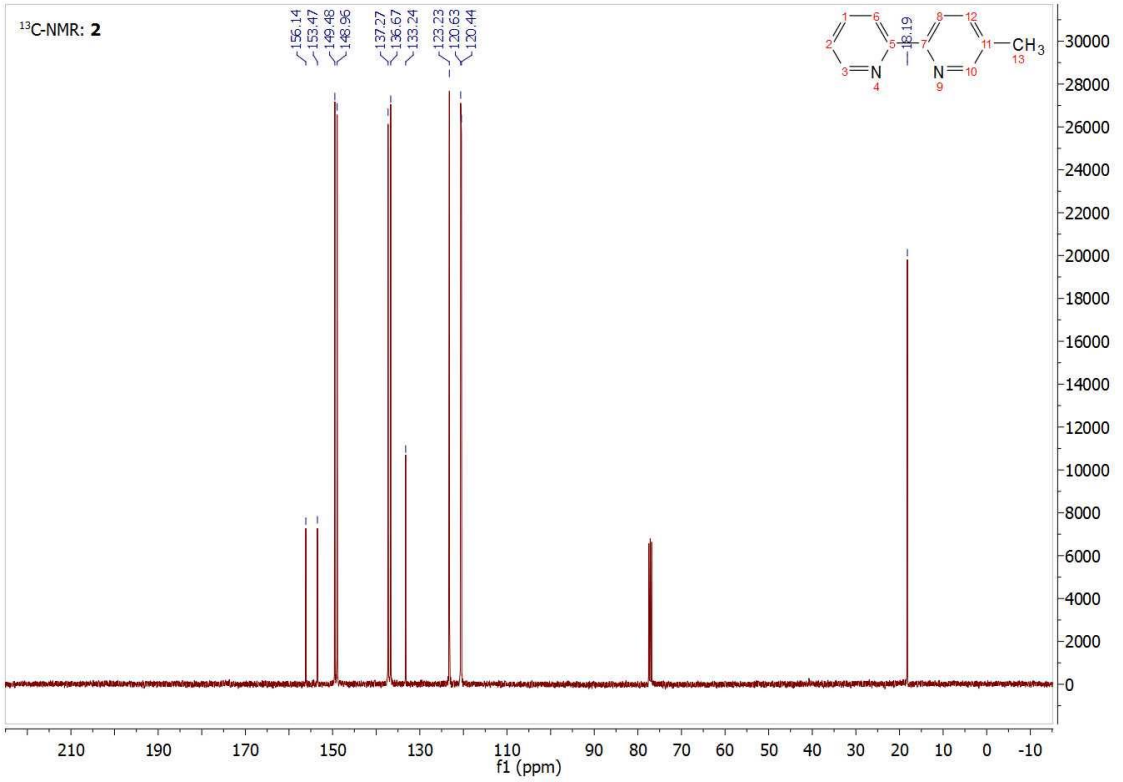
13C-NMR: 2
156.14
153.47
149.48
148.96
137.27
136.67
133.24
123.23
120.63
120.44
18.19
CH3
f1 (ppm)

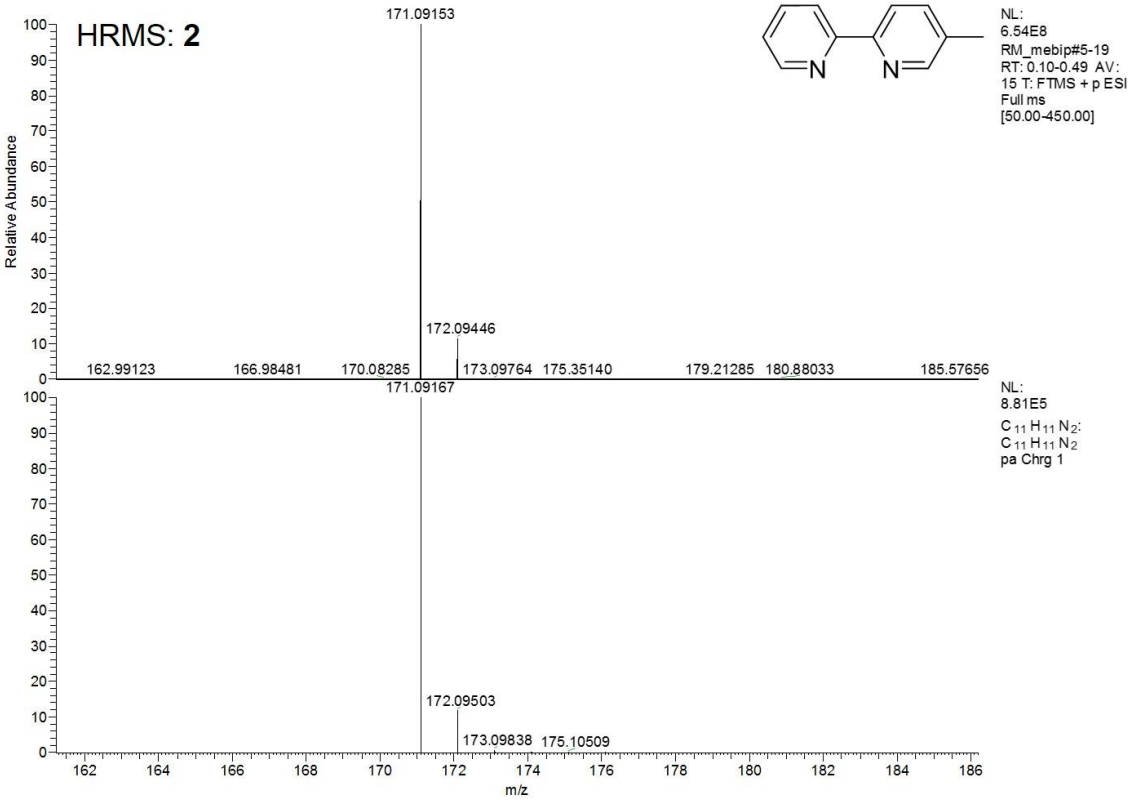
HRMS: 2
171.09153
172.09446
171.09167
172.09503
173.09838
175.10509
NL:
6.54E8
RM_mebip#5-19
RT: 0.10-0.49 AV:
15 T: FTMS + p ESI
Full ms
[50.00-450.00]
NL:
8.81E5
C11 H11 N2:
C11 H11 N2
pa Chrg 1
Relative Abundance
m/z

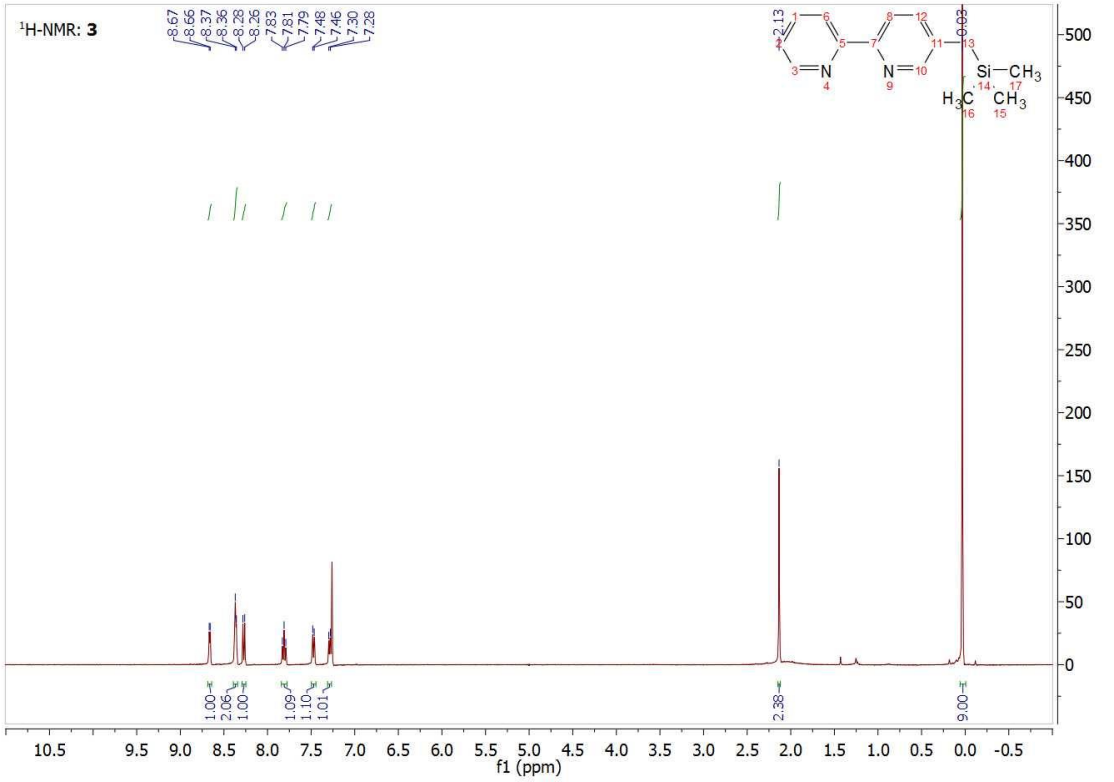
¹H-NMR: 3
8.67
8.66
8.37
8.36
8.28
8.26
7.83
7.81
7.79
7.48
7.46
7.30
7.28
2.13
0.03
1.00
2.06
1.00
1.09
1.10
1.01
2.38
9.00
f1 (ppm)

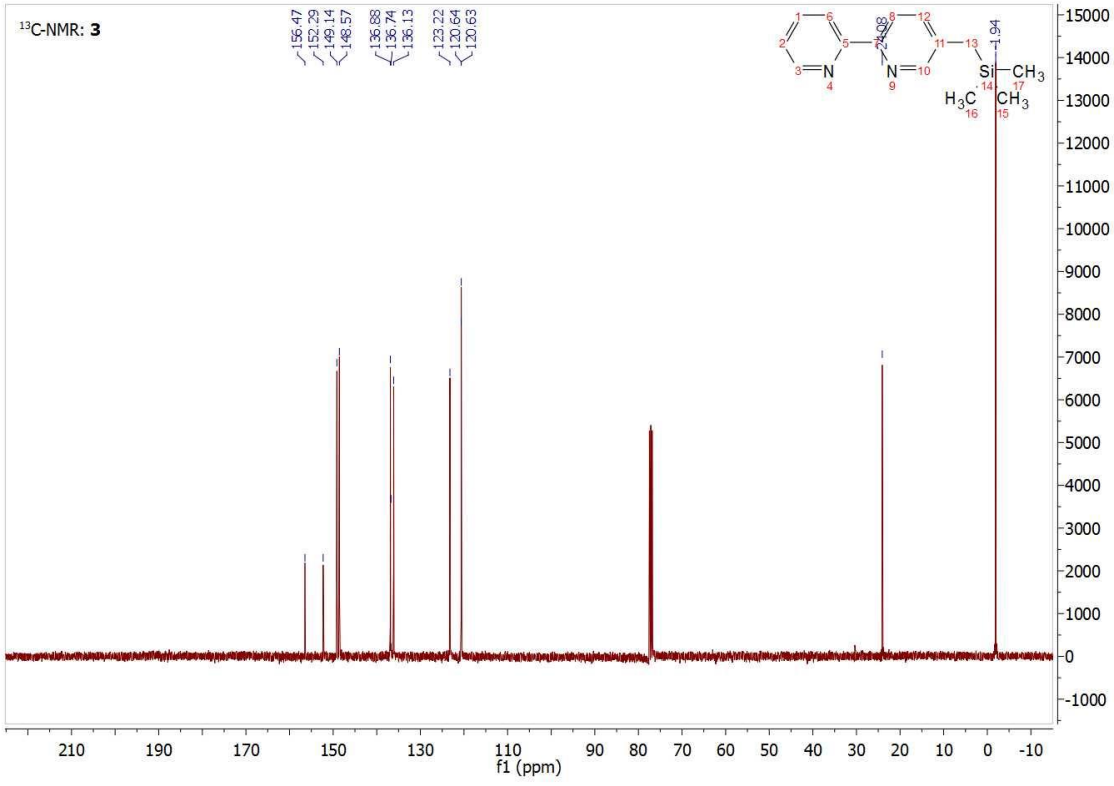
¹³C-NMR: 3
156.47
152.29
149.14
148.57
136.88
136.74
136.13
123.22
120.64
120.63
24.08
1.94
f1 (ppm)

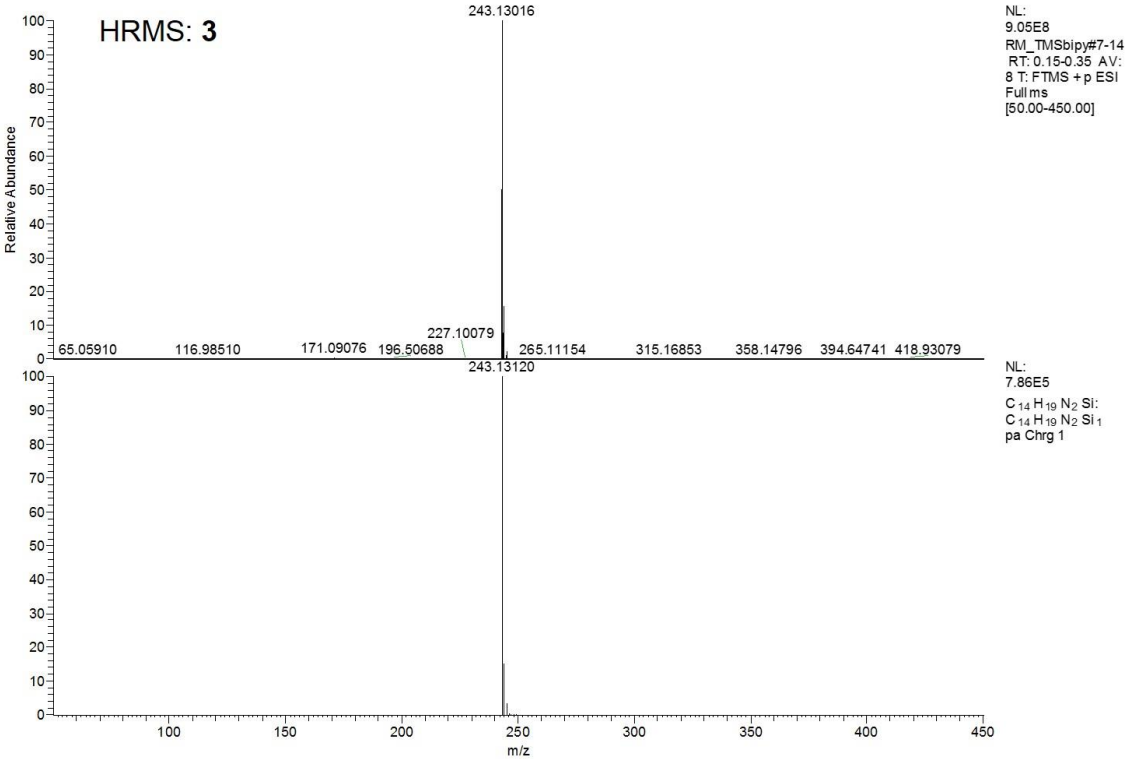
HRMS: 3
243.13016
NL:
9.05E8
RM_TMSbipy#7-14
RT: 0.15-0.35 AV:
8 T: FTMS + p ESI
Full ms
[50.00-450.00]
Relative Abundance
227.10079
65.05910
116.98510
171.09076
196.50688
265.11154
315.16853
358.14796
394.64741
418.93079
243.13120
NL:
7.86E5
C 14 H 19 N 2 Si:
C 14 H 19 N 2 Si 1
pa Chrg 1
m/z

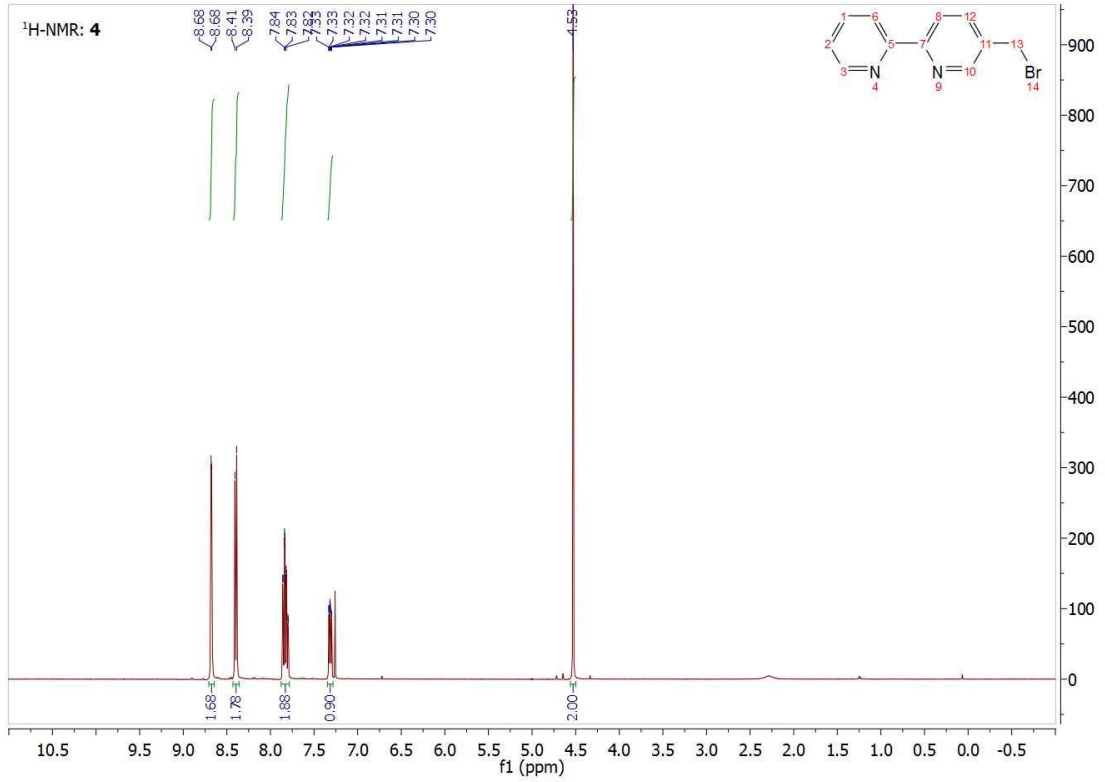
1H-NMR: 4
8.68
8.68
8.41
8.39
7.84
7.83
7.33
7.32
7.32
7.31
7.31
7.30
7.30
4.53
Br
1.68
1.78
1.88
0.90
2.00
f1 (ppm)

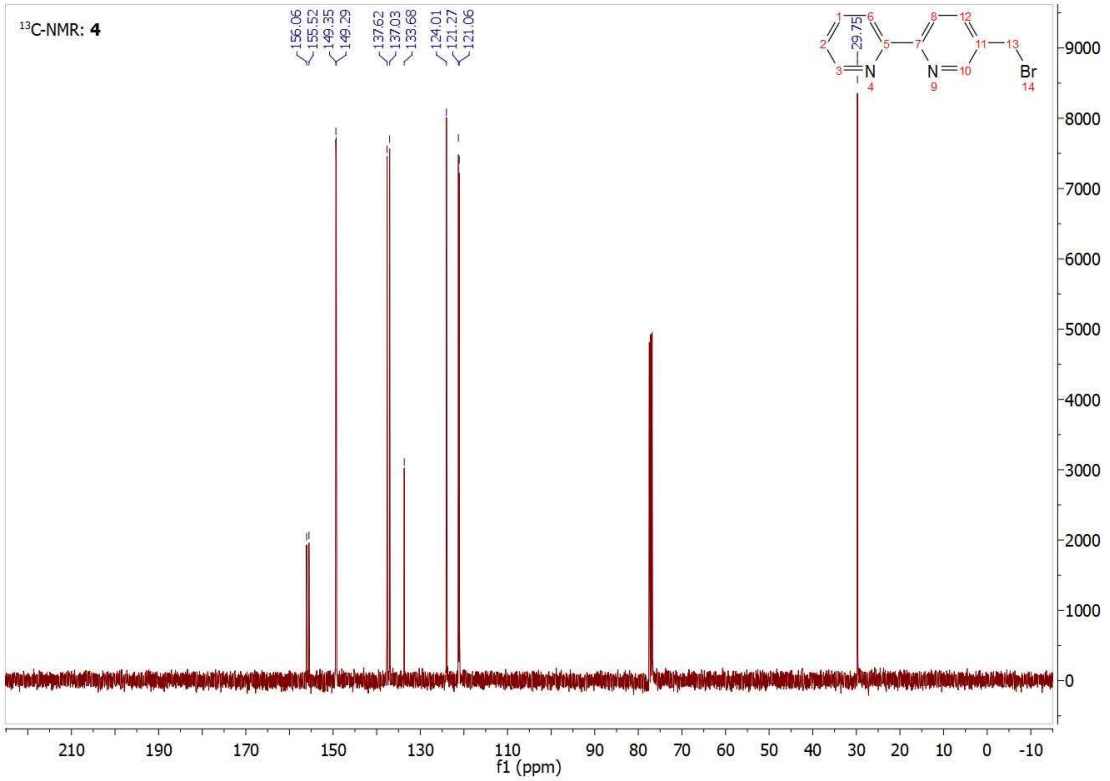
^{13}C-NMR: **4**
156.06
155.52
149.35
149.29
137.62
137.03
133.68
124.01
121.27
121.06
29.75
Br
f1 (ppm)

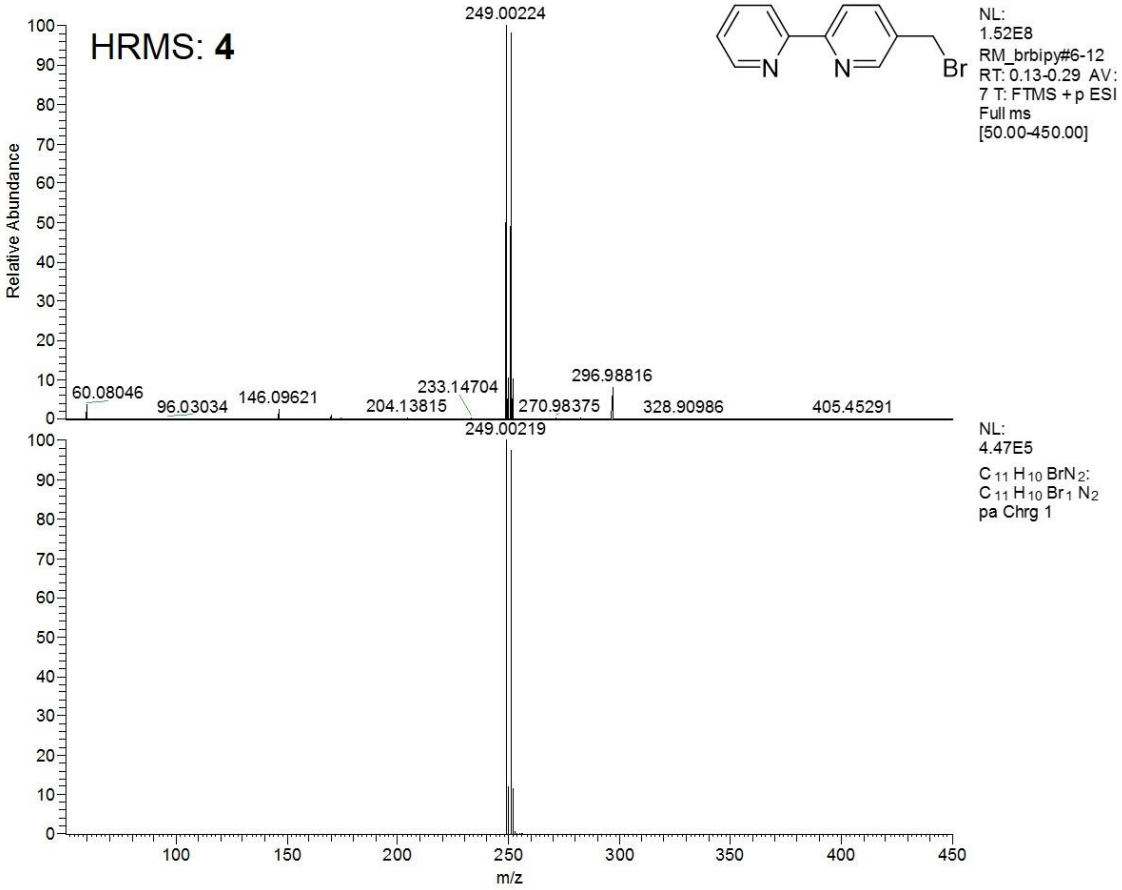
HRMS: **4**
249.00224
Br
NL:
1.52E8
RM_brbipy#6-12
RT: 0.13-0.29 AV:
7 T: FTMS + p ESI
Full ms
[50.00-450.00]
Relative Abundance
60.08046
96.03034
146.09621
204.13815
233.14704
249.00219
270.98375
296.98816
328.90986
405.45291
NL:
4.47E5
$C_{11}H_{10}BrN_2$:
$C_{11}H_{10}Br_1N_2$
pa Chrg 1
m/z

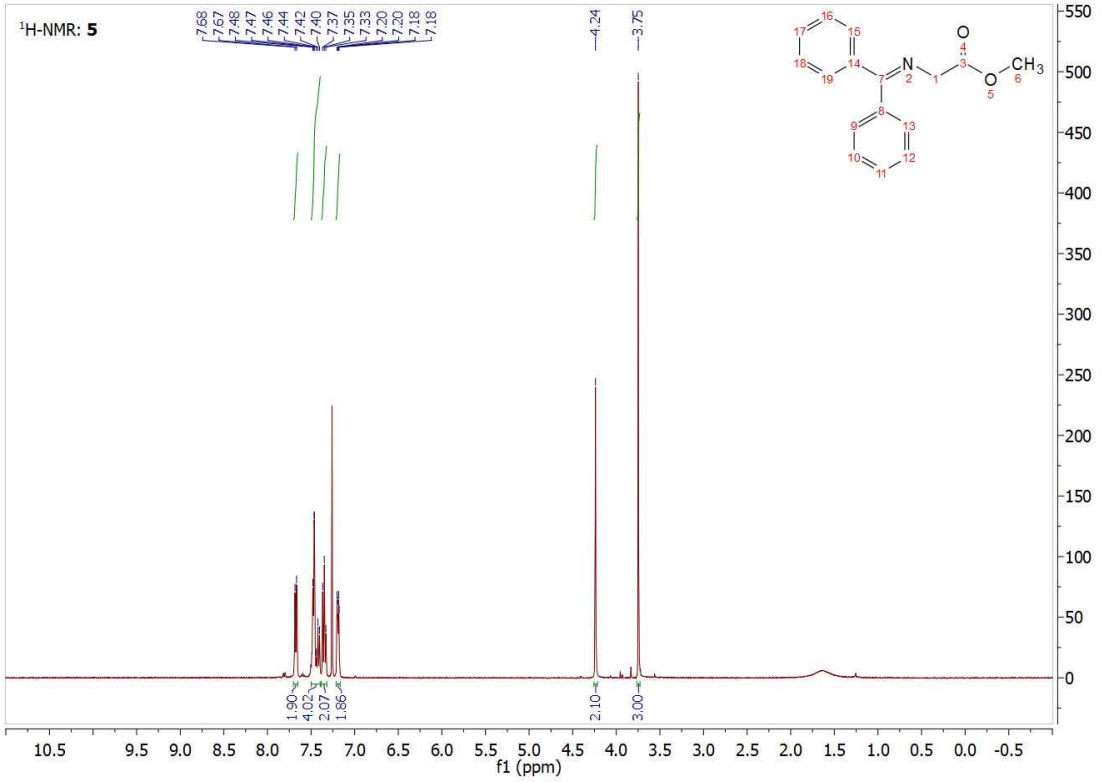
¹H-NMR: 5
7.68
7.67
7.48
7.47
7.46
7.44
7.42
7.40
7.37
7.35
7.33
7.20
7.18
7.18
4.24
3.75
1.90
4.02
2.07
1.86
2.10
3.00
f1 (ppm)

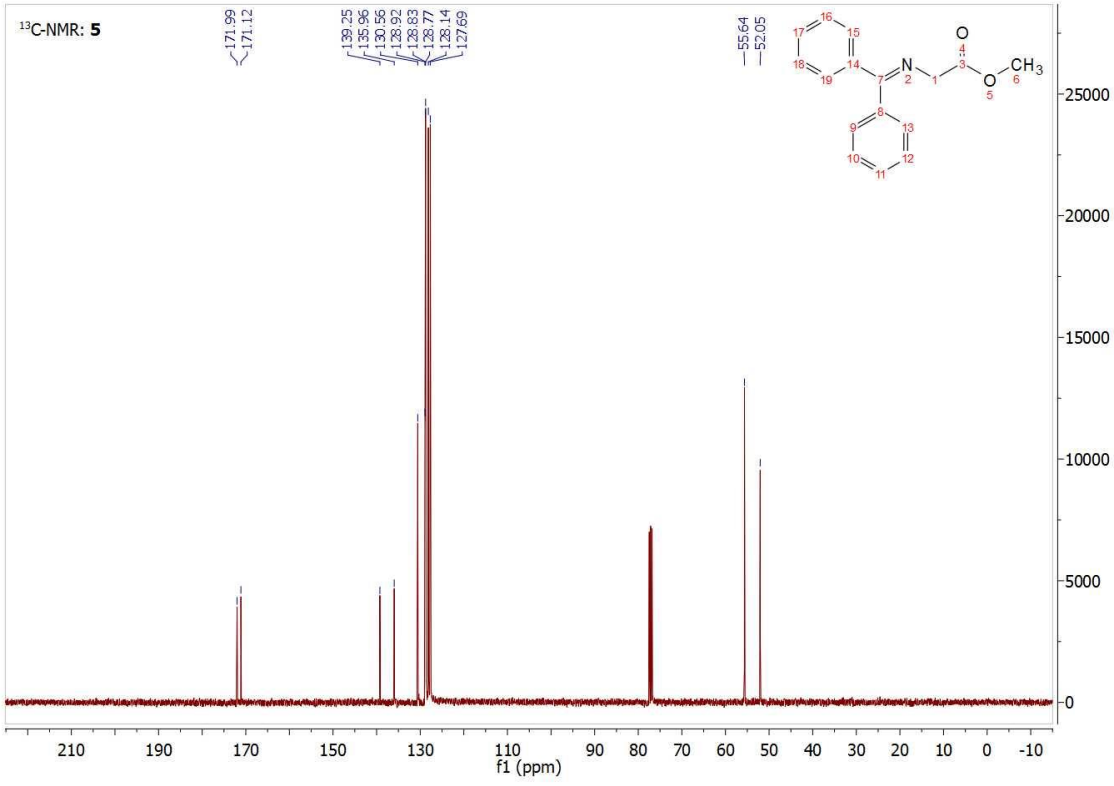
¹³C-NMR: 5
171.99
171.12
139.25
135.96
130.56
128.92
128.83
128.77
128.14
127.69
55.64
52.05
f1 (ppm)

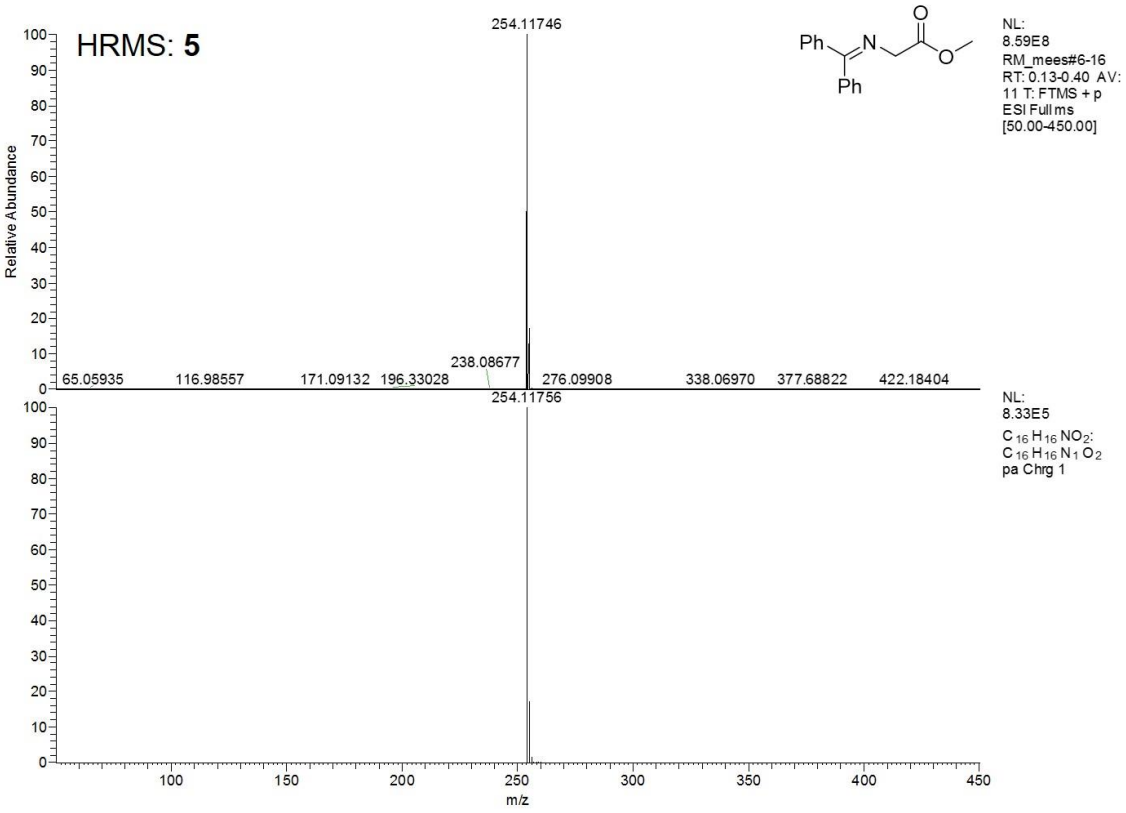
HRMS: 5
254.11746
NL:
8.59E8
RM_mees#6-16
RT: 0.13-0.40 AV:
11 T: FTMS + p
ESI Full ms
[50.00-450.00]
Relative Abundance
65.05935
116.98557
171.09132
196.33028
238.08677
276.09908
338.06970
377.68822
422.18404
254.11756
NL:
8.33E5
C16 H16 NO2:
C16 H16 N1 O2
pa Chrg 1
m/z

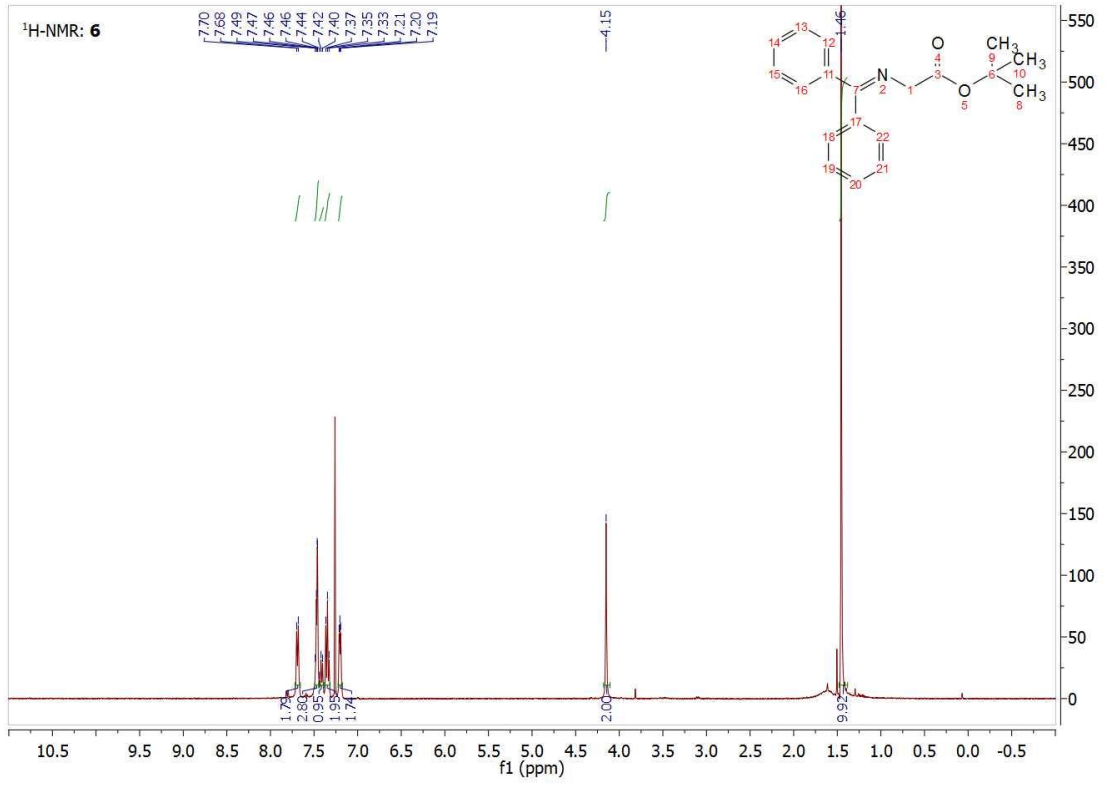
1H-NMR: 6
7.70
7.68
7.49
7.47
7.46
7.46
7.44
7.42
7.40
7.37
7.35
7.33
7.21
7.20
7.19
4.15
1.46
1.79
2.80
0.95
1.95
1.74
2.00
9.92
f1 (ppm)

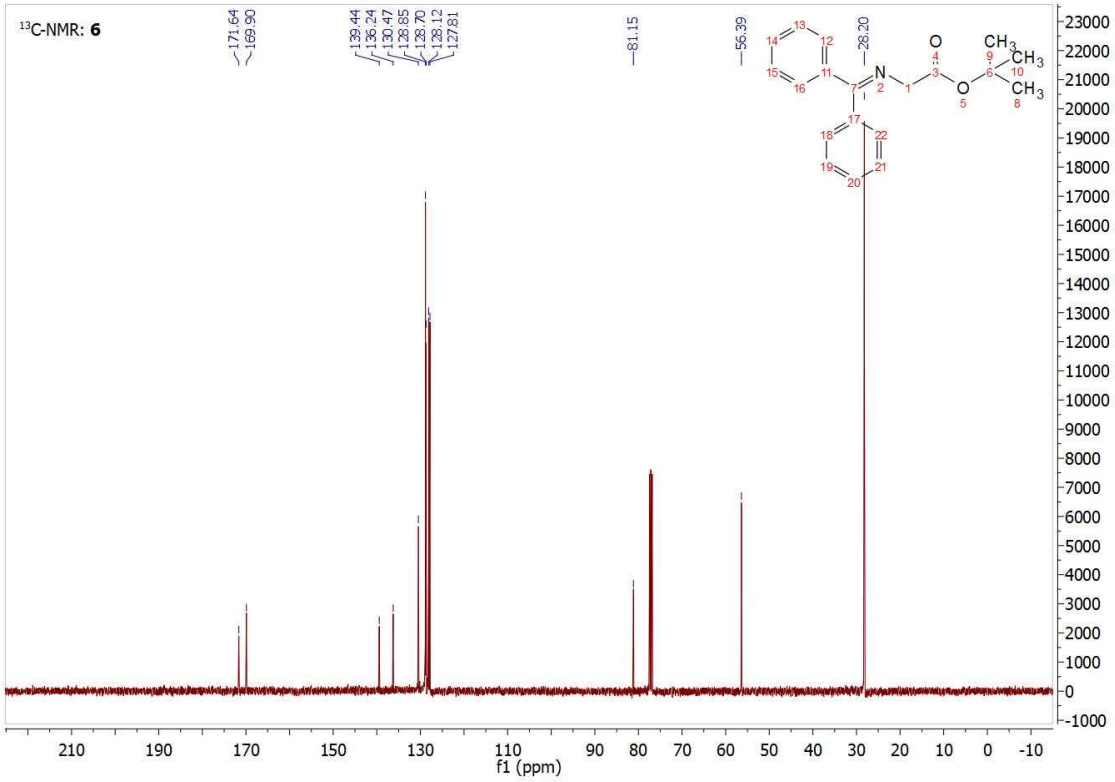
13C-NMR: 6
171.64
169.90
139.44
136.24
130.47
128.85
128.70
128.12
127.81
81.15
56.39
28.20
f1 (ppm)

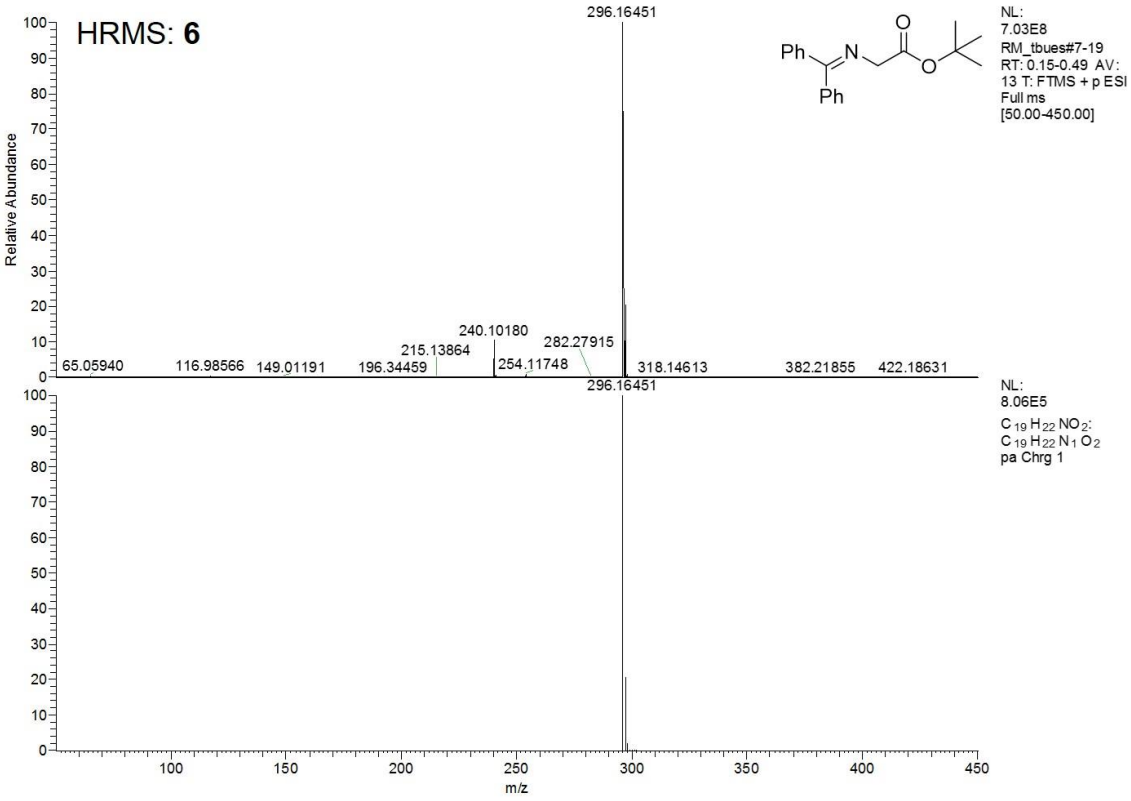
HRMS: 6
296.16451
NL:
7.03E8
RM_tbues#7-19
RT: 0.15-0.49 AV:
13 T: FTMS + p ESI
Full ms
[50.00-450.00]
Relative Abundance
65.05940
116.98566
149.01191
196.34459
215.13864
240.10180
254.11748
282.27915
318.14613
382.21855
422.18631
NL:
8.06E5
C19H22NO2:
C19H22N1O2
pa Chrg 1
m/z

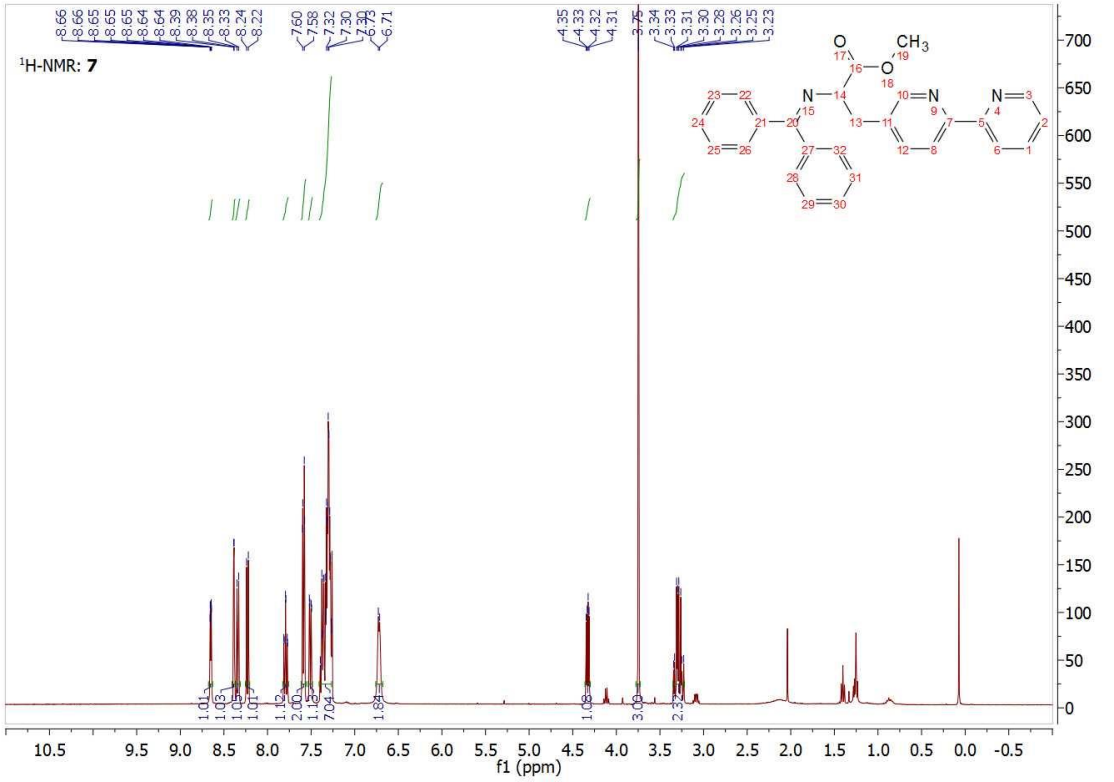
^{1}H-NMR: **7**
f1 (ppm)

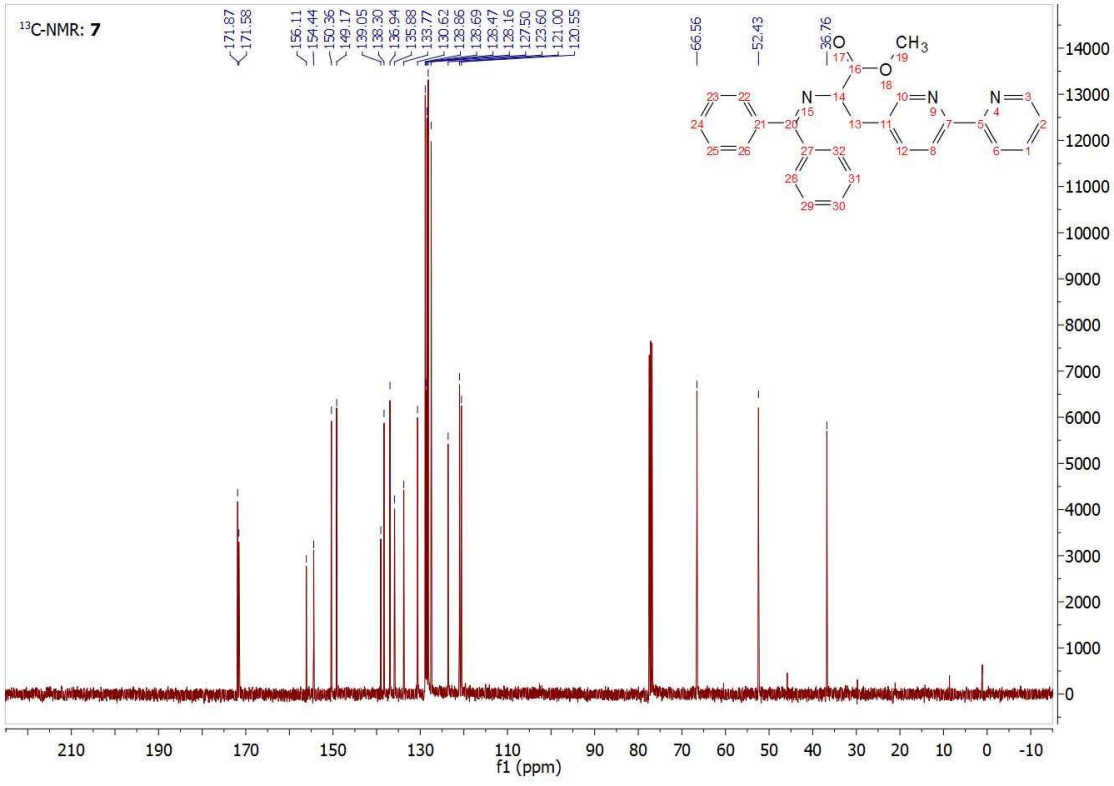
^{13}C-NMR: **7**
f1 (ppm)

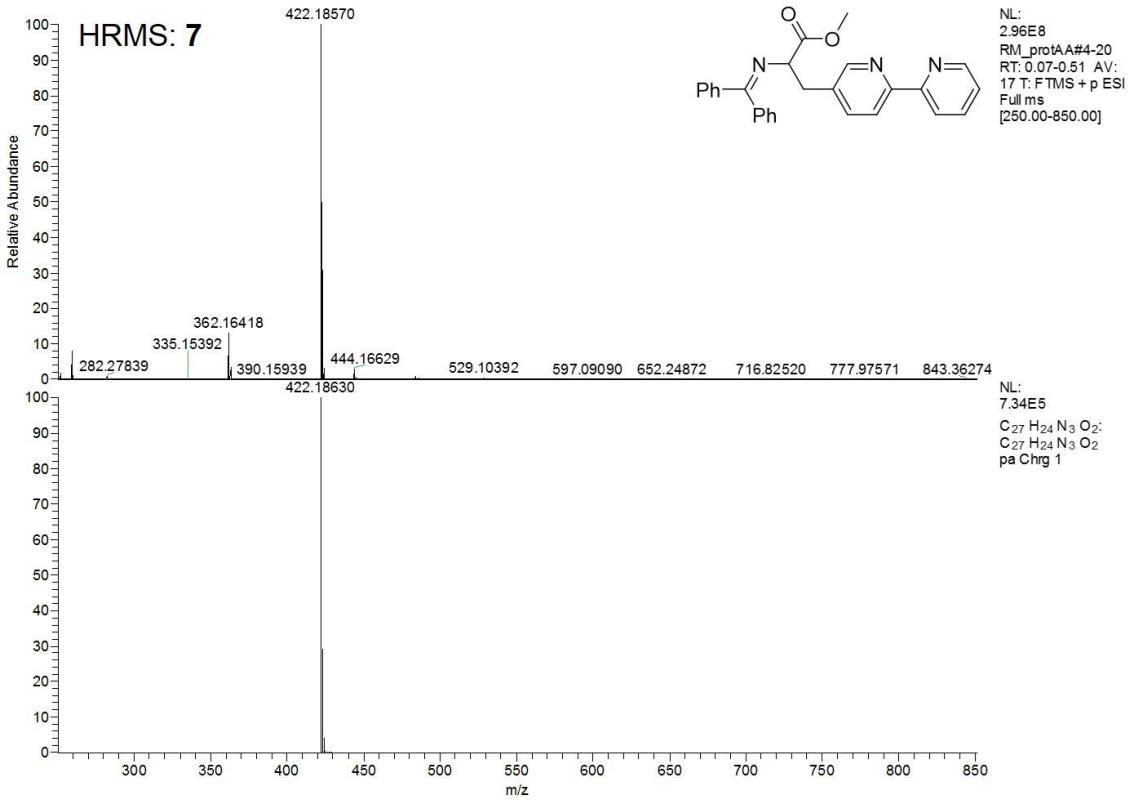
HRMS: 7
422.18570
NL:
2.96E8
RM_protAA#4-20
RT: 0.07-0.51 AV:
17 T: FTMS + p ESI
Full ms
[250.00-850.00]
Relative Abundance
362.16418
335.15392
282.27839
390.15939
444.16629
529.10392
597.09090
652.24872
716.82520
777.97571
843.36274
422.18630
NL:
7.34E5
C27 H24 N3 O2:
C27 H24 N3 O2
pa Chrg 1
m/z

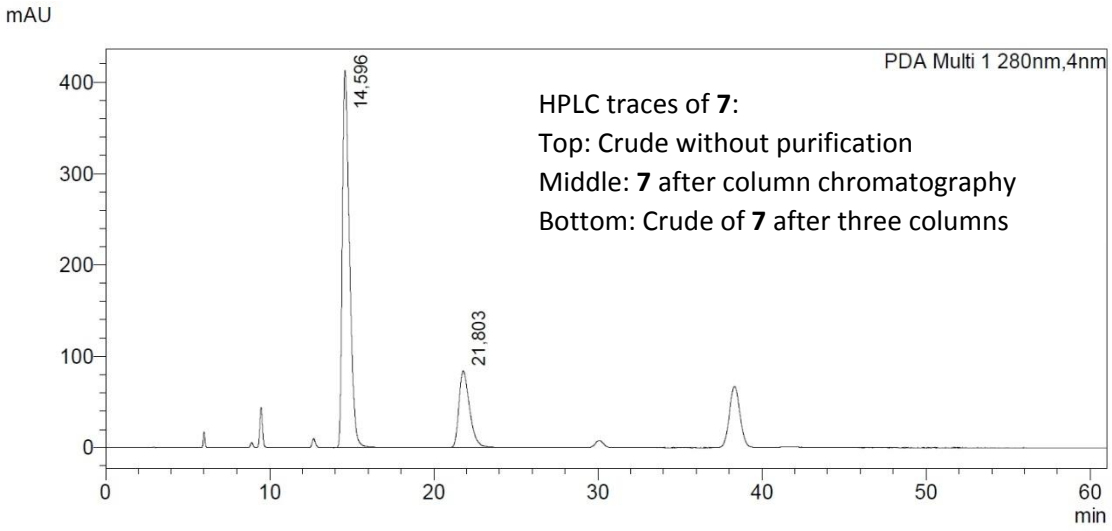

HPLC traces of **7**:
Top: Crude without purification
Middle: **7** after column chromatography
Bottom: Crude of **7** after three columns

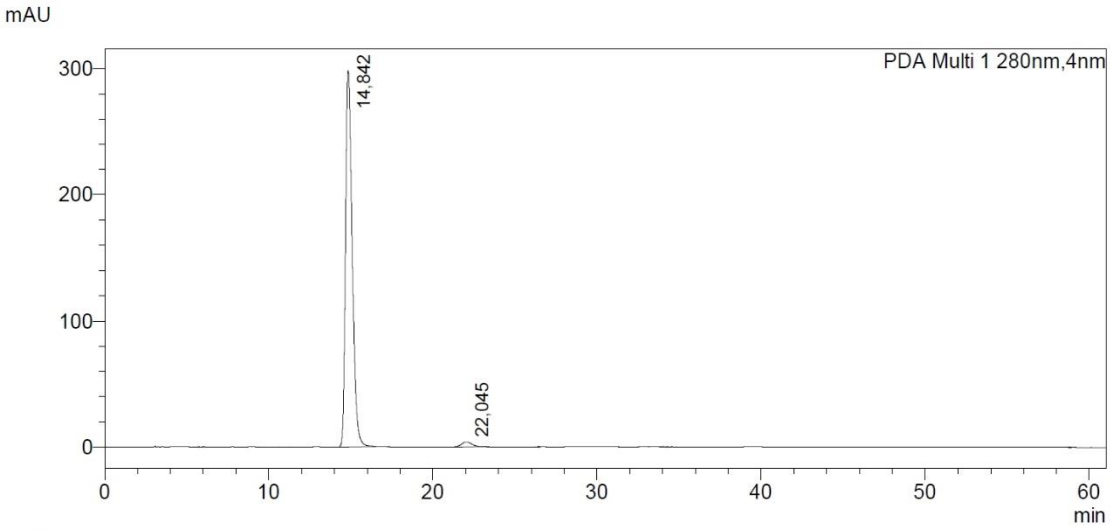

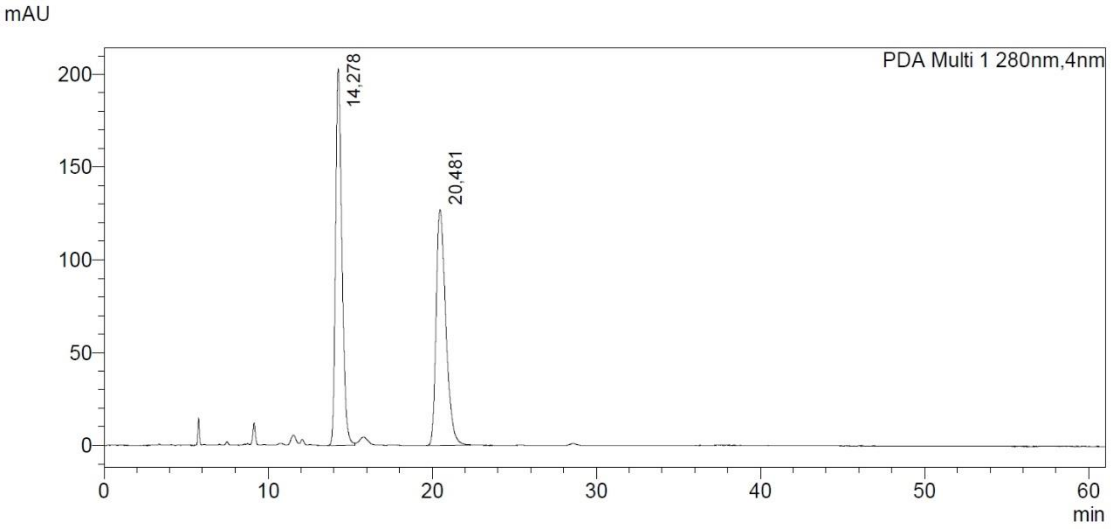

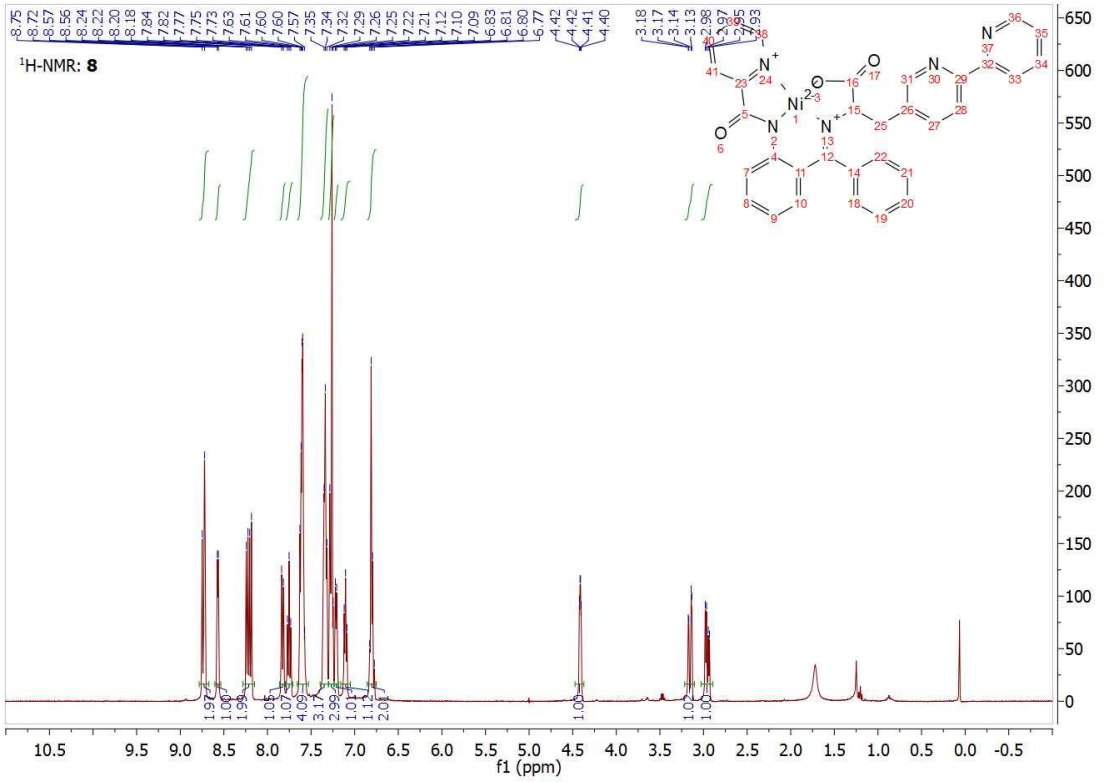
^{1}H-NMR: **8**
f1 (ppm)

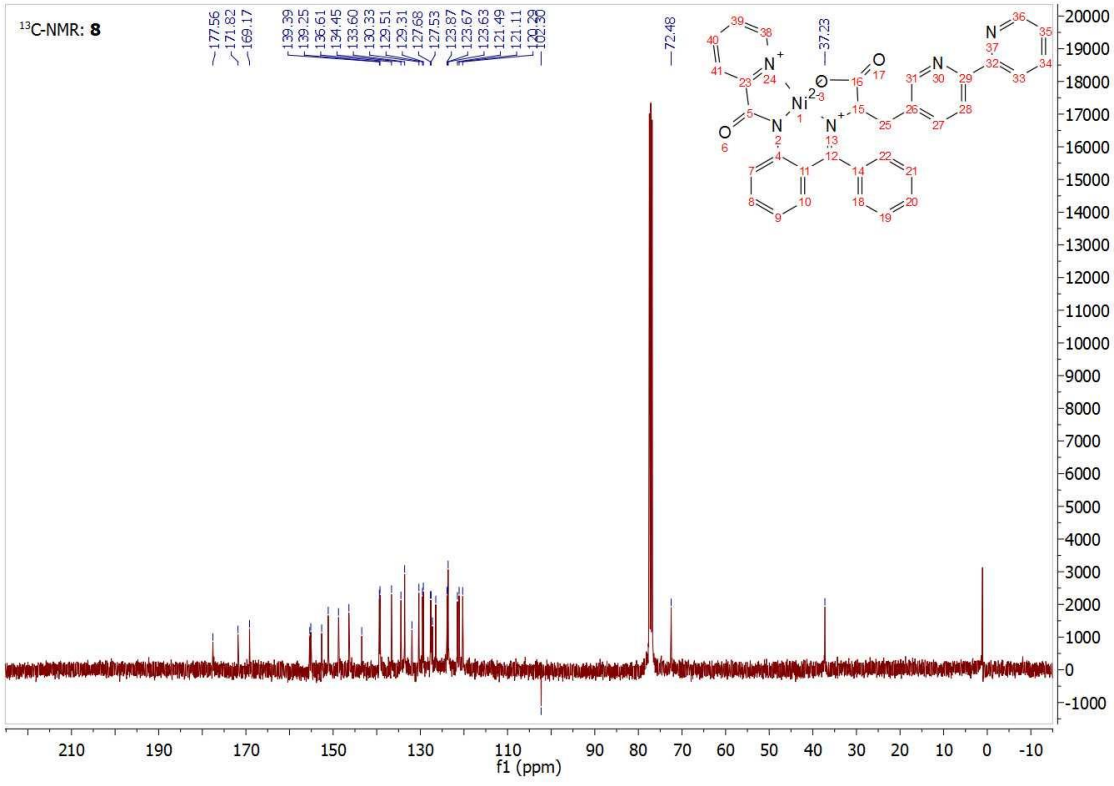
^{13}C-NMR: **8**
f1 (ppm)

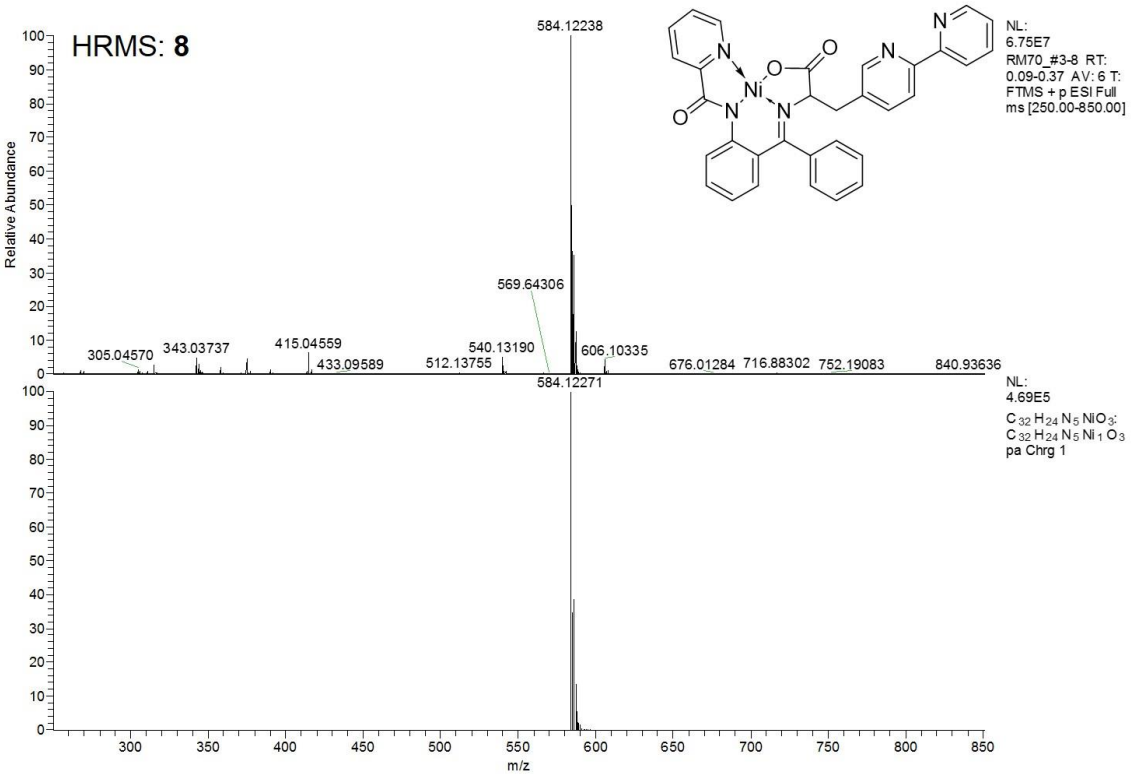
HRMS: 8
584.12238
569.64306
305.04570
343.03737
415.04559
433.09589
512.13755
540.13190
584.12271
606.10335
676.01284
716.88302
752.19083
840.93636
Relative Abundance
m/z
NL:
6.75E7
RM70_#3-8 RT:
0.09-0.37 AV: 6 T:
FTMS + p ESI Full
ms [250.00-850.00]
NL:
4.69E5
C32 H24 N5 NiO3:
C32 H24 N5 Ni1 O3
pa Chrg 1

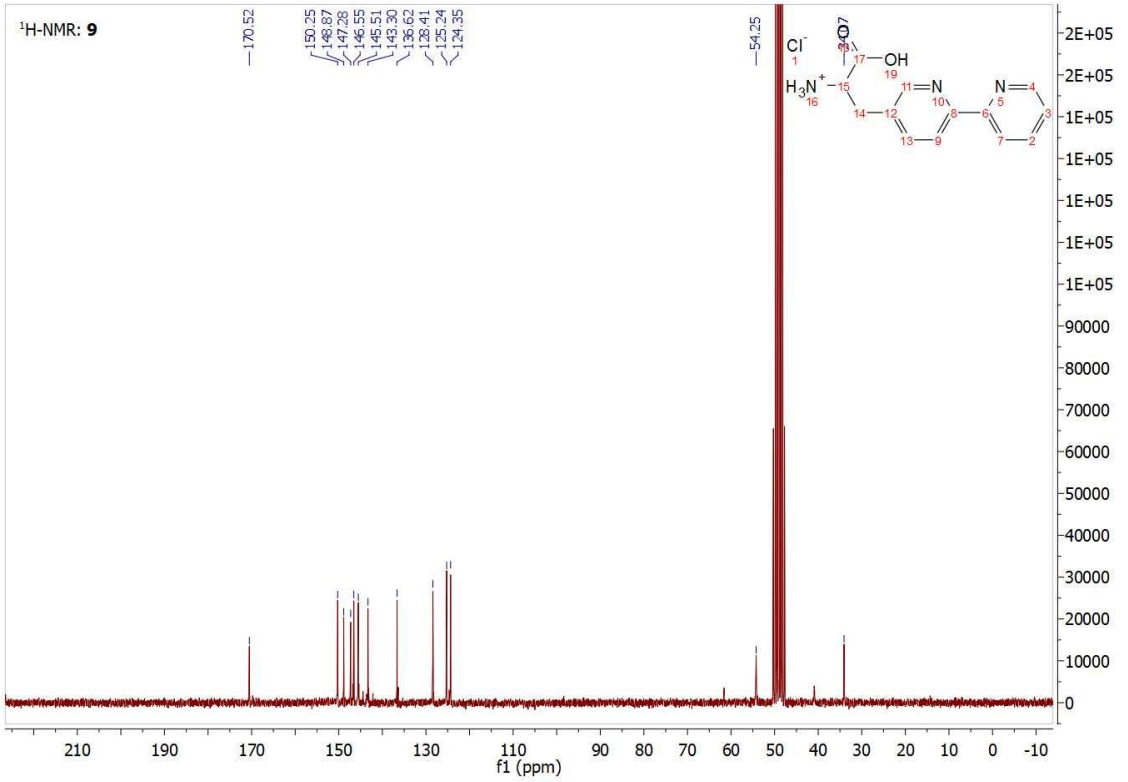
1H-NMR: 9
170.52
150.25
148.87
147.28
146.55
145.51
143.30
136.62
128.41
125.24
124.35
54.25
f1 (ppm)

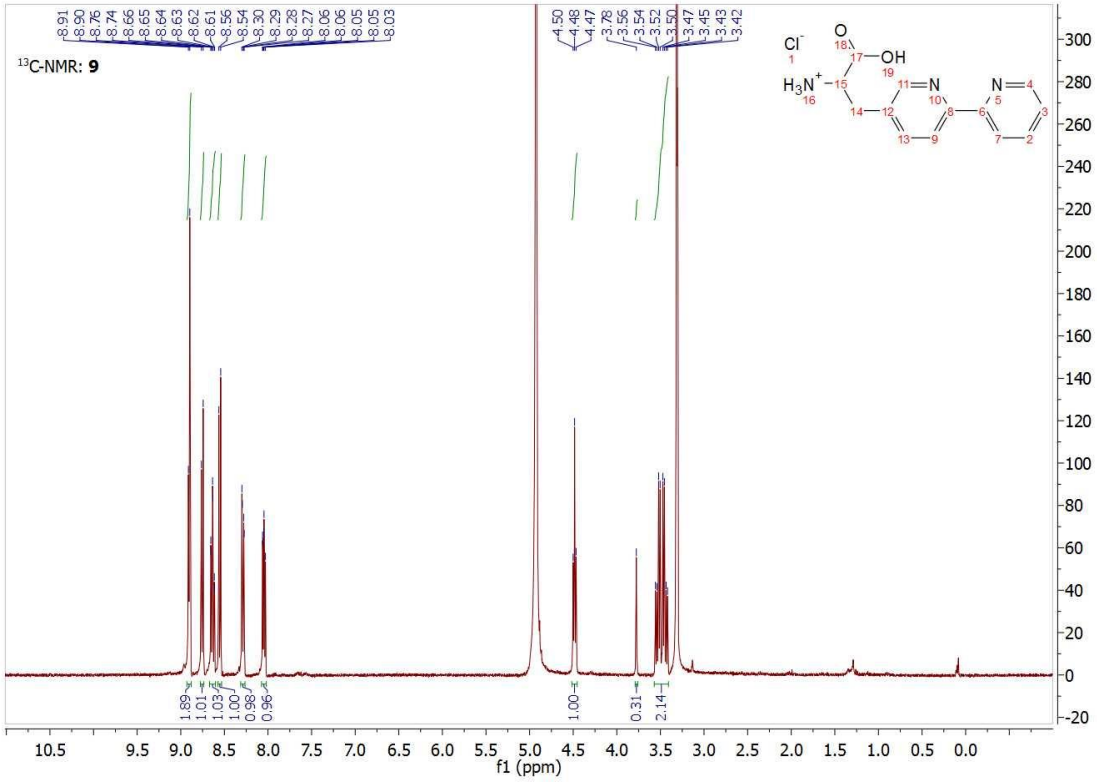
^{13}C-NMR: **9**
f1 (ppm)

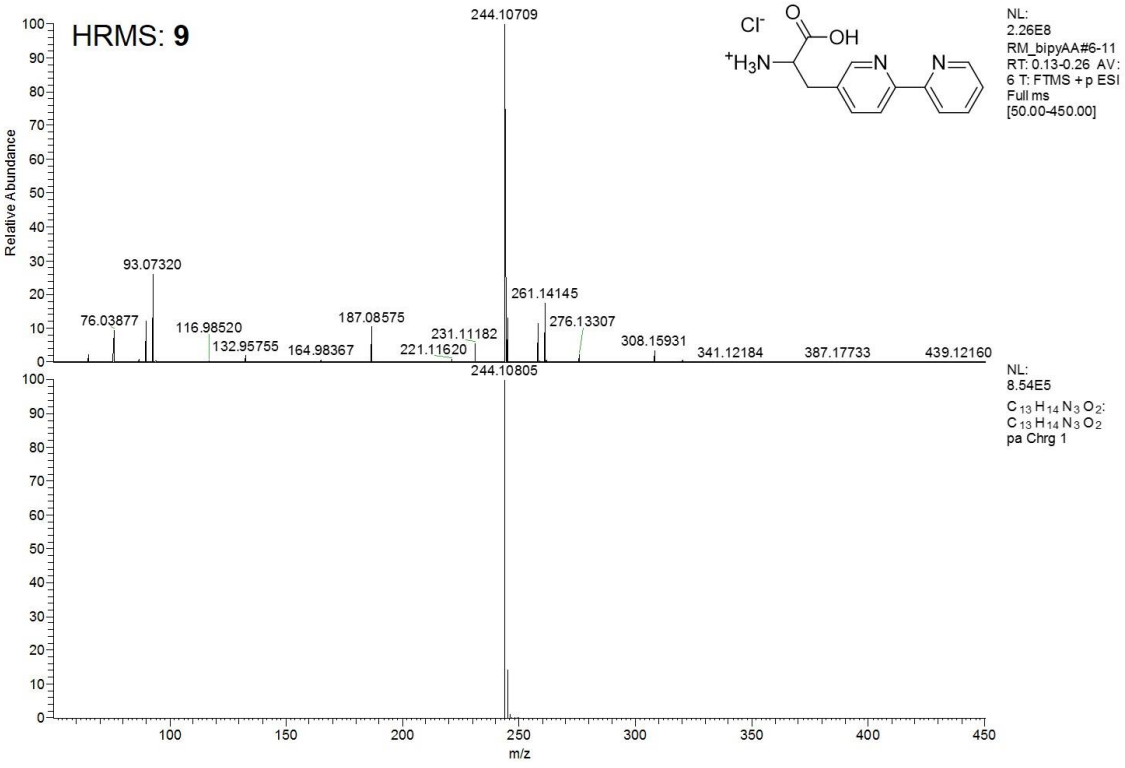
HRMS: **9**
244.10709
93.07320
261.14145
276.13307
187.08575
116.98520
76.03877
132.95755
164.98367
221.11620
231.11182
308.15931
341.12184
387.17733
439.12160
244.10805
Relative Abundance
m/z

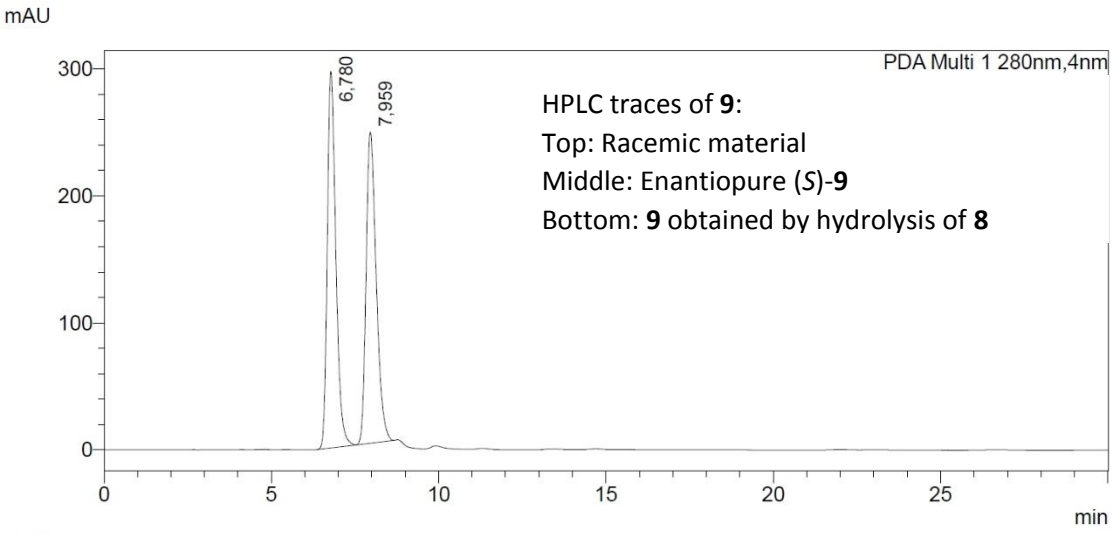

HPLC traces of **9**:
Top: Racemic material
Middle: Enantiopure (*S*)-**9**
Bottom: **9** obtained by hydrolysis of **8**

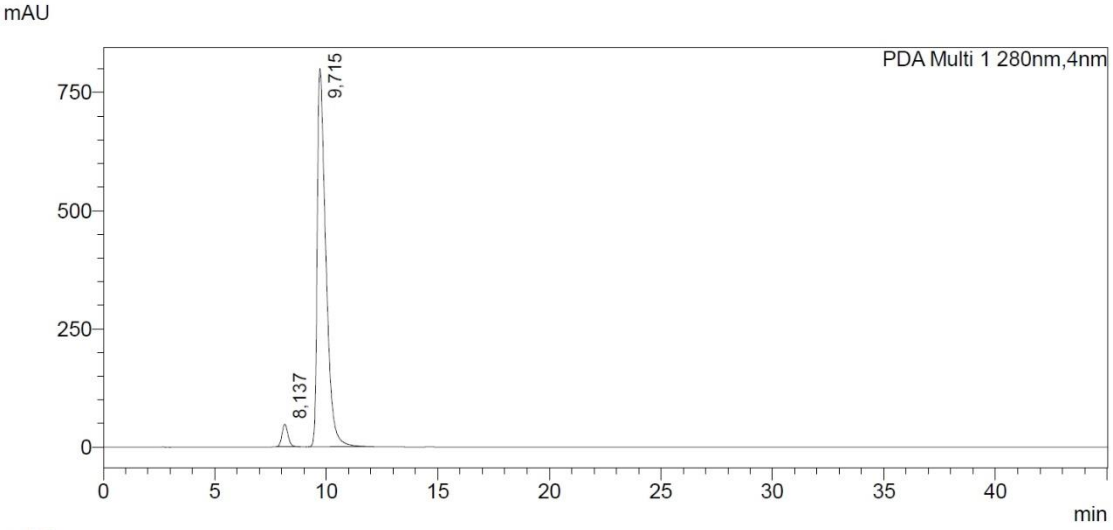

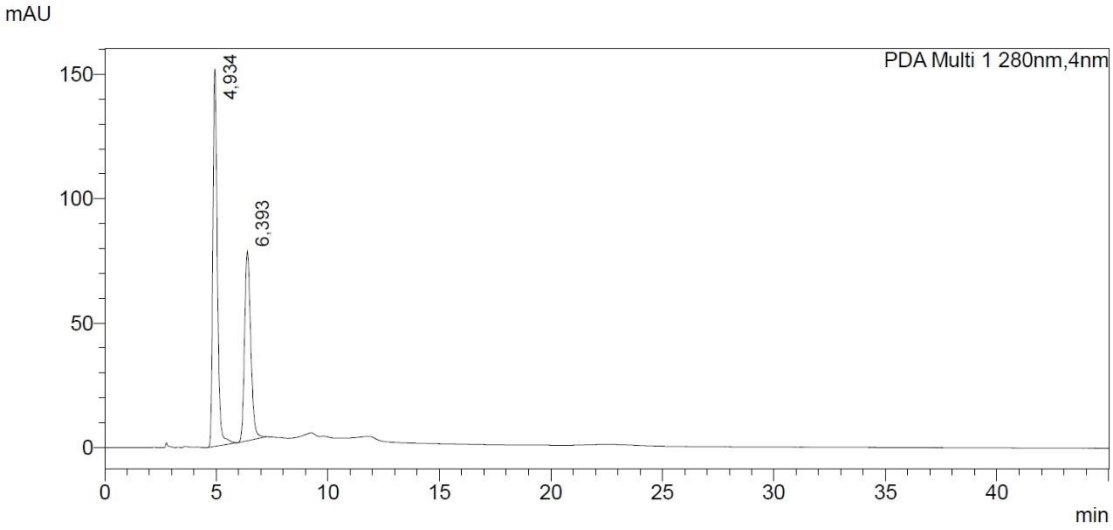

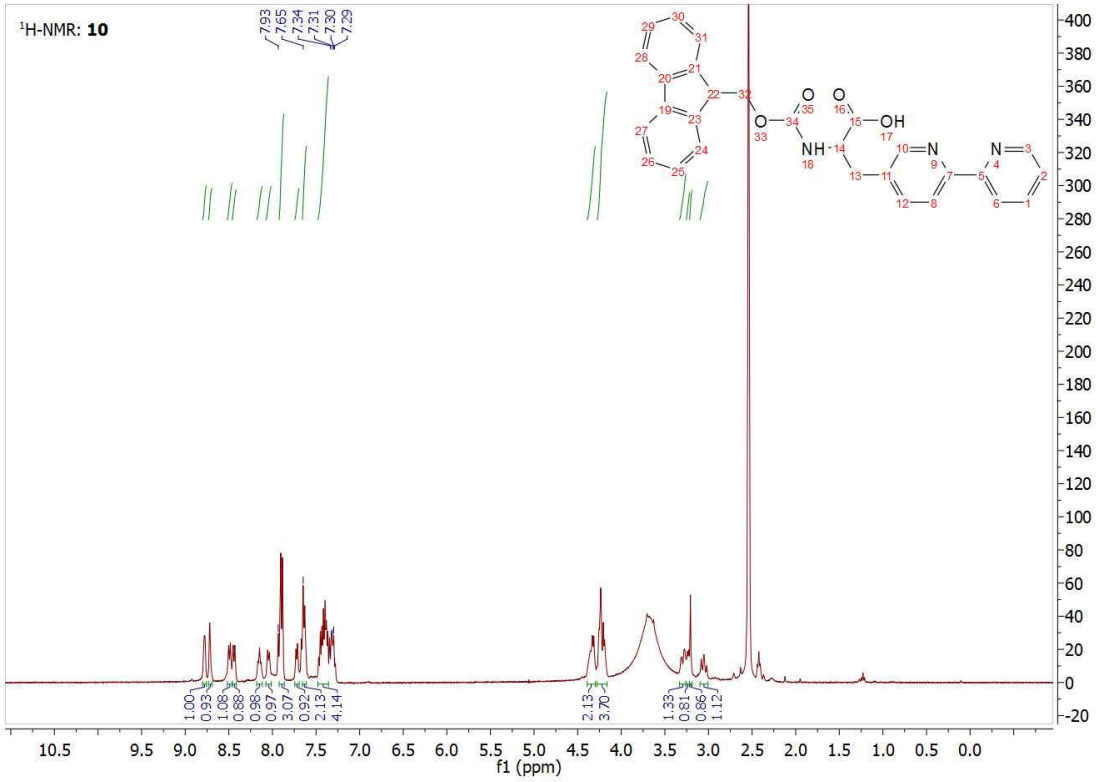
¹H-NMR: 10
f1 (ppm)

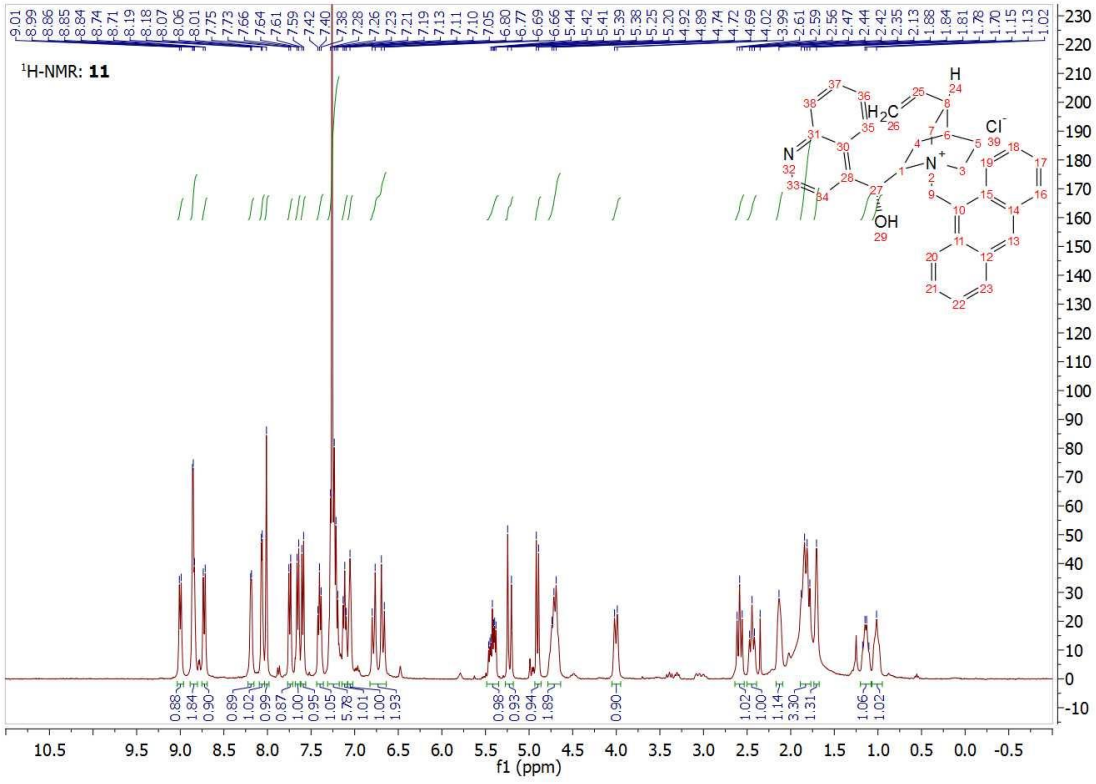
¹H-NMR: 11
f1 (ppm)

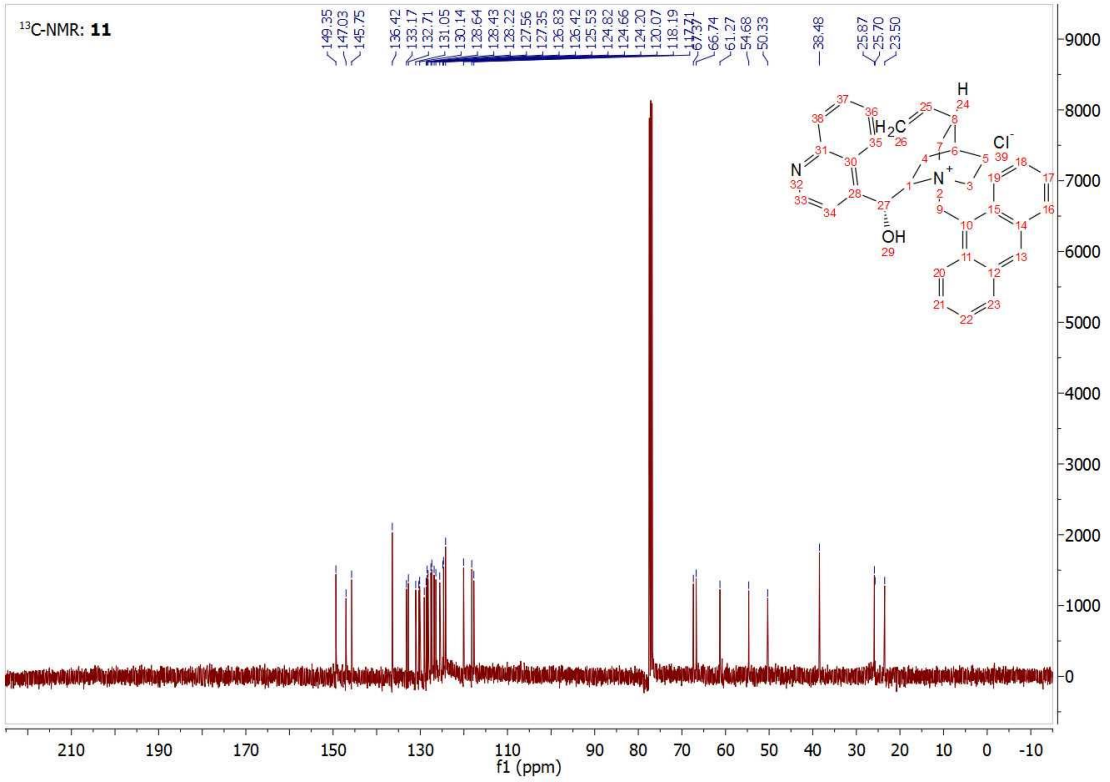
13C-NMR: 11
149.35
147.03
145.75
136.42
133.17
132.71
131.05
130.14
128.64
128.43
128.22
127.56
127.35
126.83
126.42
125.53
124.82
124.66
124.20
120.07
118.19
67.71
66.74
61.27
54.68
50.33
38.48
25.87
25.70
23.50
f1 (ppm)

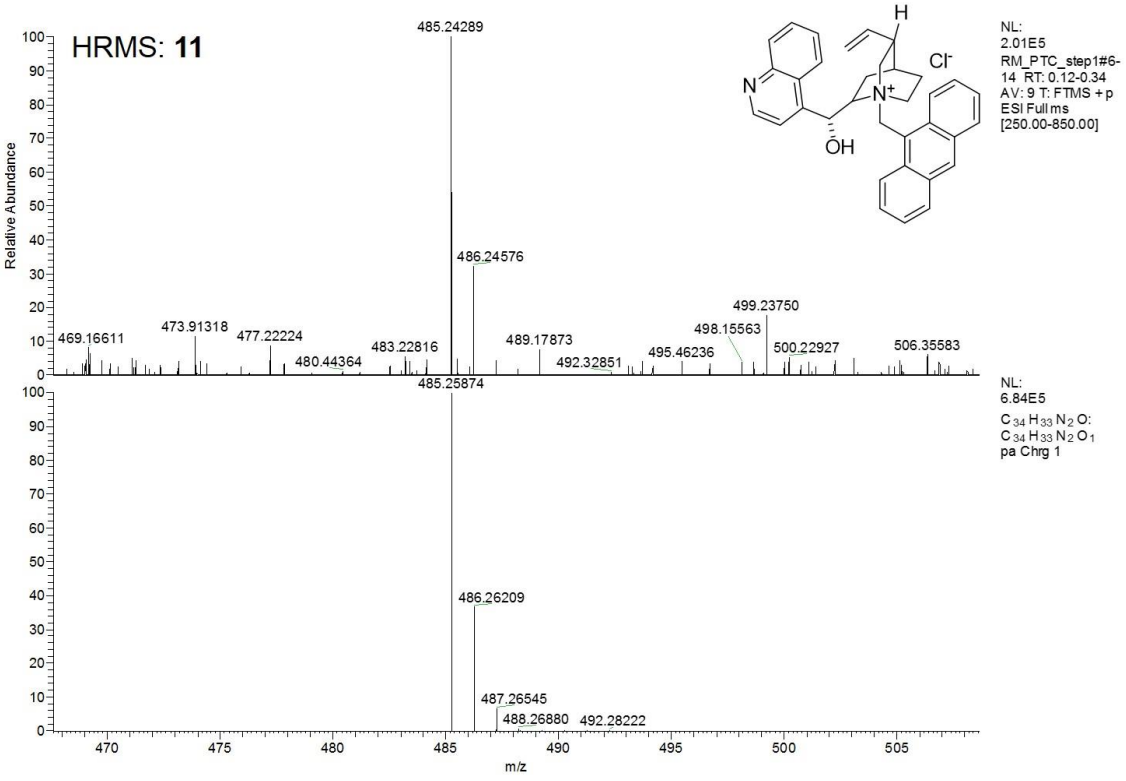
HRMS: 11
485.24289
486.24576
499.23750
498.15563
469.16611
473.91318
477.22224
480.44364
483.22816
489.17873
492.32851
495.46236
500.22927
506.35583
Relative Abundance
NL:
2.01E5
RM_PTC_step1#6-14 RT: 0.12-0.34 AV: 9 T: FTMS + p ESI Full ms [250.00-850.00]
485.25874
486.26209
487.26545
488.26880
492.28222
m/z
NL:
6.84E5
C34 H33 N2 O:
C34 H33 N2 O1
pa Chrg 1

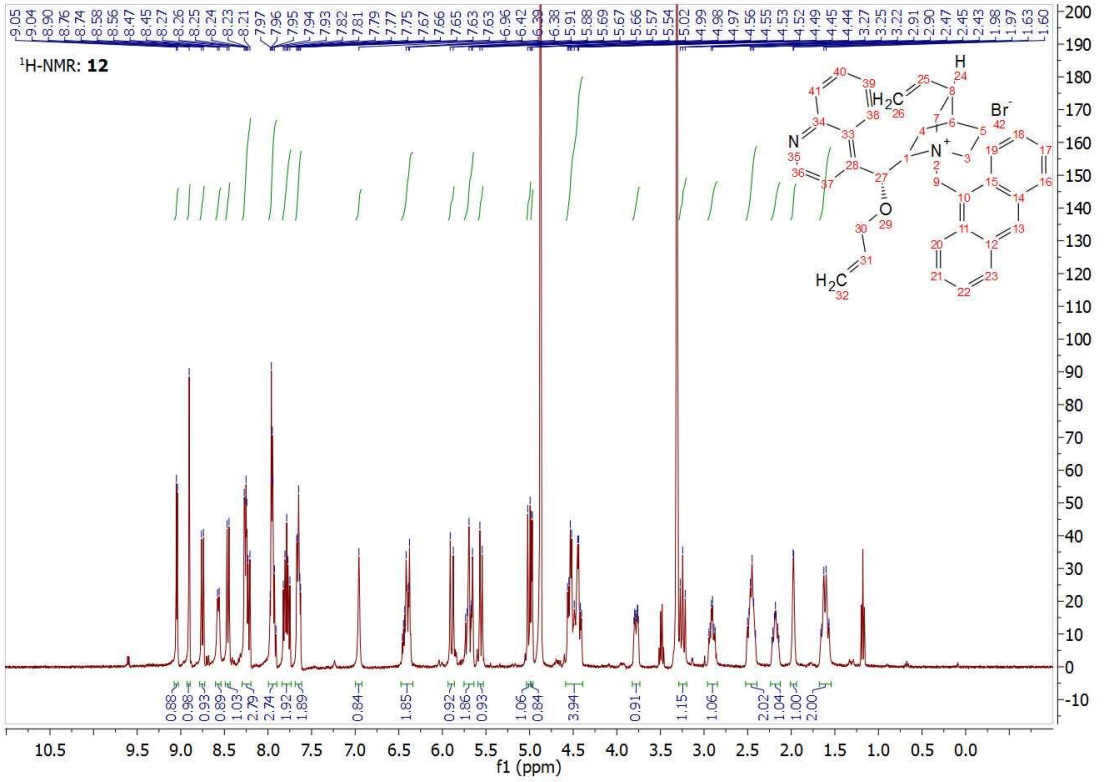
^{1}H-NMR: **12**
f1 (ppm)

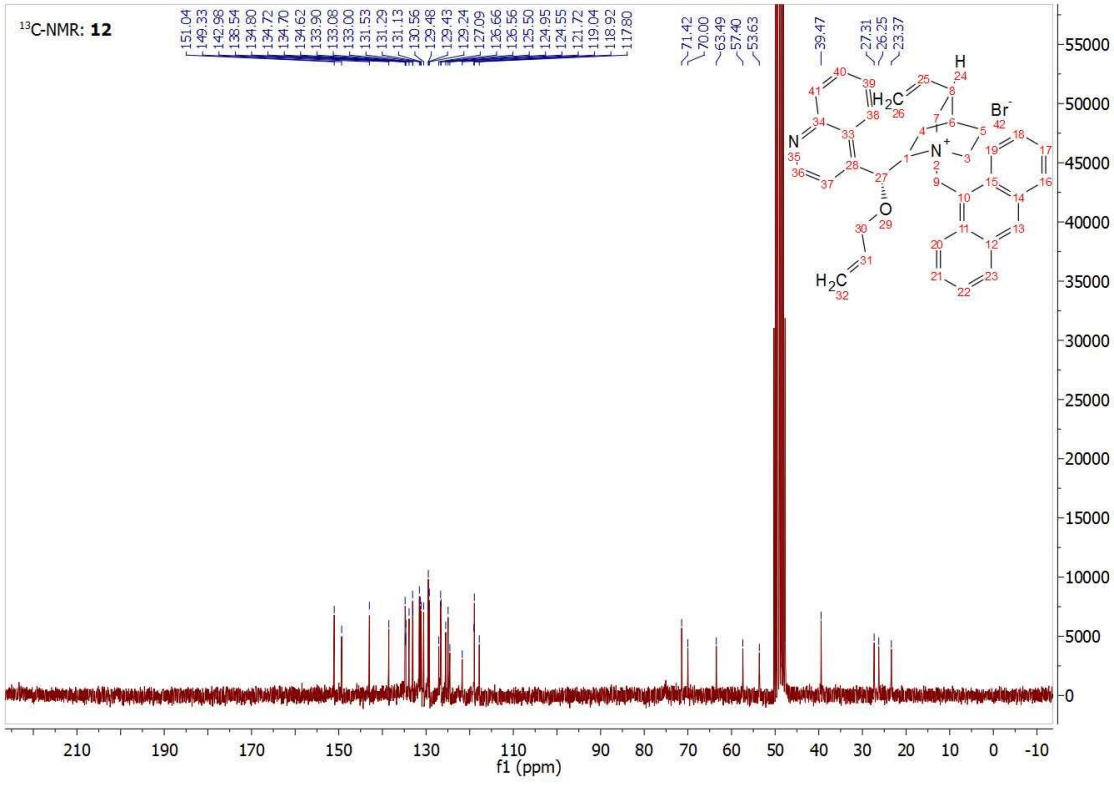
^{13}C-NMR: **12**
f1 (ppm)

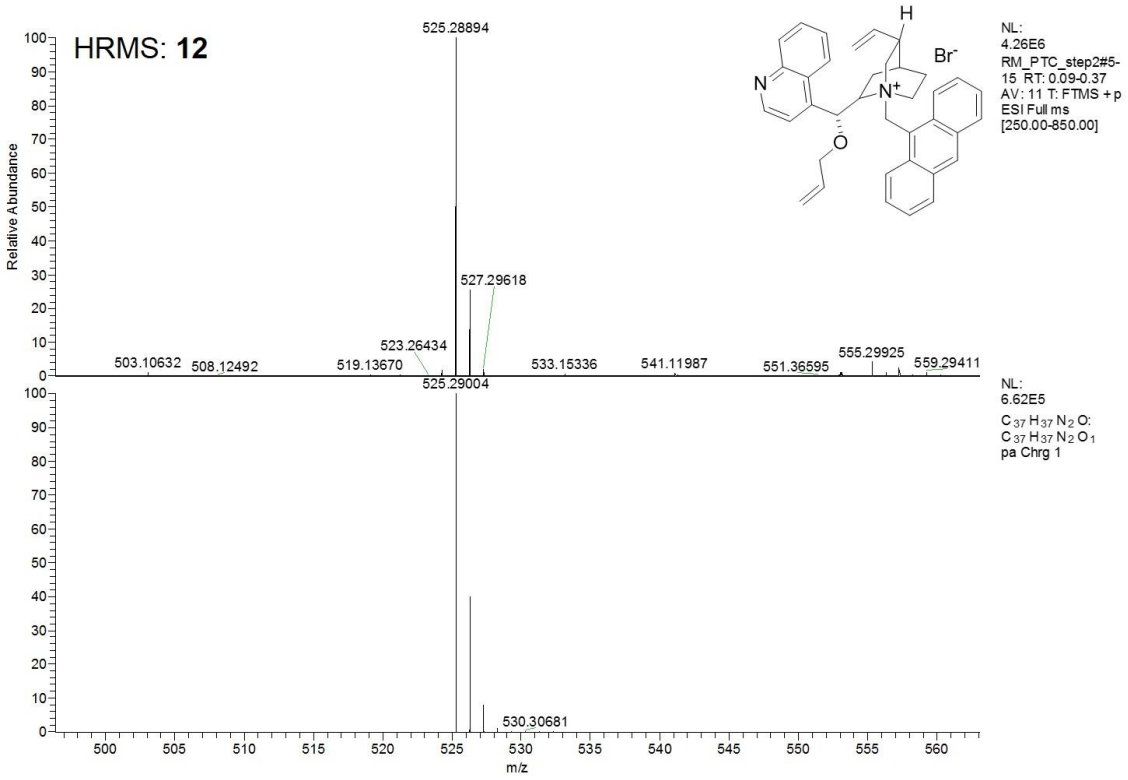
HRMS: 12
Relative Abundance
m/z
525.28894
527.29618
523.26434
503.10632
508.12492
519.13670
533.15336
541.11987
551.36595
555.29925
559.29411
525.29004
530.30681
NL:
4.26E6
RM_PTC_step2#5-15 RT: 0.09-0.37
AV: 11 T: FTMS + p
ESI Full ms
[250.00-850.00]
NL:
6.62E5
C37 H37 N2 O:
C37 H37 N2 O1
pa Chrg 1
Br⁻
N
N+
O
H

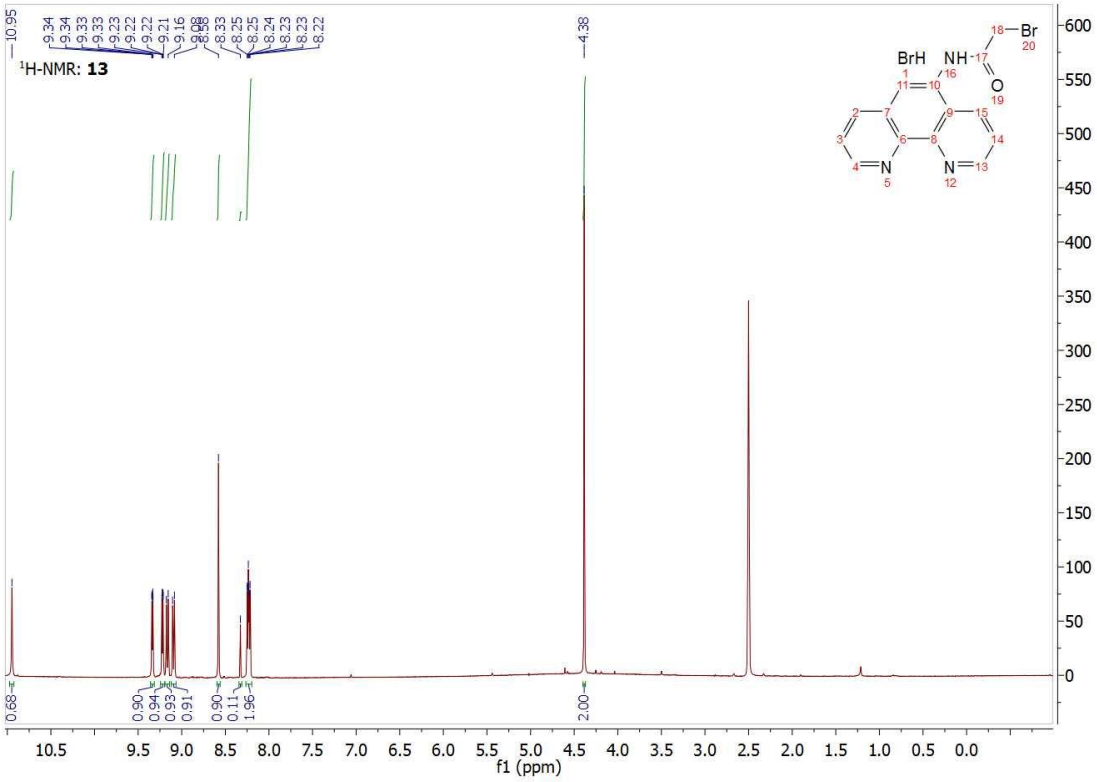
¹H-NMR: 13
f1 (ppm)
10.95
9.34
9.34
9.33
9.33
9.23
9.22
9.22
9.21
9.16
8.33
8.25
8.25
8.24
8.23
8.23
8.22
4.38
0.68
0.90
0.94
0.93
0.91
0.90
0.11
1.96
2.00
BrH
NH
O
N
Br

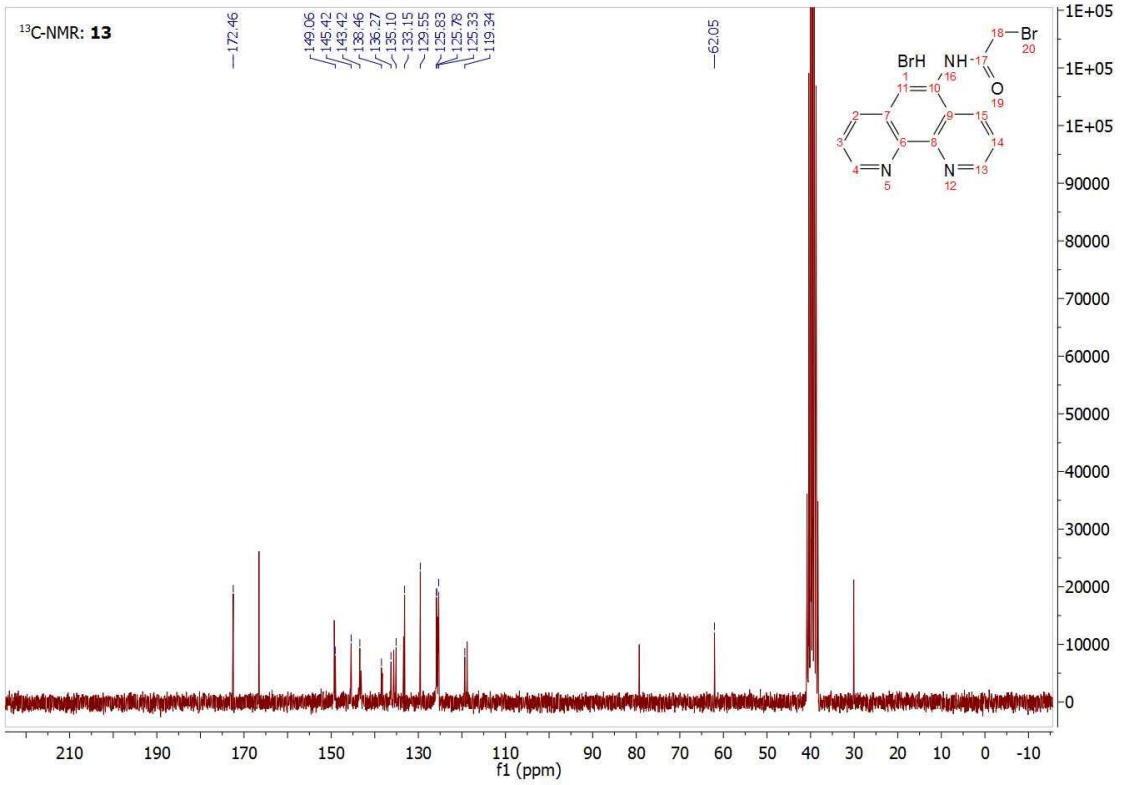
13C-NMR: 13
172.46
149.06
145.42
143.42
138.46
136.27
135.10
133.15
129.55
125.83
125.78
125.33
119.34
62.05
f1 (ppm)

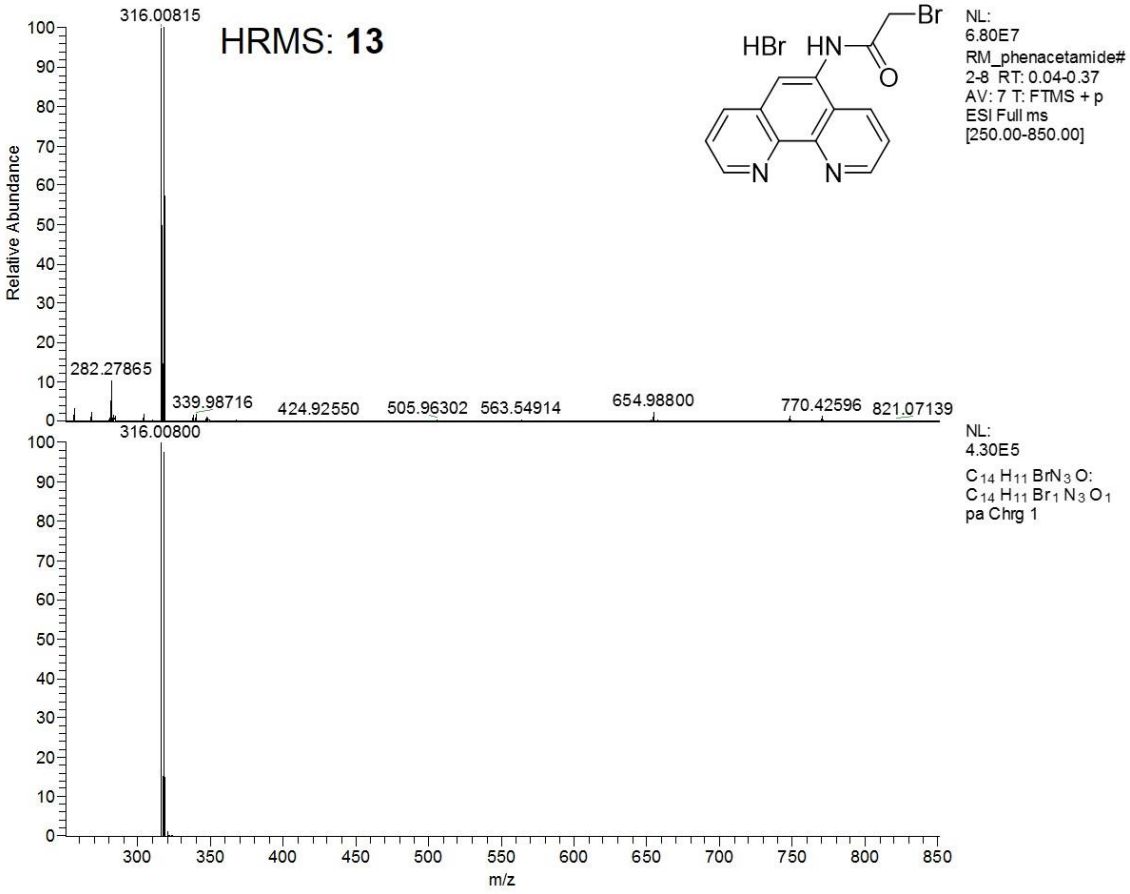
HRMS: 13
316.00815
316.00800
282.27865
339.98716
424.92550
505.96302
563.54914
654.98800
770.42596
821.07139
Relative Abundance
m/z
NL:
6.80E7
RM_phenacetamide#
2-8 RT: 0.04-0.37
AV: 7 T: FTMS + p
ESI Full ms
[250.00-850.00]
NL:
4.30E5
C14 H11 BrN3 O:
C14 H11 Br1 N3 O1
pa Chrg 1

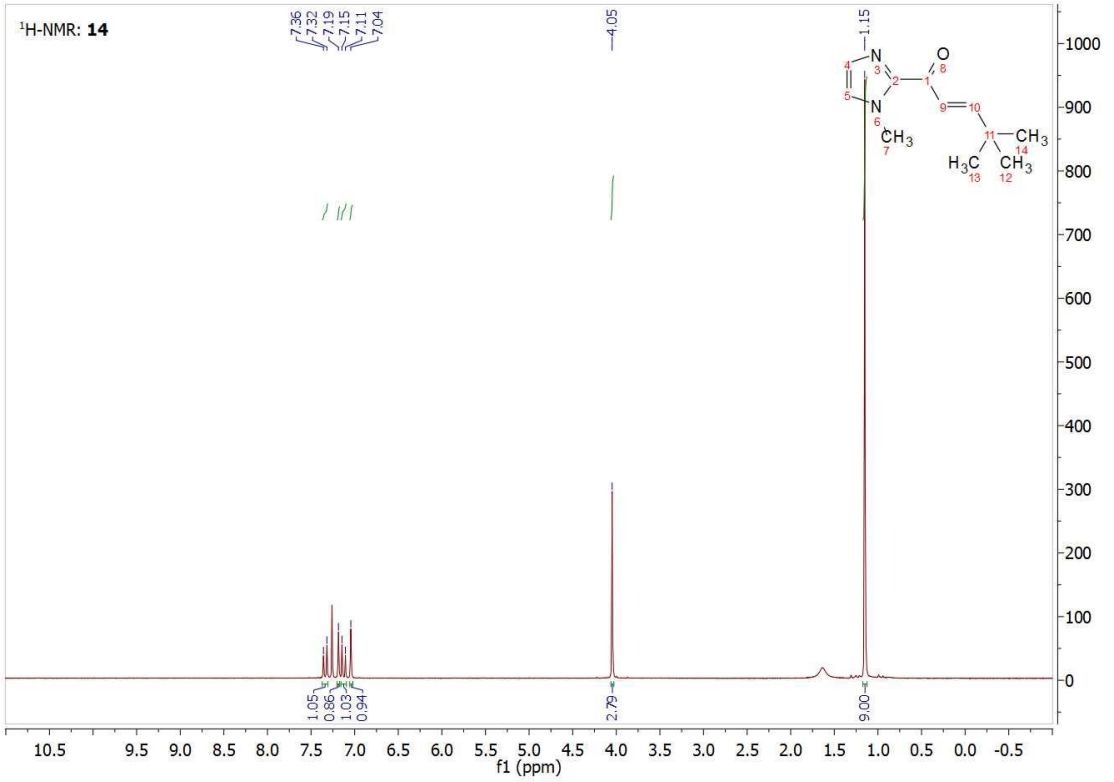
¹H-NMR: 14
7.36
7.32
7.19
7.15
7.11
7.04
4.05
1.15
1.05
0.86
1.03
0.94
2.79
9.00
f1 (ppm)

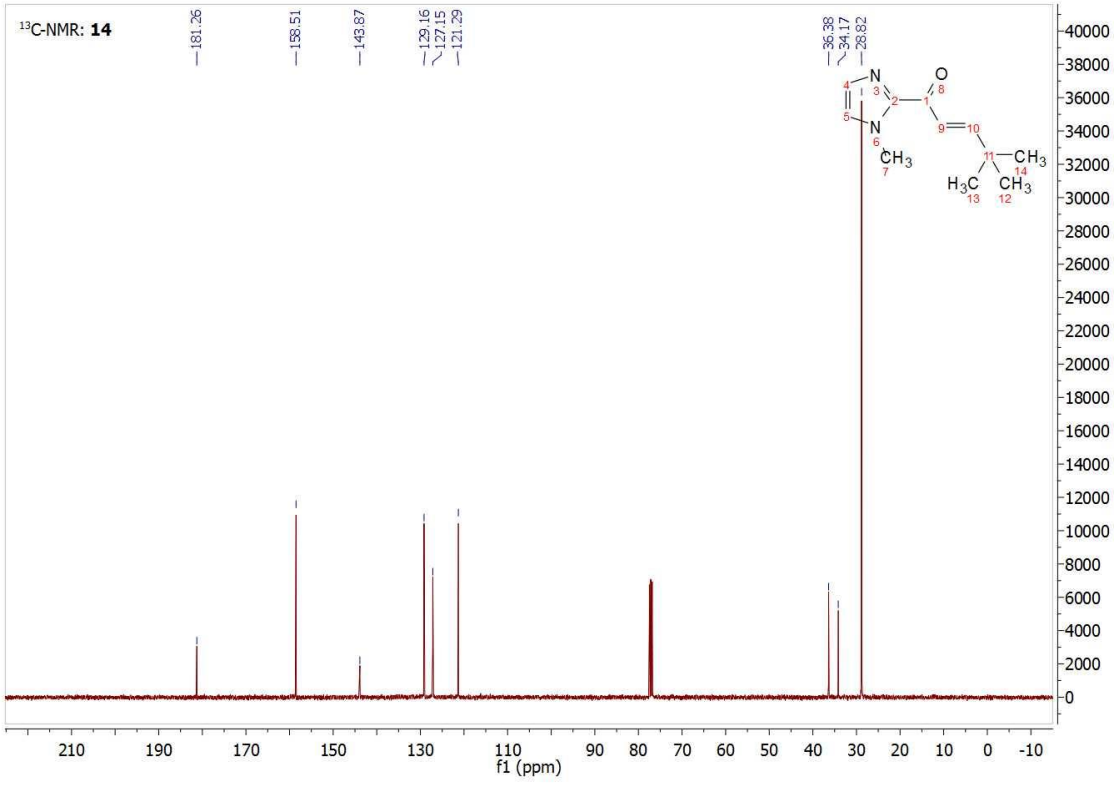
¹³C-NMR: 14
181.26
158.51
143.87
129.16
127.15
121.29
36.38
34.17
28.82
f1 (ppm)

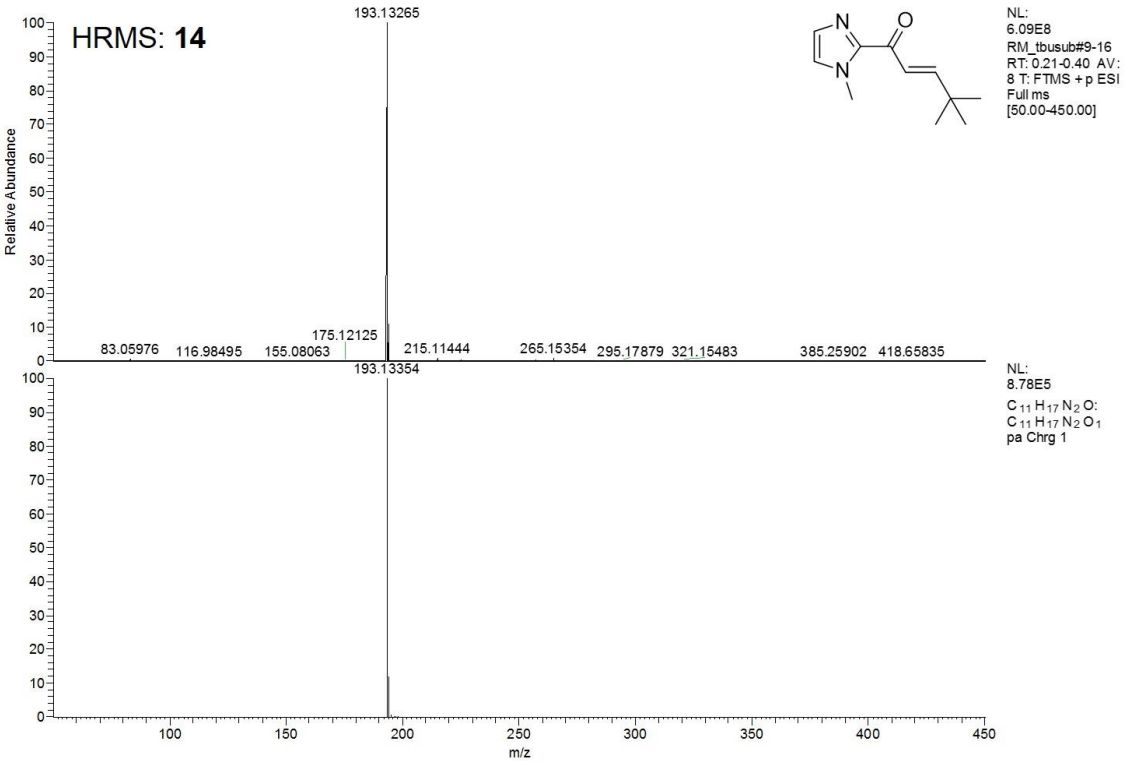
HRMS: **14**
193.13265
NL:
6.09E8
RM_tbusub#9-16
RT: 0.21-0.40 AV:
8 T: FTMS + p ESI
Full ms
[50.00-450.00]
Relative Abundance
83.05976
116.98495
155.08063
175.12125
215.11444
265.15354
295.17879
321.15483
385.25902
418.65835
193.13354
NL:
8.78E5
C 11 H 17 N 2 O:
C 11 H 17 N 2 O 1
pa Chrg 1
m/z

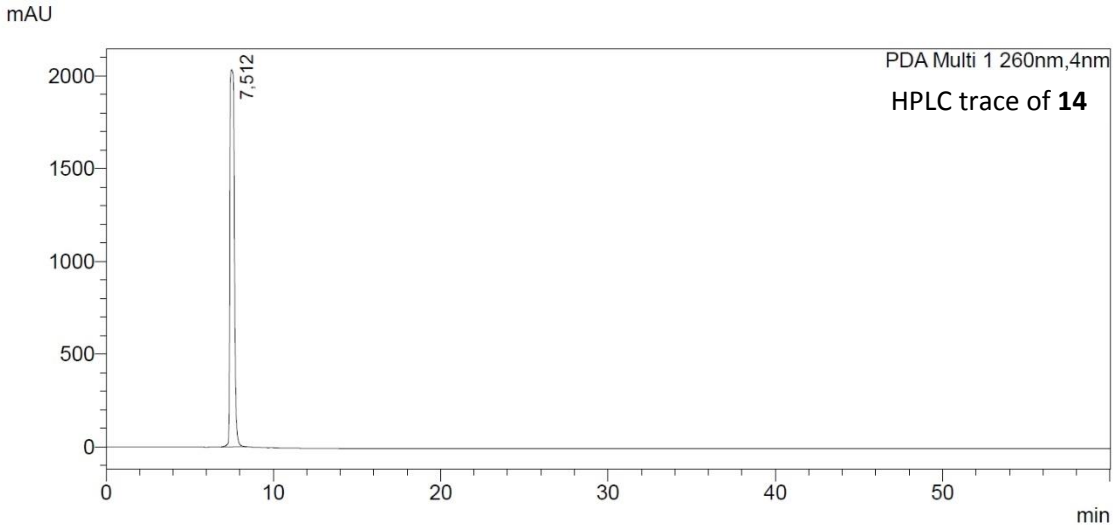
mAU
PDA Multi 1 260nm,4nm
HPLC trace of **14**
7,512
min

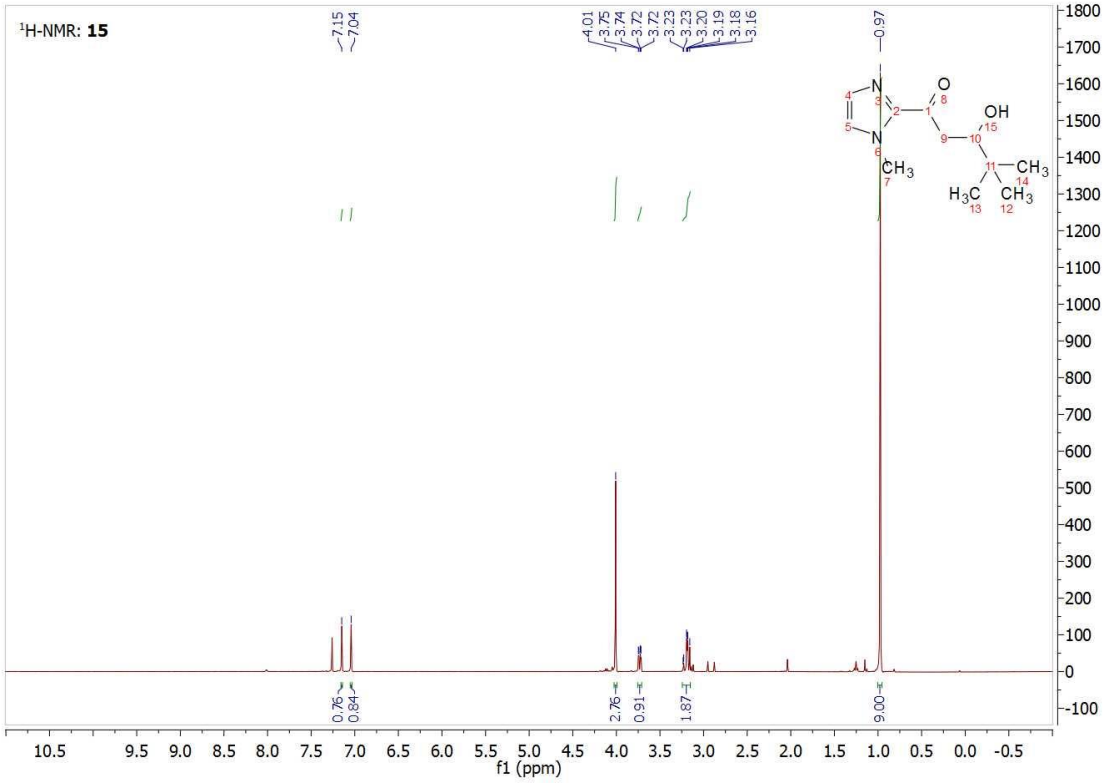
1H-NMR: 15
7.15
7.04
4.01
3.75
3.74
3.72
3.72
3.23
3.23
3.20
3.19
3.18
3.16
0.97
0.76
0.84
2.76
0.91
1.87
9.00
f1 (ppm)

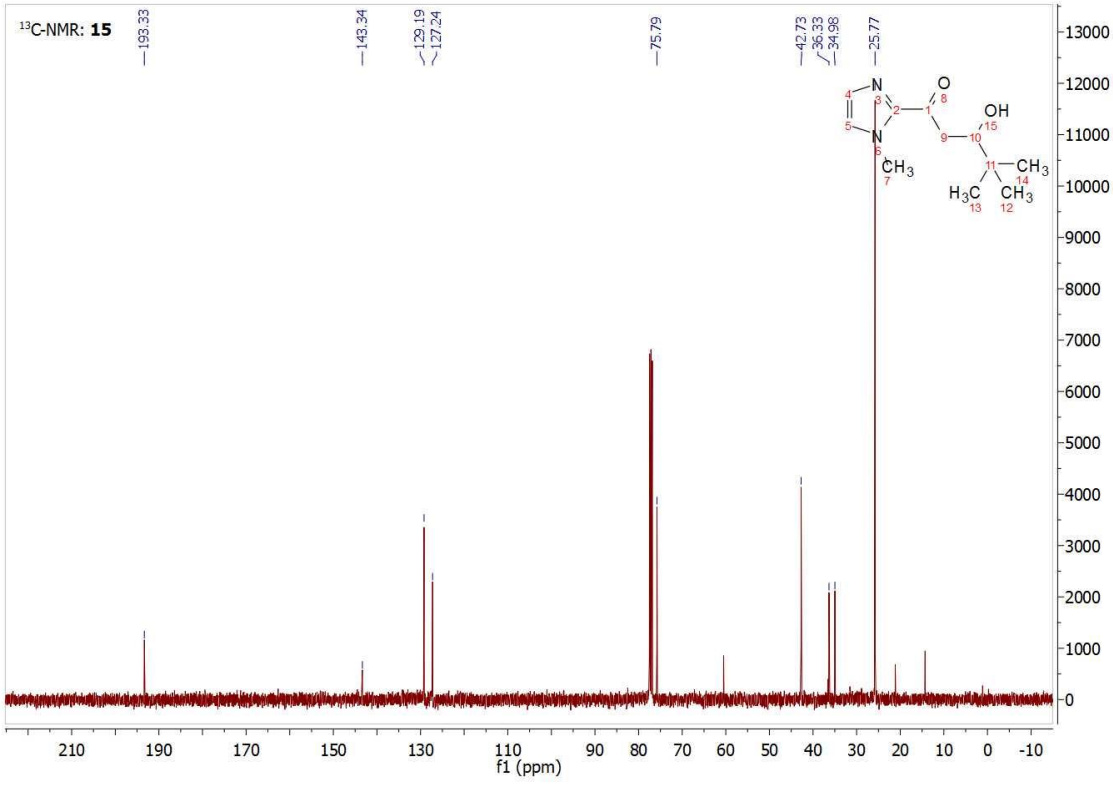
13C-NMR: 15
193.33
143.34
129.19
127.24
75.79
42.73
36.33
34.98
25.77
f1 (ppm)

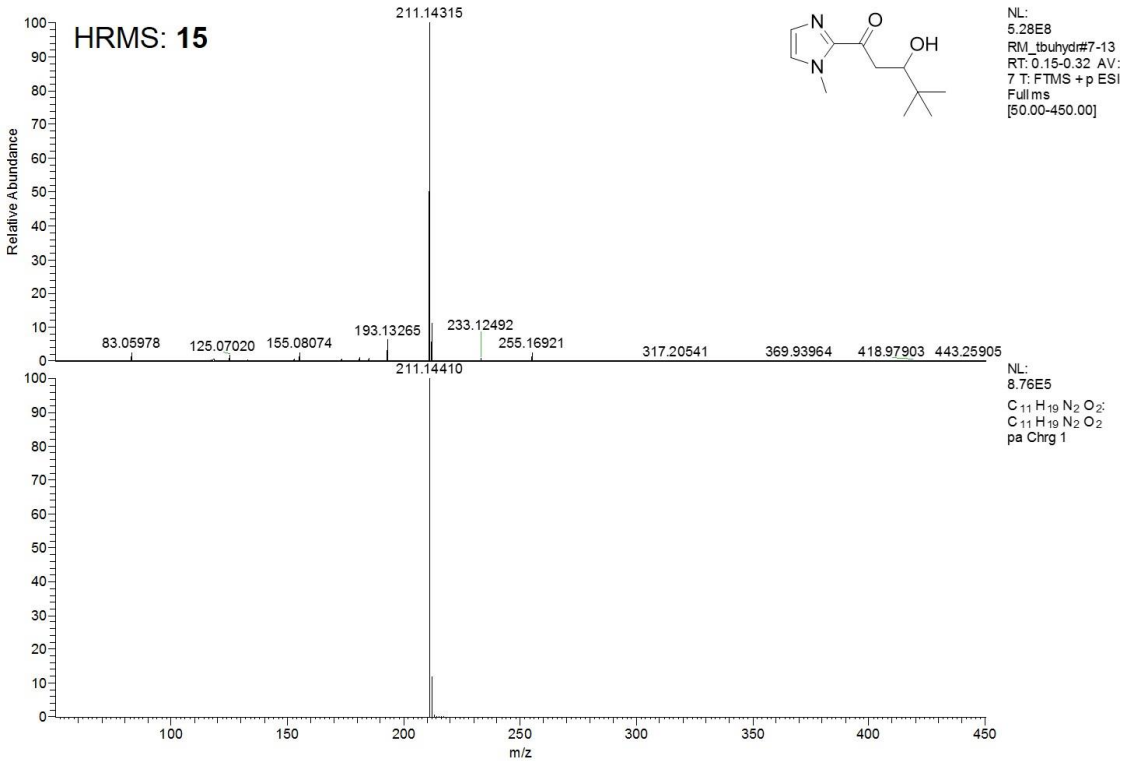
HRMS: **15**
211.14315
NL:
5.28E8
RM_tbuhydr#7-13
RT: 0.15-0.32 AV:
7 T: FTMS + p ESI
Full ms
[50.00-450.00]
Relative Abundance
83.05978
125.07020
155.08074
193.13265
233.12492
255.16921
317.20541
369.93964
418.97903
443.25905
211.14410
NL:
8.76E5
$C_{11}H_{19}N_2O_2$:
$C_{11}H_{19}N_2O_2$
pa Chrg 1
m/z

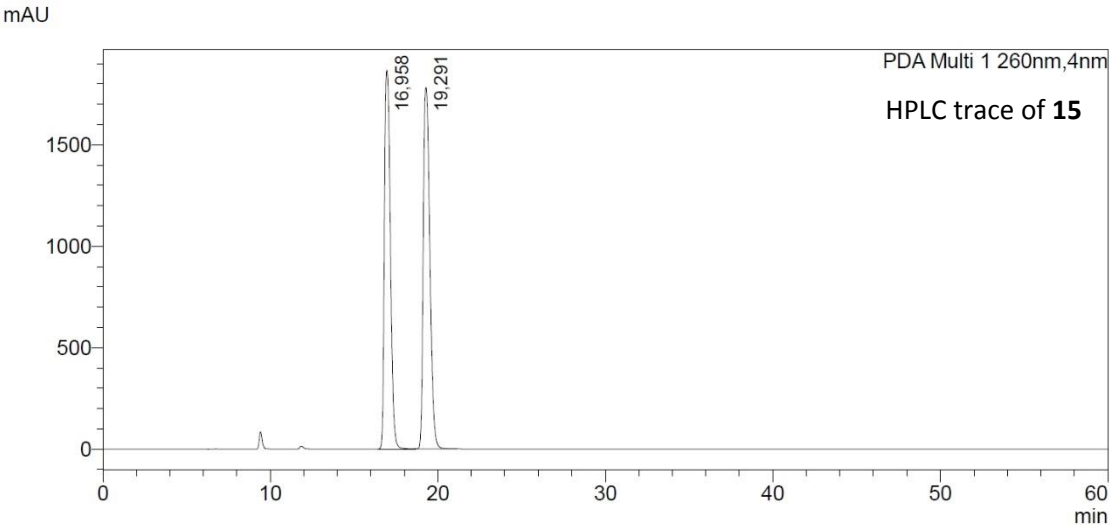
mAU
PDA Multi 1 260nm,4nm
HPLC trace of **15**
16,958
19,291
min

Appendix C: Characterization of peptides

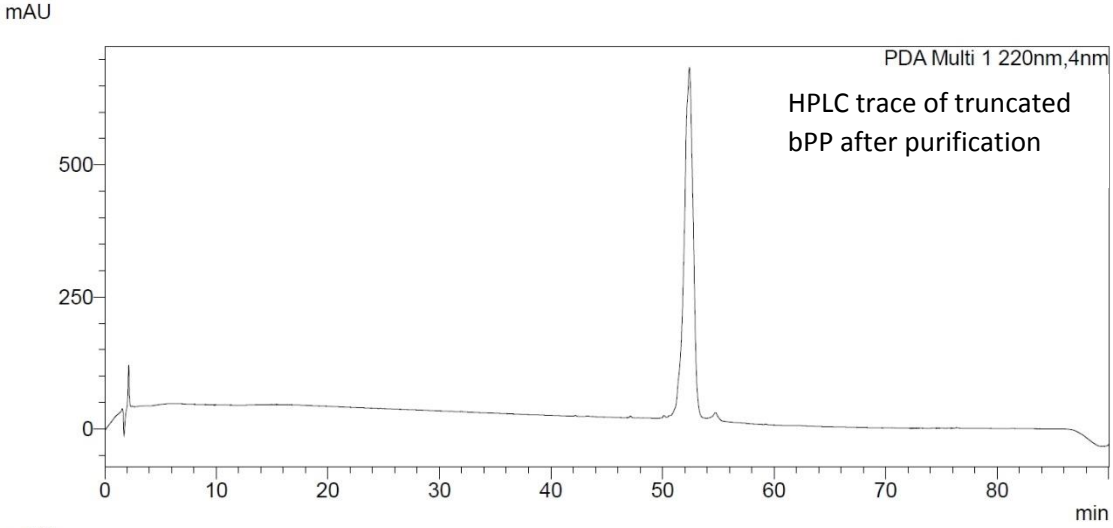

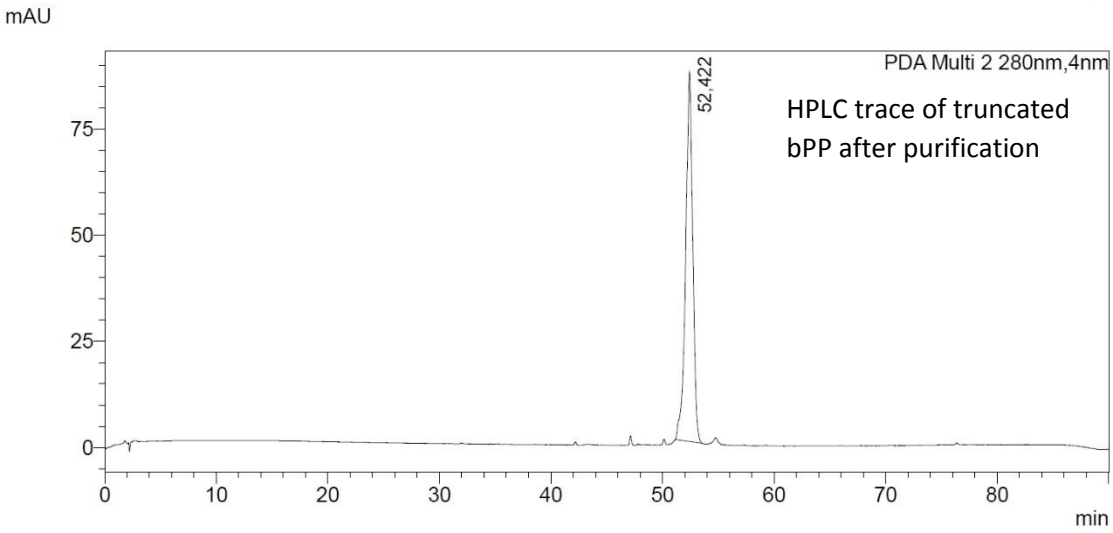

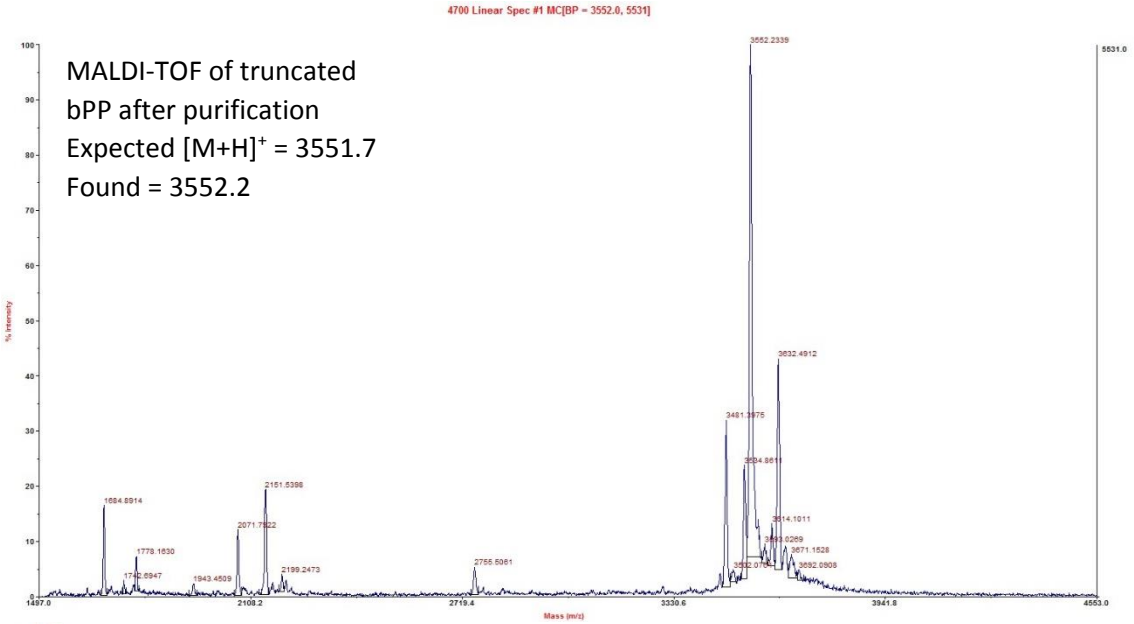
4700 Linear Spec #1 MC[BP = 3552.0, 5531]
MALDI-TOF of truncated
bPP after purification
Expected [M+H]+ = 3551.7
Found = 3552.2
% Intensity
Mass (m/z)
1497.0
2108.2
2719.4
3330.6
3941.8
4553.0
3552.2339
5531.0
3632.4912
3481.3975
3634.8611
3514.1011
3693.6269
3671.1526
3692.0808
2151.5398
2071.7922
1884.8914
1778.1630
1742.6947
1943.4509
2199.2473
2755.5061

mAU

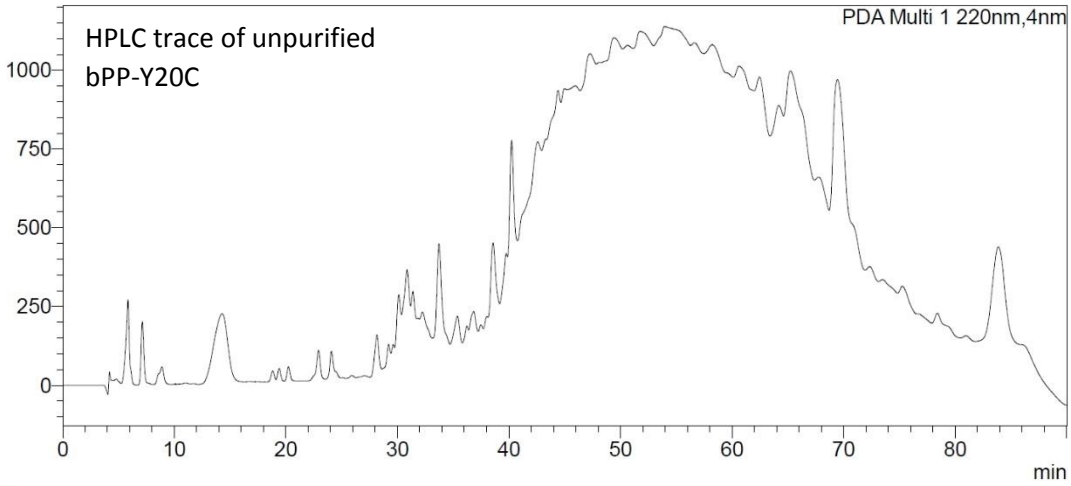
HPLC trace of unpurified
bPP-Y20C
PDA Multi 1 220nm,4nm
1000
750
500
250
0
0
10
20
30
40
50
60
70
80
min

mAU

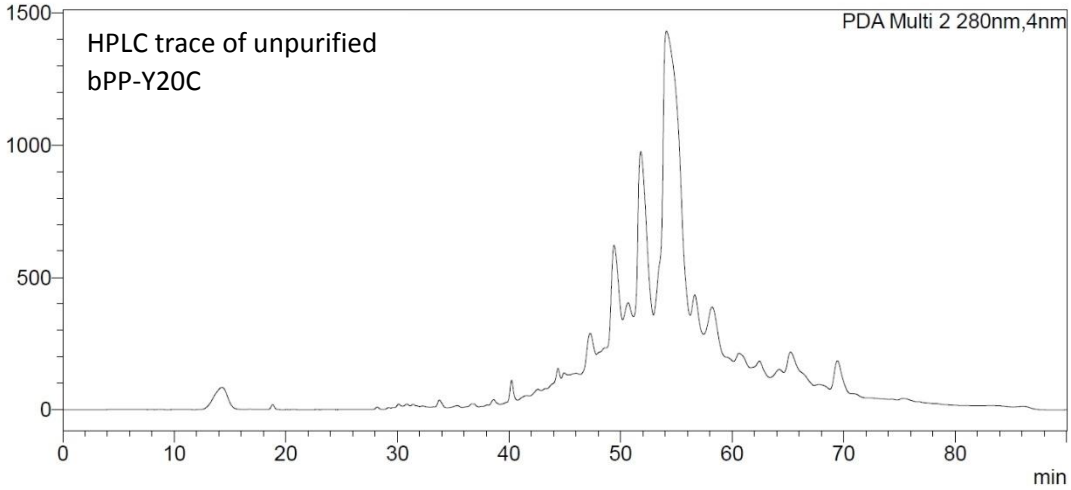
HPLC trace of unpurified
bPP-Y20C
PDA Multi 2 280nm,4nm
1500
1000
500
0
0
10
20
30
40
50
60
70
80
min

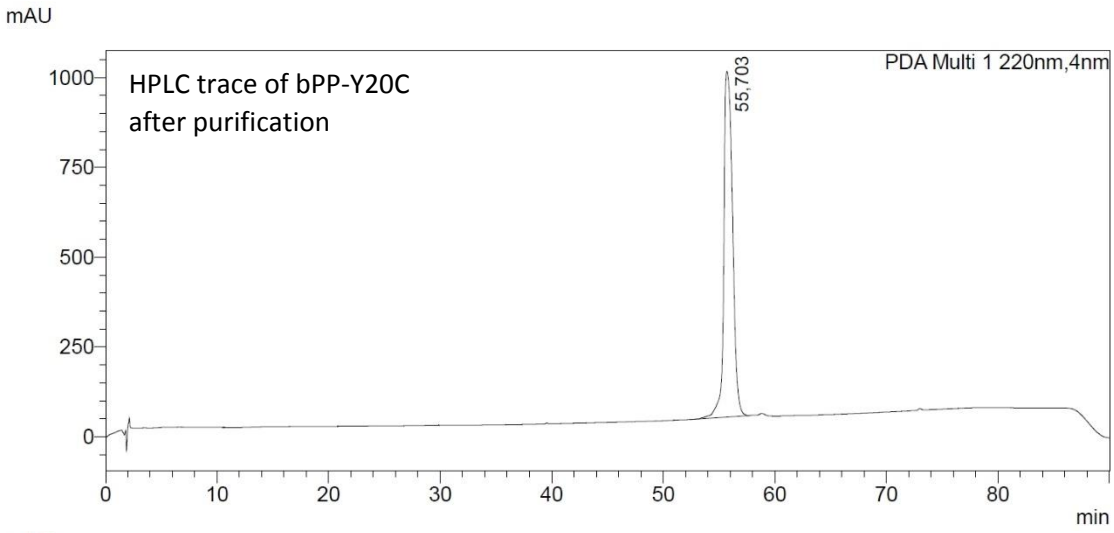
mAU
HPLC trace of bPP-Y20C
after purification
PDA Multi 1 220nm,4nm
55,703
1000
750
500
250
0
0
10
20
30
40
50
60
70
80
min

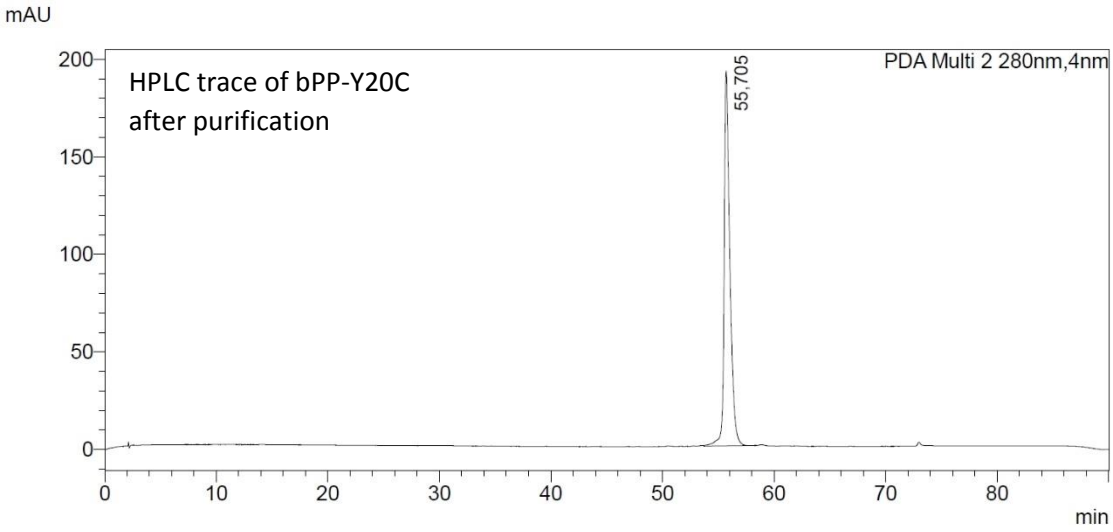
mAU
HPLC trace of bPP-Y20C
after purification
PDA Multi 2 280nm,4nm
55,705
200
150
100
50
0
0
10
20
30
40
50
60
70
80
min

Applied Biosystems Voyager System 6363

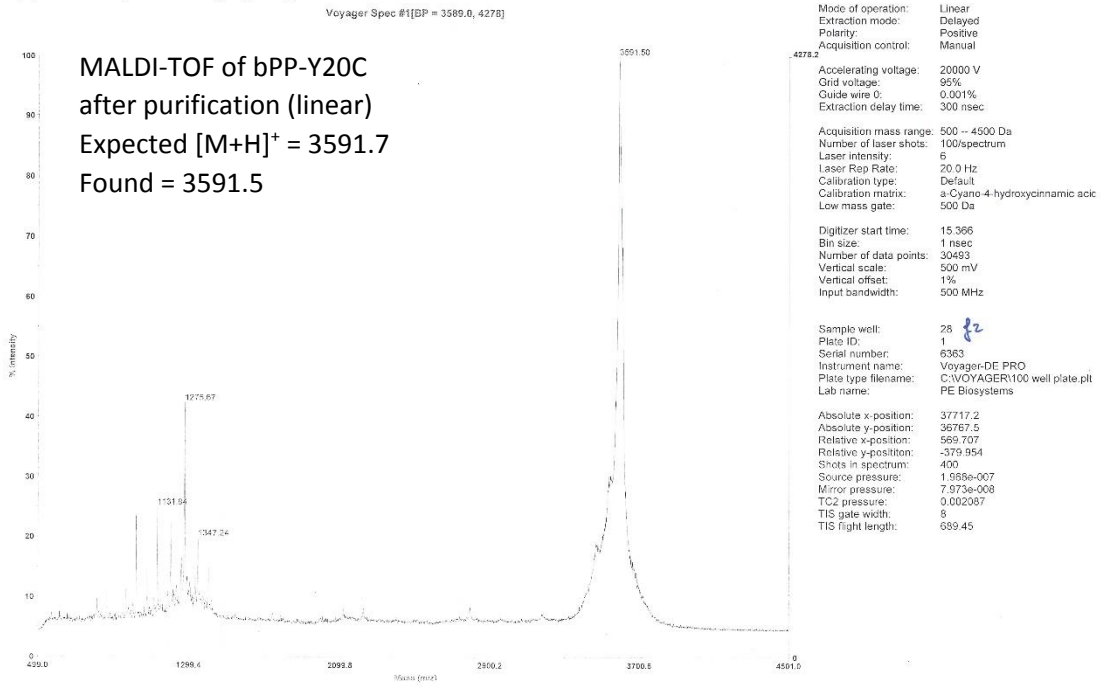

Applied Biosystems Voyager System 6363

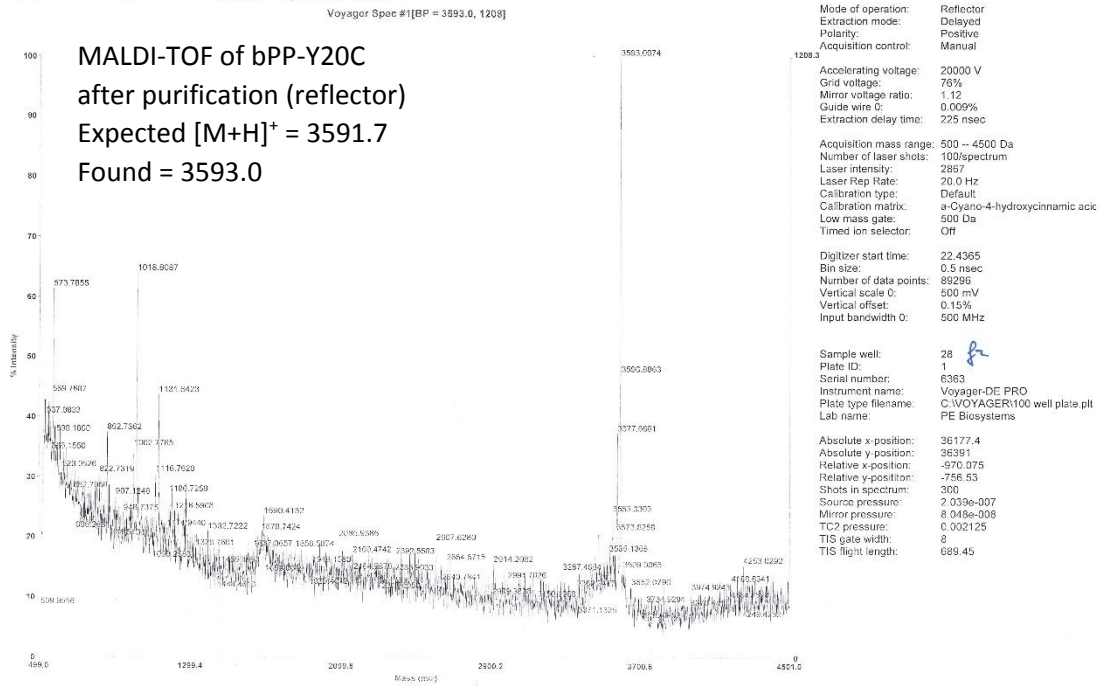

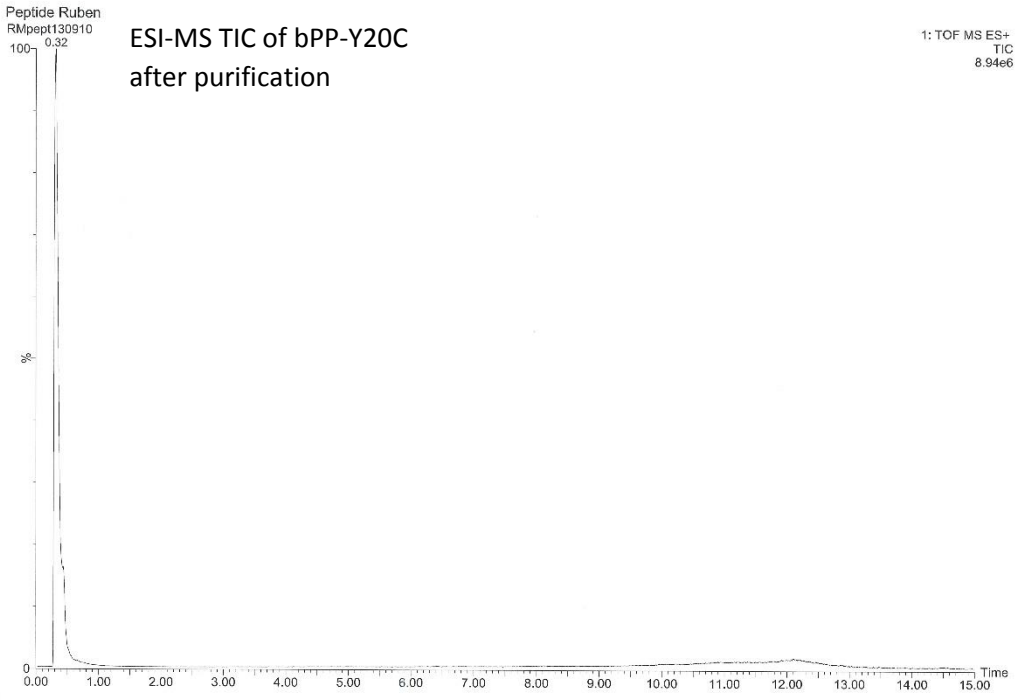

ESI-MS TIC of bPP-Y20C after purification

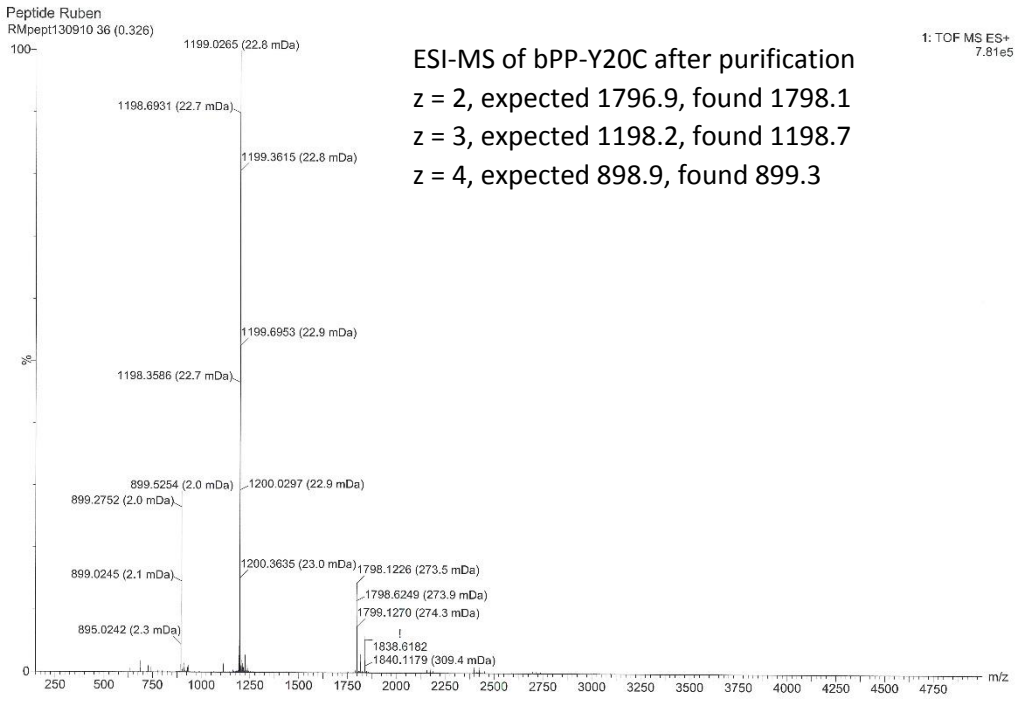

ESI-MS of bPP-Y20C after purification
z = 2, expected 1796.9, found 1798.1
z = 3, expected 1198.2, found 1198.7
z = 4, expected 898.9, found 899.3

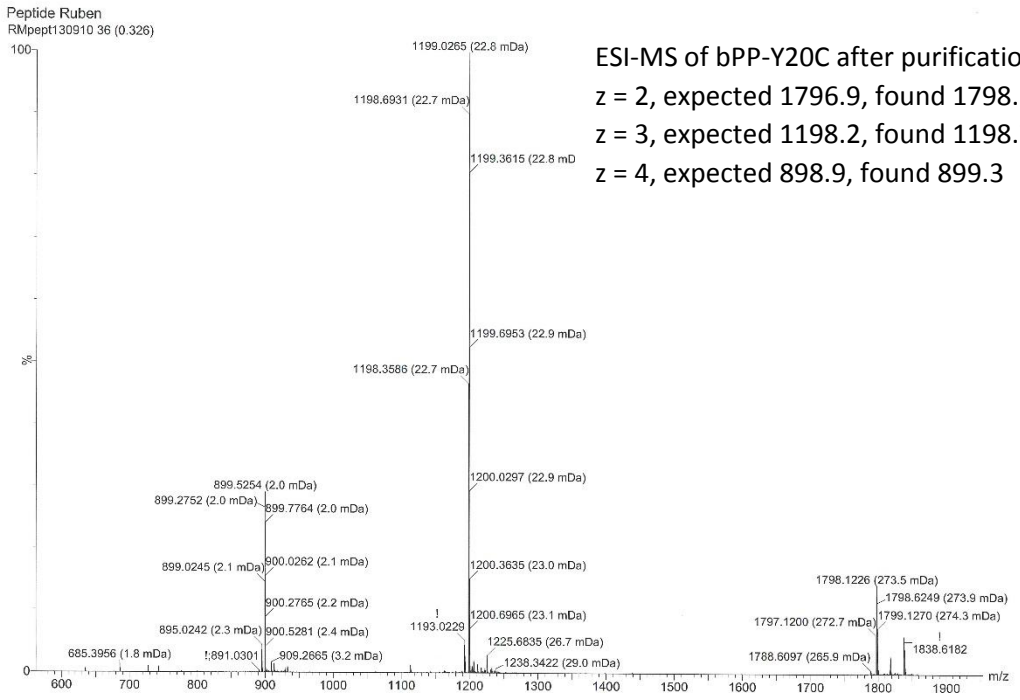

ESI-MS of bPP-Y20C after purification
z = 2, expected 1796.9, found 1798.1
z = 3, expected 1198.2, found 1198.7
z = 4, expected 898.9, found 899.3

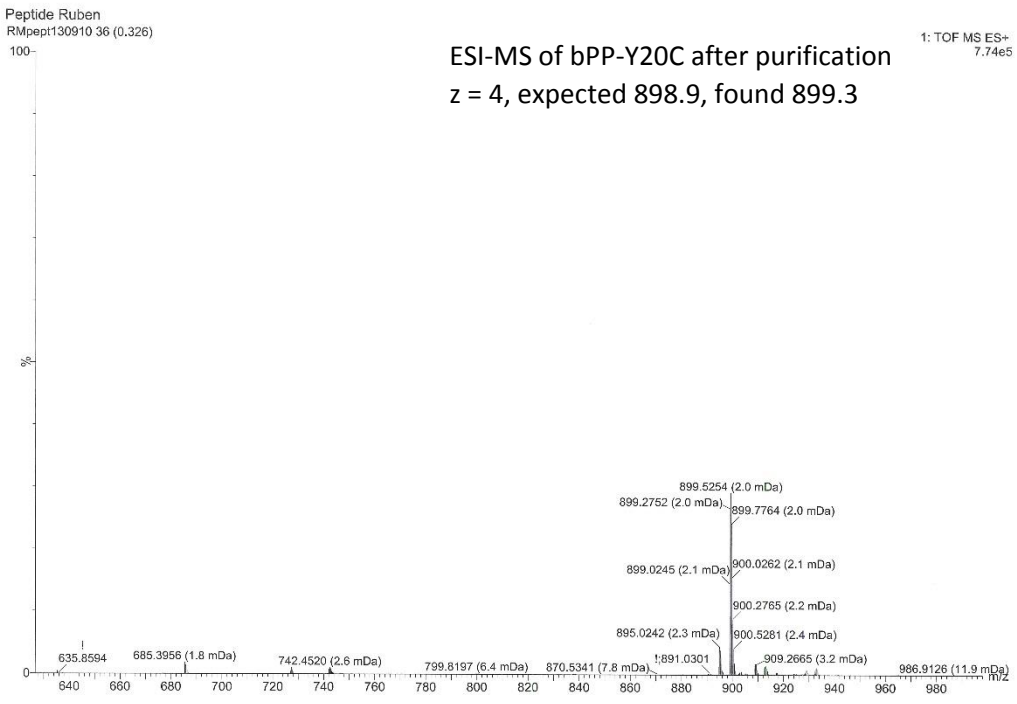

ESI-MS of bPP-Y20C after purification
z = 4, expected 898.9, found 899.3

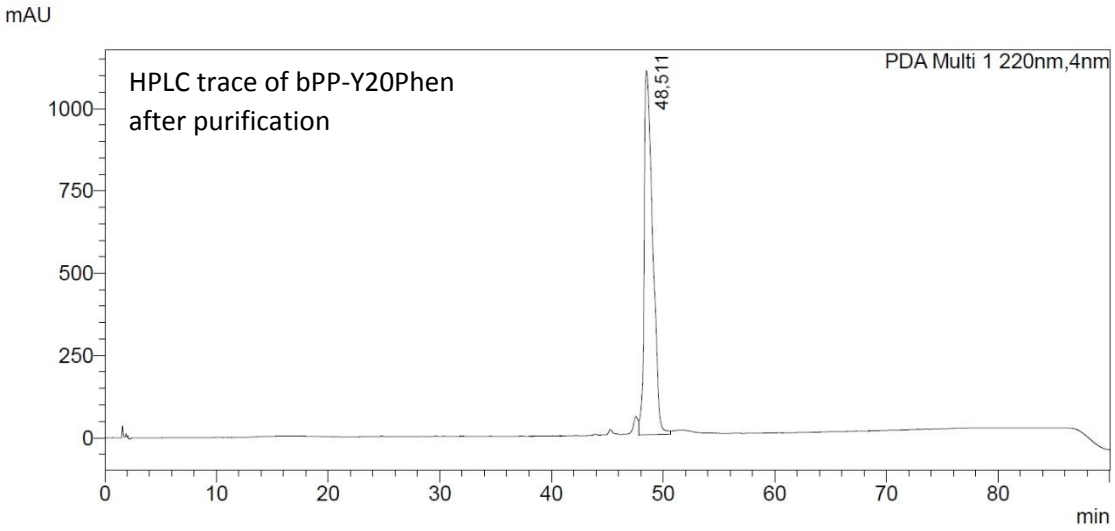
mAU
HPLC trace of bPP-Y20Phen
after purification
PDA Multi 1 220nm,4nm
48,511
1000
750
500
250
0
0
10
20
30
40
50
60
70
80
min

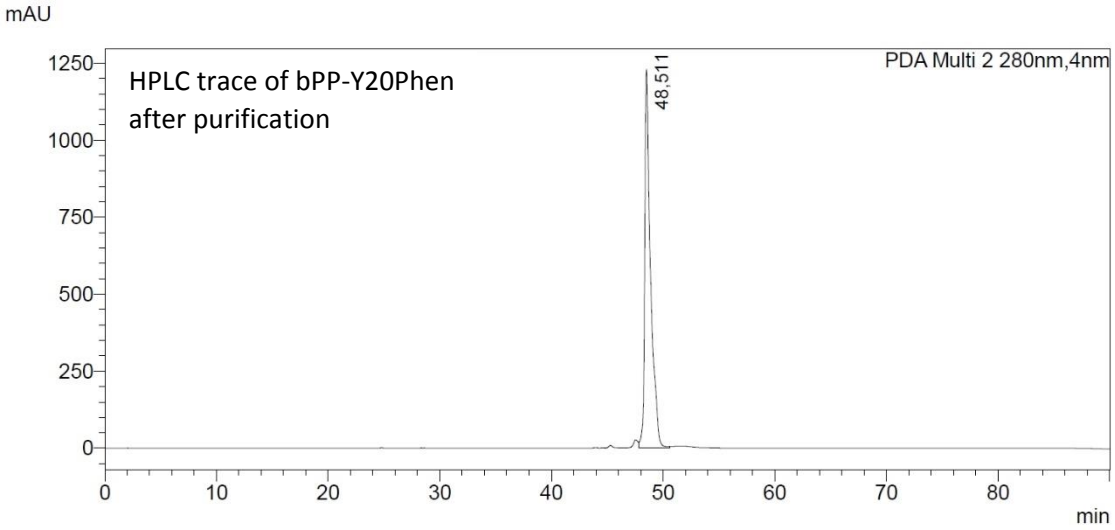
mAU
HPLC trace of bPP-Y20Phen
after purification
PDA Multi 2 280nm,4nm
48,511
1250
1000
750
500
250
0
0
10
20
30
40
50
60
70
80
min

Applied Biosystems Voyager System 6363

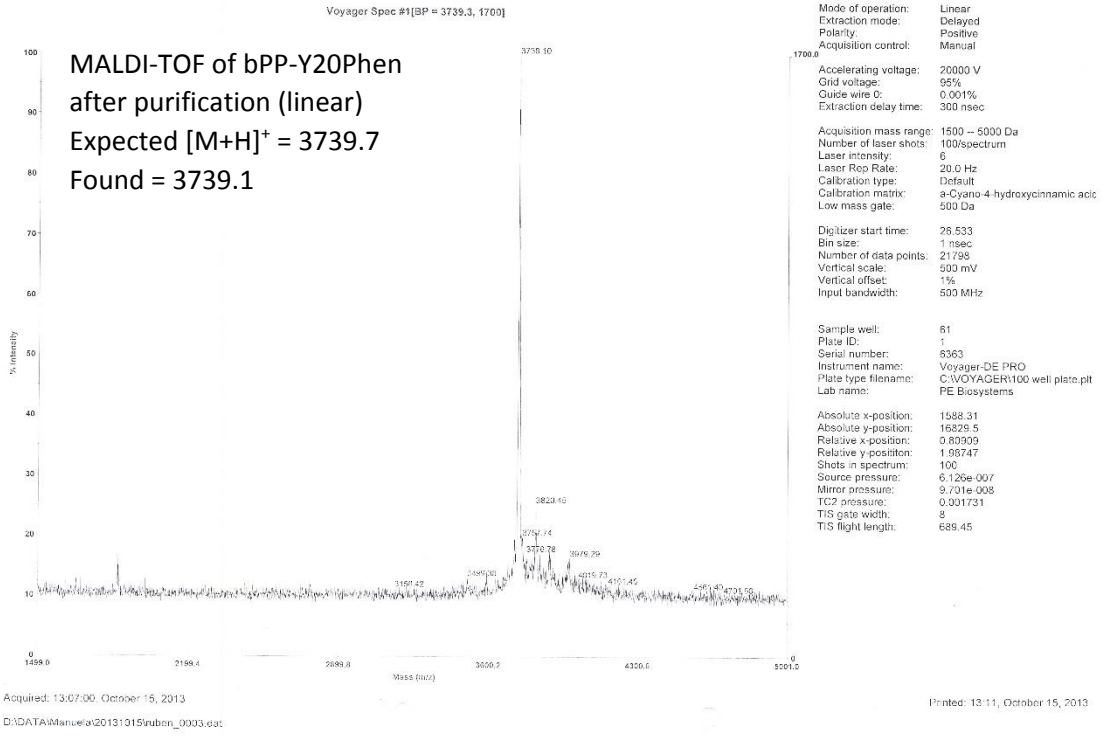

Applied Biosystems Voyager System 6363

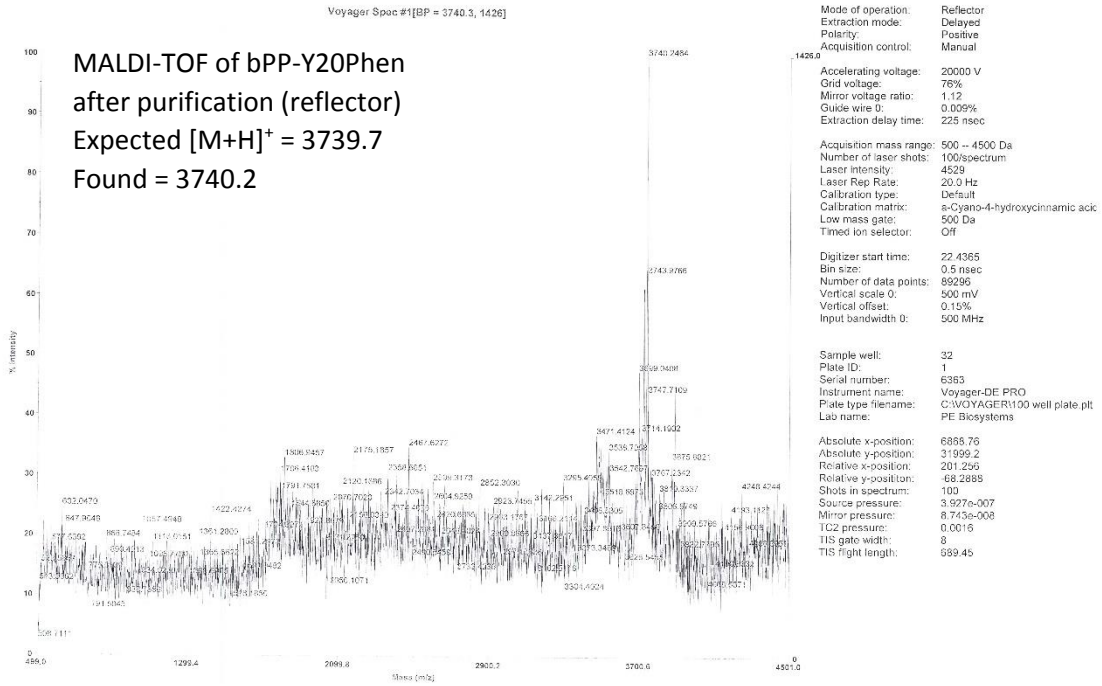

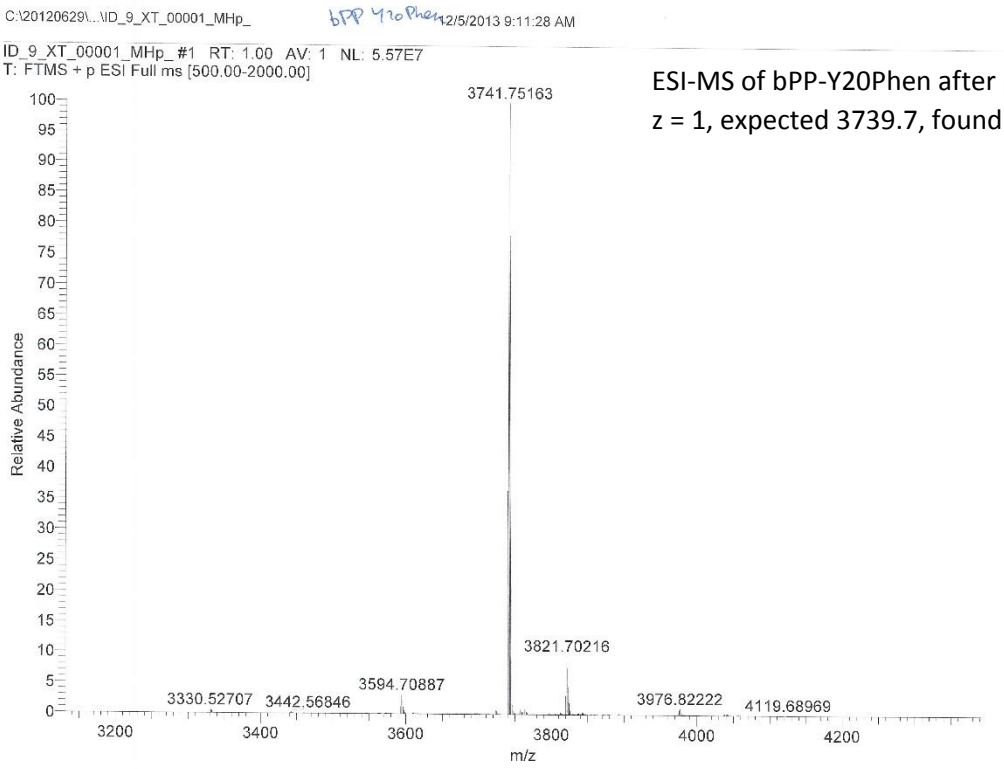

ESI-MS of bPP-Y20Phen after purification
z = 1, expected 3739.7, found 3741.8

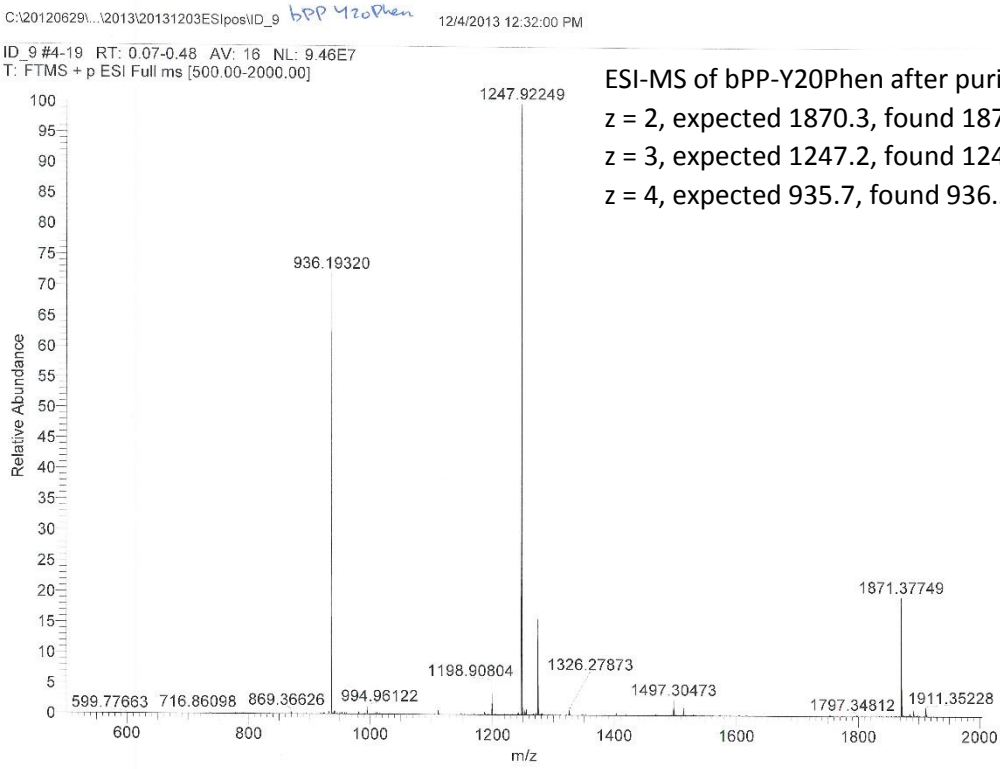

ESI-MS of bPP-Y20Phen after purification
z = 2, expected 1870.3, found 1871.4
z = 3, expected 1247.2, found 1247.9
z = 4, expected 935.7, found 936.2

Appendix D: HPLC-traces of correction factor and catalysis

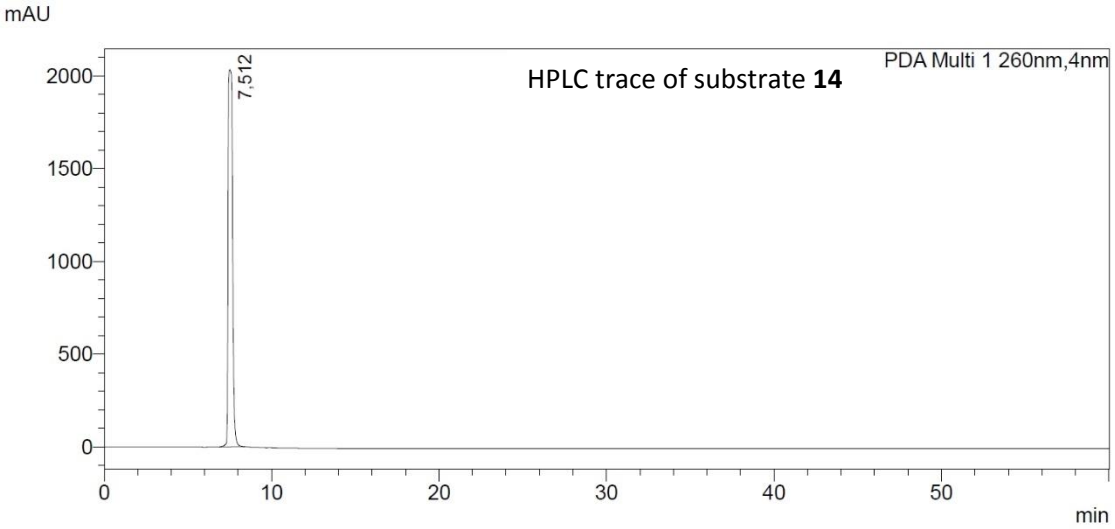

HPLC trace of substrate **14**

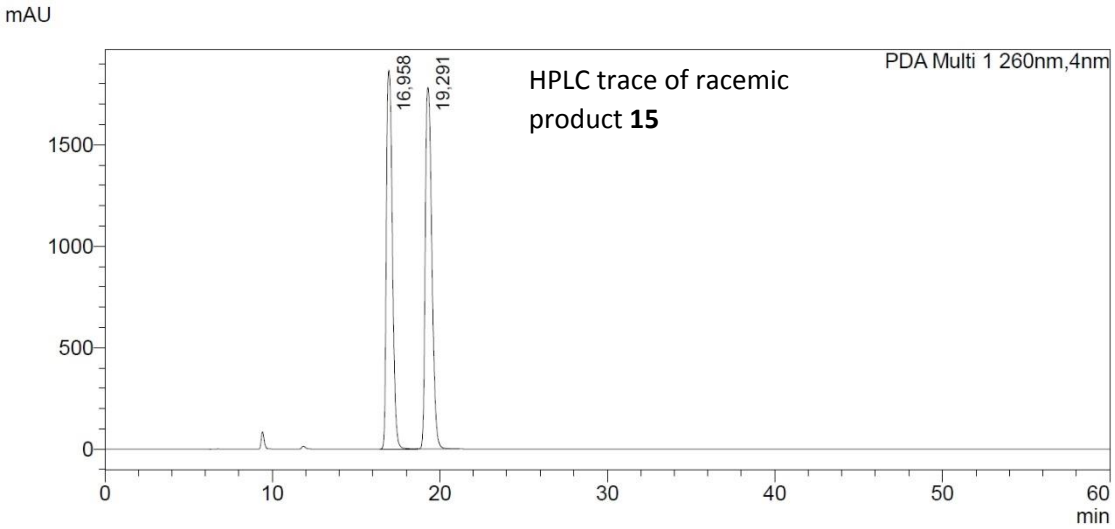

HPLC trace of racemic product **15**

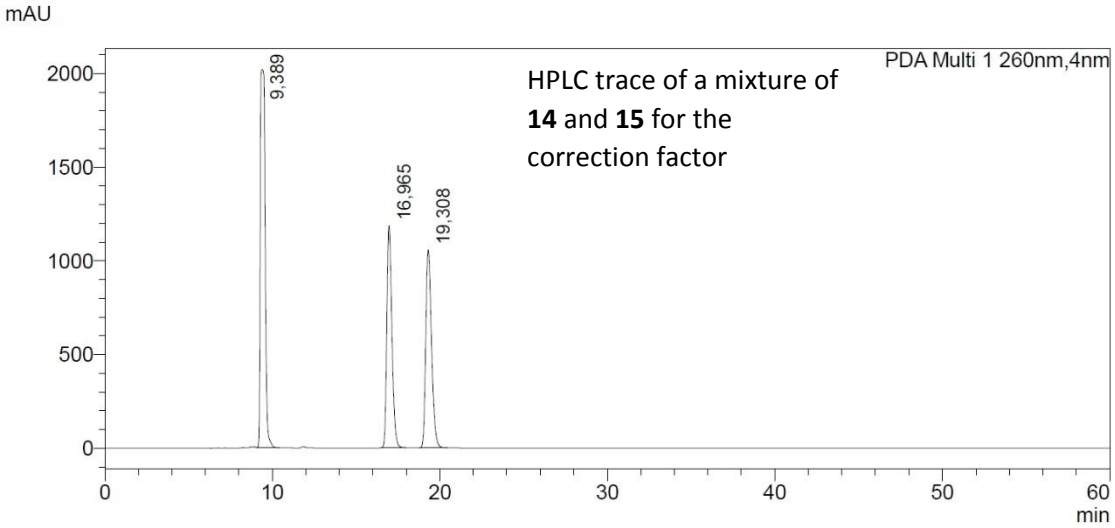

HPLC trace of a mixture of **14** and **15** for the correction factor

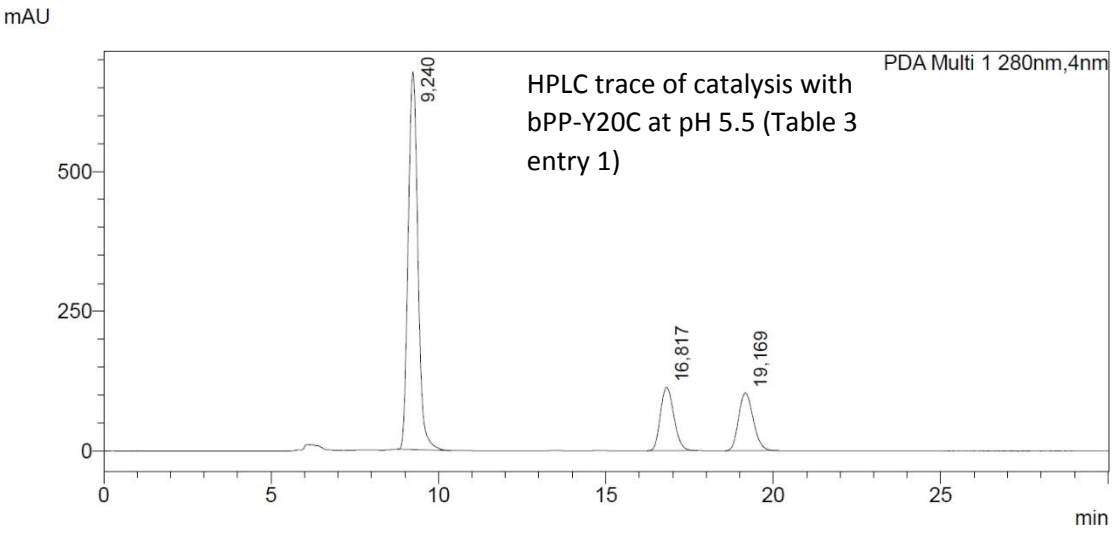
mAU
PDA Multi 1 280nm,4nm
HPLC trace of catalysis with bPP-Y20C at pH 5.5 (Table 3 entry 1)
9,240
16,817
19,169
500
250
0
0
5
10
15
20
25
min

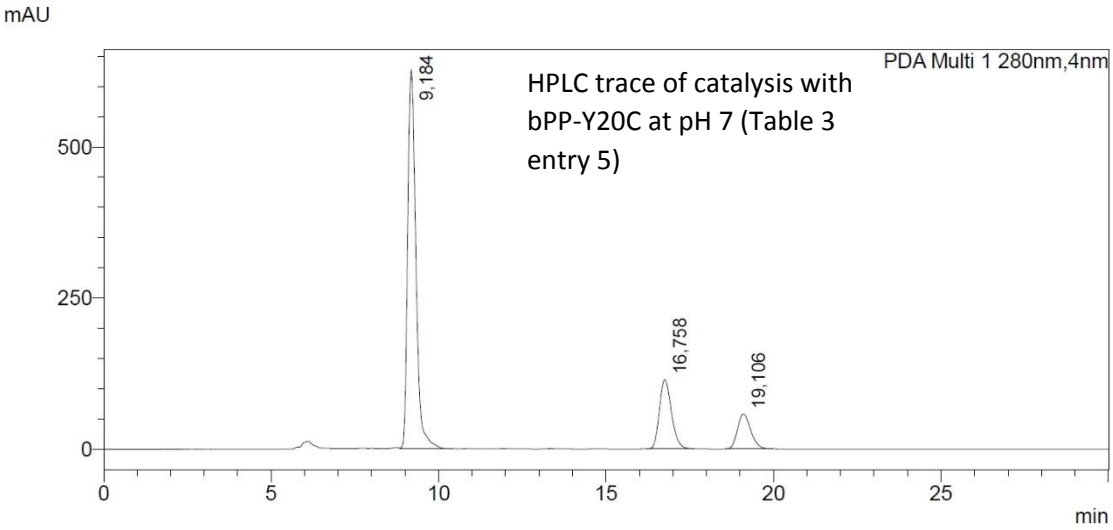
mAU
PDA Multi 1 280nm,4nm
HPLC trace of catalysis with bPP-Y20C at pH 7 (Table 3 entry 5)
9,184
16,758
19,106
500
250
0
0
5
10
15
20
25
min

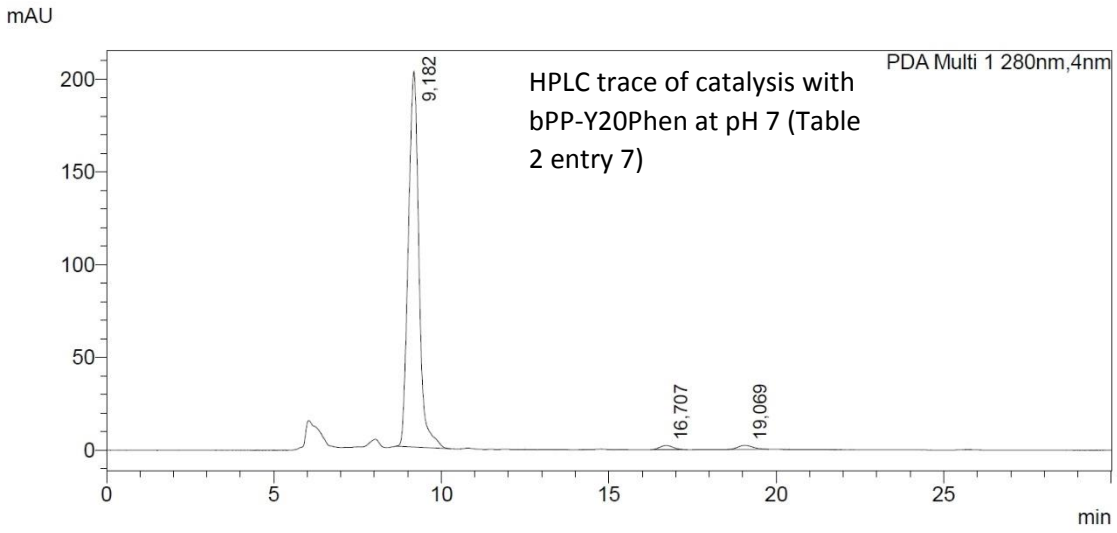

HPLC trace of catalysis with bPP-Y20Phen at pH 7 (Table 2 entry 7)

Correction factor for HPLC-based conversion with data points in red